Spring 2019

CLIMATE ADAPTATION FOR COASTAL ROAD INFRASTRUCTURE IN THE NORTHEAST

Jayne Fifield Knott
University of New Hampshire, Durham

CLIMATE ADAPTATION FOR COASTAL ROAD INFRASTRUCTURE IN THE NORTHEAST

BY

JAYNE FIFIELD KNOTT

Bachelor of Arts in Geology and Physics, Mount Holyoke College, 1978

Master of Science in Civil and Environmental Engineering,

Massachusetts Institute of Technology, 1981

DISSERTATION

Submitted to the University of New Hampshire

in Partial Fulfillment of the Requirements

for the Degree of

Doctor of Philosophy

in

Civil and Environmental Engineering

May 2019

This dissertation has been examined and approved in partial fulfillment of the requirements for the degree of Doctor of Philosophy in Civil and Environmental Engineering by:

Dissertation Director, Jennifer M. Jacobs, Professor of Civil and Environmental Engineering

Jo E. Sias, Professor of Civil and Environmental Engineering

Eshan V. Dave, Associate Professor of Civil and Environmental Engineering

David M. Burdick, Research Associate Professor, Natural Resources and the Environment

Paul Kirshen, Professor, School for the Environment, University of Massachusetts – Boston

On April 8, 2019

Approval signatures are on file with the University of New Hampshire Graduate School.

DEDICATION

This dissertation is dedicated to my husband, Andrew M. Knott, whose love, encouragement, and support has sustained me throughout this journey. It is also dedicated to my brother, Capt. Douglas T. Fifield whose interest in science throughout our lives and climate change, recently, has motivated me.

ACKNOWLEDGEMENTS

I would like to express my sincere gratitude to my advisors, Dr. Jennifer Jacobs and Dr. Jo Sias, for giving me this opportunity, including me in ICNet, UCIRC, TRB and AGU, and supporting me with guidance and funding throughout this journey. Special thanks goes to Dr. Paul Kirshen who has been a mentor for many years and who continued to provide valuable guidance on this research through meetings and conversation even after moving to the University of Massachusetts. I am grateful for Dr. Eshan Dave's contributions to my pavement education and his insights at the weekly asphalt meetings. Dr. David Burdick's work on wetlands is highly respected and I appreciate his perspective on this interdisciplinary climate-change work. I would also like to thank the UNH asphalt research group who contributed to this work, as well as Michelle Mancini, Kristen Parenteau, Maddy Wasiewski, and Kelly Shaw for their support.

I am grateful for my family's support and willingness to participate in climate-change conversation as well as their patience when I was too busy to participate in family life. I also hope this work will inspire our children and grandchildren who will face the challenge of climate change in their lifetimes.

This work was made possible through the New Hampshire Sea Grant Project No. R/RCE-2, the University of New Hampshire Center for Infrastructure to Climate (UCIRC), and the Infrastructure and Climate Network (ICNet) supported by the National Science Foundation via the RCN-SEES: Engineering Research Collaboratory for Sustainable Infrastructure in a Changing Climate (Grant Number: CBET 1231326). Contributions to this research came from the NH Seacoast Transportation Climate Working Group; NH Department of Transportation (NHDOT); NH Department of Environmental Services (NHDES); and the NH Coastal Adaptation Workgroup (NH CAW).

TABLE OF CONTENTS

LIST OF TABLES

LIST OF FIGURES

ABSTRACT

CLIMATE ADAPTATION FOR COASTAL ROAD INFRASTRUCTURE IN THE NORTHEAST

By

Jayne Fifield Knott

University of New Hampshire

The climate is changing, and these changes are expected to accelerate. In the northeast region of the United States, temperatures and sea levels are projected to rise with climate change. These changes have the potential to impact coastal communities in many ways, but this dissertation focuses on climate-change impacts to pavement life. A well-maintained and fully functional roadway system is essential to maintaining a high quality of life and economic vitality in a region. When pavements fail prematurely, the agency and user costs of full-pavement rehabilitation or reconstruction are much higher than the costs of routine maintenance and pavement overlays. Pavement life is sensitive to changes in temperature and the moisture content of the underlying layers. This research investigates the individual and combined effects of rising groundwater from sea-level rise (SLR) and rising temperatures on pavement life. Adaptation strategies are evaluated with respect to performance, cost, and long-term viability.

A three-dimensional groundwater model is used to characterize groundwater rise caused by SLR in coastal New Hampshire and to establish a groundwater-rise zone (GWRZ). Roads vulnerable to reduced pavement life caused by increasing moisture content in underlying pavement layers from rising groundwater are identified. A top-down, or scenario-based, approach is

used to quantify projected pavement life reductions in years 2030, 2060, 2090, and 2100 under a high emissions SLR scenario using pavement layered-elastic analysis. Adaptation options including layer-thickness and base-layer material modifications are evaluated.

A hybrid bottom-up/top-down approach is then introduced to evaluate seasonal and long-term changes in pavement life due to climate-change induced temperature rise over a 60-year pavement management period. This approach differs from the top-down approach by beginning with a sensitivity analysis of pavement performance with incremental temperature rise over the entire range (low to high emissions scenarios) of projected temperature rise. Pavement performance is quantified using an optimal hot-mix asphalt (HMA) thickness or the thickness required to achieve a minimum of 85% reliability under the simulated conditions. Next, downscaled Global Climate Model (GCM) output is used to determine the timing of the effects. Finally, a pavement adaptation framework consisting of the hybrid bottom-up/top-down approach, adaptation pathway mapping, and cost analysis is introduced and demonstrated at a case-study site in coastal New Hampshire for the combined effects of temperature and groundwater rise.

This research shows that climate change, specifically temperature and SLR-induced groundwater rise, will produce significant reductions in coastal-road pavement life without adaptation planning and implementation. Pavement adaptation in the form of structural modifications can maintain the pavement's design life with climate change but choosing the best adaptation strategy and the timing of its' implementation is challenging with an uncertain climate future. Developing adaptation pathways, consisting of a series of performance-based adaptation actions with regular re-evaluation, will result in a cost-effective, stepwise, and flexible adaptation plan that that can help transportation agencies avoid the high cost of premature pavement failure or robust over-design.

CHAPTER 1 – INTRODUCTION

A key factor in a community's ability to be resilient in the face of climate change and other threats is the integrity of the transportation network [*Jacobs, Culp et al.,* 2018; *Kossin et al.,* 2017; *Muench and Van Dam,* 2015]. Coastal communities rely almost exclusively on the network of local roads and connectors for the transportation of people, goods, and services [*Jacobs, Culp et al.,* 2018]. Given the long lifespan of roads (50 to 100 years) transportation agencies should prepare for climate change in their long-term design and management strategies to avoid the costs of more frequent pavement maintenance and rehabilitation [*Chinowsky et al.,* 2013; *Mallick et al.,* 2016]. Unfortunately, most existing road infrastructure design and management practices use historic climate records and do not anticipate long-term changes in sea levels, streamflow, storm frequency and intensity, and temperature when predicting pavement service life [*Muench and Van Dam,* 2015; *National Research Council,* 2011; *Transport & ICT,* 2015]. Research on climate-change impacts on pavement performance raises the possibility that the frequency, duration, and severity of pavement rutting and cracking will increase [*Meagher et al.,* 2012; *Mills et al.,* 2009; *Stoner et al.,* 2019]. Better understanding of potential modes and consequences of road infrastructure failure is critical in the evaluation of adaptation options to maintain current service levels [*Chinowsky et al.,* 2013; *Elshaer, Ghayoomi and Daniel,* 2017a; *Mallick et al.,* 2014; *Mallick et al.,* 2016; *TRB,* 2009].

Many studies have investigated seasonal temperature and groundwater variability and their impact on pavement performance [*Ping et al.,* 2010; *Salour and Erlingsson,* 2014; *Silva et al.,* 2014; *Wang et al.,* 2016]. Few have investigated the combined and dynamic effects of long-term temperature and groundwater changes over the road's lifespan. In this dissertation, a traditional top-down, or scenario-based, approach will be used to analyze SLR-induced rising

groundwater impacts on pavement service life and adaptation options will be evaluated. A hybrid bottom-up/top-down framework for designing a climate-ready coastal road will then be introduced and demonstrated at a case-study site in the NH coastal region. Comparisons will be made between the traditional scenario-based and the hybrid bottom-up/top-down approaches for coastal road adaptation planning.

1.1 CLIMATE CHANGE

Greenhouse gas emissions have caused an increase in global atmospheric and oceanic temperatures since the mid-20th century and the rate of warming is projected to increase through the 21st century and beyond [*IPCC,* 2014; *Melillo et al.,* 2014; *USGCRP*, 2017; *van Vuuren et al.,* 2011].

1.1.1 Sea-Level Rise

Coastal communities with high population density and infrastructure close to the shoreline are vulnerable to the effects of climate change and SLR. The causes of SLR are 1) thermal expansion of ocean waters, 2) water transfer between glaciers and oceans, 3) vertical land movement, 4) shifts in the Earth's magnetic field, and 5) ocean dynamics [*IPCC,* 2014; *Parris et al.,* 2012; *USGCRP*, 2017]. SLR can cause erosion, storm-surge damage, increase the frequency of nuisance flooding [*Jacobs, Cattaneo et al.,* 2018; *Moftakhari et al.,* 2015], flood coastal communities, and damage coastal infrastructure [*Fleming et al.,* 2018; *Melillo et al.,* 2014].

SLR caused by climate change has been the focus of many studies over the past decade [*Horton et al.,* 2014; *IPCC,* 2014; *Kemp et al.,* 2011; *Parris et al.,* 2012; *Sallenger et al.,* 2012a; *Sweet et al.,* 2017; *Vermeer and Rahmstorf,* 2009]. Approximately 18 to 20 cm of global

average SLR has occurred since 1900 with 8 cm occurring since 1993 [*USGCRP*, 2017]. Some areas have experienced more SLR than others. A study of saltmarsh sediments in North Carolina revealed a SLR rate of 2.1 mm/year from 1880 to 1920 in response to 20th century warming [*Kemp et al.*, 2011]. In the northeastern United States sea level has risen approximately 30 cm since 1900 which exceeds the global average. This accelerated SLR is due to factors such as changing ocean circulation patterns in the northwest Atlantic Ocean and land subsidence [*Church et al.*, 2010; *Ezer and Atkinson*, 2014; *Goddard et al.*, 2015; *Kopp, Robert E. et al.*, 2014; *Sallenger et al.*, 2012b; *Sweet et al.*, 2017].

Global average sea levels are expected to continue to rise [*USGCRP*, 2017]. Uncertainties exist in SLR projections due to uncertainties in the rate of greenhouse gas emission reductions that will be adopted globally and uncertainties in the rate and magnitude of ice loss from the Greenland and West Antarctica ice sheets [*DeConto and Pollard*, 2016; *Kopp, R. E. et al.*, 2017; *Melillo et al.*, 2014]. An analysis of a large sample of expert opinions on SLR concluded that there is a 66-percent probability that global mean sea level will rise 0.4 to 0.6 m in a low emission scenario and 0.7 to 1.2 m in a high emission scenario by the end of the century [*Horton et al.*, 2014]. Global SLR ranging from 0.8 to 1.9 m was projected over the period of 1990 to 2100 in a study linking global SLR to global temperature [*Vermeer and Rahmstorf*, 2009]. The National Oceanic and Atmospheric Administration (NOAA) assessed a large body of SLR studies and produced scenarios of global mean SLR ranging from 0.2 to 2 m by the end of the century [*Parris et al.*, 2012]. The low scenario is based on an extrapolation of the historical record. The high scenario is based on the IPCC SRES (Intergovernmental Panel on Climate Change Special Report on Emissions Scenarios) AR4 global SLR projections [*IPCC*, 2007] and an estimate of the maximum amount of glacial and ice sheet loss by the end of the century. A recent report

by NOAA increases the range of global mean SLR to 0.3 to 2.5 m by year 2100 [*Sweet et al.,* 2017]. In the Northeast, relative sea level (RSL) rise, which includes both ocean-level changes and vertical land movement, is projected to add 0.3 to 0.5 m to the global mean SLR under the intermediate emissions scenario [*Sweet et al.,* 2017].

NOAA recommends infrastructure adaptation plans be designed according to the highest emission scenario where risk tolerance is low [*Parris et al.,* 2012], but choosing the right SLR scenario must begin with an understanding of the specific asset or system being evaluated. The expected future performance, asset criticality, the time horizon of interest, and stakeholder's goals and preferences all must be considered when developing adaptation plans [*Hall et al.,* 2016]. The latest projections of global mean SLR and RSL rise in the northeast, illustrate the need to develop flexible adaptation plans that can be modified if or when projections change in the future.

1.1.2 Temperature

The observed annual average temperature from 1986 to 2016 in the Northeast region is 0.79°C warmer than early in the century (1901 to 1960) [*Vose et al.,* 2017; *Vose et al.,* 2014]. The annual average minimum temperature is 0.94ºC higher [*USGCRP,* 2017]. Data analysis from 73 weather stations in New England and New York revealed a regional average 100-year temperature increase of approximately 1.11°C, which is more than the global average of 0.6°C over the same period [*Trombulak and Wolfson,* 2004].

The Northeast region is projected to continue this accelerated warming trend with a 2°C temperature rise predicted to occur 20 to 30 years sooner than the 2°C global mean temperature rise [*Karmalkar and Bradley,* 2017]. Statistical downscaling of global climate projections using

Localized Constructed Analogs (LOCA), predict Northeast average annual temperature changes by mid-century of 2.2°C under Representative Concentration Pathway (RCP) 4.5 and 2.8°C under RCP 8.5. In late century, the projected change is 2.9°C and 5.1°C, respectively [*Pierce et al.,* 2014]. RCPs represent plausible climate futures in terms of projected greenhouse gas concentrations. RCP 4.5 is an intermediate greenhouse gas concentration pathway and RCP 8.5 is the highest concentration pathway [*Moss et al.*, 2008]. Global temperature rise is projected to accelerate [*IPCC,* 2014] and in southeastern New Hampshire (NH), by mid-century (2040 to 2069) under RCP 8.5, the summer maximum and the winter minimum temperatures are projected to be between 3 and 4ºC and between 4 and 5ºC warmer, respectively, than during the years 1979 to 2008 [*Wolfe et al.,* 2018]. The number of days per year with maximum temperature over 32.2°C has historically (1979 to 2008) been between 10 and 15 days in southeastern NH. This is projected to increase 20 to 25 days by mid-century and 50 to 60 days by the end of the century under RCP8.5. The projections are about 50% less under RCP 4.5 [*Wolfe et al.,* 2018].

Uncertainties exist in the climate projections, however. These uncertainties include scientific uncertainty (or model uncertainty), uncertainty in greenhouse gas emissions scenarios, and natural climate variability [*Hawkins, E. and Sutton,* 2011; *Meehl et al.*, 2007; *Melillo et al.,* 2014]. Model uncertainty is large in the short term, becoming less important in the long term relative to greenhouse gas emissions scenario uncertainty. The scenario uncertainty is low in the short term and increases from mid-century to end-of-century [*Hawkins, Ed and Sutton,* 2009]. For example, future annual mean temperatures at Boston Logan airport differ by approximately 1°C between the low and high greenhouse gas emissions scenarios by the year 2020 increasing to approximately 6°C by the end of the century [*Hayhoe et al.,* 2015]. The natural climate variability is large in the short term, but is relatively less important toward the end of the century when

greenhouse gas emissions scenario uncertainty dominates [*Hawkins, Ed and Sutton,* 2009]. In addition, natural variability is larger on a regional versus global scale making local adaptation planning difficult [*Hawkins, E. and Sutton,* 2011; *Stott et al.,* 2010].

1.2 SEA-LEVEL RISE INDUCED GROUNDWATER RISE

Tidal surface-water flooding is commonly recognized as a significant consequence of SLR, but modeling studies have shown that SLR-induced groundwater rise will also have consequences in coastal areas [*Bjerklie et al.,* 2012; *Cooper, H. et al.,* 2015; *Habel et al.,* 2017; *Manda et al.,* 2015; *Masterson,* 2004; *Masterson and Garabedian,* 2007; *Masterson et al.,* 2014; *Oude Essink et al.,* 2010; *Rotzoll and Fletcher,* 2013; *Walter et al.,* 2016]. Scientifically-based numerical models are useful for simulating future conditions over the long-time frames associated with SLR [*Pitz,* 2016] and groundwater models have been used to predict future groundwater levels [*Bjerklie et al.,* 2012; *Habel et al.,* 2017; *Walter et al.,* 2016]. The historical SLR signal has also been measured in coastal Massachusetts. Groundwater rise of 2.1 mm/year was estimated from a long-term (1950 to 2001) monitoring well 300 m from the coast on Cape Cod. This rate of groundwater rise is close to the 2.6 mm/year SLR recorded at the Boston tide gauge from 1921 to 2000 [*McCobb and Weiskel,* 2003].

Groundwater modeling has been used to project climate-change effects on groundwater levels, groundwater flow patterns, and saltwater intrusion [*Masterson,* 2004; *Masterson and Garabedian,* 2007; *Oude Essink et al.,* 2010; *Pitz,* 2016; *Walter et al.,* 2016]. Simulated SLR-induced groundwater rise has been predicted farther inland than tidal surface-water inundation on Cape Cod [*Masterson and Garabedian,* 2007; *Walter et al.,* 2016]. The groundwater signal was predicted at inland locations where existing groundwater levels were 5.2 to 7.3 m above mean

sea level (MSL) in New Haven, CT [*Bjerklie et al.,* 2012]. As groundwater rises, the unsaturated or vadose zone between the ground surface and the groundwater table decreases [*Masterson et al.,* 2014]. This has important consequences for infrastructure including roads, septic systems, underground utilities, and foundations in areas where groundwater is currently near the ground surface [*Hoover et al.,* 2017; *Manda et al.,* 2015; *Walter et al.,* 2016]. A study conducted in urban Honolulu, Hawaii found that the combined area of surface-water inundation and SLR-induced groundwater inundation (GWI) was twice that of tidal surface water alone [*Rotzoll and Fletcher,* 2013]. A study in Miami-Dade County, Florida predicts flooding problems at the Homestead Air Reserve Base from SLR-induced groundwater rise [*Cooper, H. et al.,* 2015] and rising groundwater is predicted to have serious consequences for ecology and water quality in barrier islands of Maryland and North Carolina [*Manda et al.,* 2015; *Masterson et al.,* 2014].

Many of the previous SLR-induced groundwater rise studies have been conducted in coastal aquifers where the bedrock is deep [*Masterson and Garabedian,* 2007; *Walter et al.,* 2016] or porous [*Cooper, H. et al.,* 2015; *Habel et al.,* 2017; *Rotzoll and Fletcher,* 2013] and the transmissivity, or the rate of groundwater flow through the geologic materials, is high. Some studies have focused on GWI and impacts to infrastructure in relatively narrow low-lying areas along the coast [*Habel et al.,* 2017; *Hoover et al.,* 2017; *Roshani,* 2014] or barrier islands where the vadose zone is small [*Manda et al.,* 2015; *Masterson et al.,* 2014].

1.3 PAVEMENT VULNERABILITY

Pavement performance is sensitive to environmental factors, specifically temperature and the moisture content of pavement sublayers [*Elshaer, Ghayoomi et al.,* 2015; *Meyer et al.,* 2014; *Wang et al.,* 2016]. Higher temperatures reduce the stiffness (strength) of the asphalt layer.

Increased moisture content reduces the stiffness of the underlying unbound layers [*Mallick and El-Korchi,* 2013].

1.3.1 Groundwater Rise

Pavement designs, including material types, layer thicknesses and drainage systems, are chosen based on the current groundwater depth determined from soil borings [*Daoulas et al.,* 2011]. Pavement life is especially vulnerable when groundwater rises into the unbound layers of the pavement structure [*Ping et al.,* 2010; *Salour and Erlingsson,* 2014; *Silva et al.,* 2014]. Increasing the groundwater level in field tests in Sweden produced a 20% increase in strain and had more effect on the stiffness of the pavement structure than either temperature or load [*Salour et al.,* 2014]. In addition, the useful life of a pavement structure decreases as the duration of unbound soil saturation increases [*Cedergren,* 1988]. Pavement structure, including layer thicknesses and material types, as well as the nature of the subgrade, influences the structural response to changes in moisture content [*Elshaer, Ghayoomi et al.,* 2015; *Salour et al.,* 2015].

Coastal-road infrastructure is increasingly at risk from surface-water flooding caused by more intense precipitation, storm surge, and wave action. Many studies have investigated the surface-water effects of SLR on road infrastructure [*Batouli and Mostafavi,* 2016; *Johnston et al.,* 2014; *Wu et al.,* 2009] but few have investigated the effect of SLR-induced groundwater rise [*Roshani,* 2014]. Pavement designs are developed under the assumption that the depth to groundwater is stationary over the pavement's lifespan. This assumption is no longer valid in areas where groundwater will rise with SLR [*Roshani,* 2014]. SLR-induced groundwater rise will intersect the unbound layers of some roads weakening the pavement structure, reducing its service life, and making it more vulnerable to damage [*Knott et al.,* 2017; *Roshani,* 2014; *Salour et*

al., 2014]. A study along the Gold Coast in Australia investigated the combined effect of SLR-induced groundwater rise and increased precipitation on roads where the land elevation is 3 m to 6.5 m above MSL. They found 32% of 9.1 km of roadway will be at high risk of failure, defined as groundwater less than 1 m below the pavement surface, by 2070 [*Roshani,* 2014].

1.3.2 Temperature Increase

Pavement performance is also sensitive to pavement temperature [*Meyer et al.,* 2014]. Asphalt-layer stiffness (strength) is quantified by the temperature-dependent modulus of the hot mix asphalt (HMA). Higher temperatures reduce the asphalt-layer stiffness, primarily due to the properties of the viscous asphalt binder [*Mallick and El-Korchi,* 2013]. The temperature dependency of binders is used in their classification. For example, a binder classified with a performance grade of PG 64-22 means the binder will meet high temperature physical property requirements up to a temperature of 64° C and low-temperature physical property requirements down to -22° C [*AASHTO,* 2017].

The temperature dependency of the asphalt-layer modulus affects the seasonal performance of pavements [*Orr and Irwin,* 2006]. Winter modulus is approximately four to six times the summer modulus in Minnesota, Maine, and New York State [*Mallick and El-Korchi,* 2013; *Orr and Irwin,* 2006; *Tanquist,* 2001]. In addition, the underlying unbound materials are also stronger when the ground is frozen [*Swett,* 2007]. DOTs often allow heavier loads to travel on low volume roads during the freezing season [*Daniel et al.,* 2017]. Seasonal load restrictions are applied during spring thaw when the pavement structure is weak from warmer temperatures and increased moisture in the underlying supportive layers. The frost depth and the freezing season duration are both important in determining when seasonal load restrictions should be applied to

prevent pavement damage [*Minnesota Department of Transportation,* 2014a]. Researchers at the Minnesota Department of Transportation (MnDOT) have recognized the importance of modulus seasonal variation and have incorporated it into their pavement design software MnPAVE [*Tanquist,* 2001; *Tanquist,* 2012].

Climate-change induced temperature increases will reduce the modulus similar to the seasonal effects resulting pavement damage over a longer time scale [*Meyer et al.,* 2014; *Stoner et al.,* 2019]. Climate-change induced temperature changes were investigated in Australia where they found a 4°C increase in the effective temperature, defined as the test temperature at which an equivalent amount of fatigue cracking (measured over a year) would occur, resulted in a projected 4-year reduction in pavement life [*Kumlai et al.,* 2017]. Gudipudi et al. (2017) studied the impact of climate-change induced temperature increases on interstate highways in Arizona, Montana, Maine and Virginia. They found daily temperature increases predicted to occur by mid-century (2040 to 2060) associated with RCP 4.5 and RCP 8.5 scenarios increased asphalt concrete fatigue cracking 2 to 9% and rutting 9 to 40%. The projected impacts were greatest in Montana and Maine [*Gudipudi et al.,* 2017]. In a study of climate-change effects on frost-thaw conditions for New England low-volume roads, Daniel et al. (2017) project a mid-century reduction in the frozen period of at least 10 to 20% increasing to 30 to 40% by the end of century [*Daniel et al.,* 2017].

1.4 ADAPTATION PLANNING

Climate-change adaptation planning for coastal-road infrastructure begins with a coastal-road vulnerability assessment and adaptation strategy evaluation to reduce the costs of potential

impacts. Three approaches have been used for adaptation planning in recent years: top-down (scenario-based), bottom-up (asset-based), and a hybrid bottom-up/top-down approach.

1.4.1 Top-Down Approach

The top-down approach to climate-change adaptation planning for coastal road infrastructure begins with downscaled global climate model (GCM) output of future changes in climate-related variables [*Bizjak et al.,* 2014; *Kirshen, Caputo et al.,* 2014; *Mallick et al.,* 2016; *Ray and Brown,* 2015; *Wilby and Harris,* 2006]. One or more climate-change scenarios are chosen for analysis based on stakeholder's needs and an asset performance model is used to evaluate the scenario's effect on the asset's future performance or lifespan. Adaptation strategies are evaluated and recommended to mitigate projected performance cost increases from lifespan reduction or other impacts. This method abandons the stationarity assumption and is an improvement over asset design or rehabilitation based on the historical climate record [*Meyer et al.,* 2014; *Ray and Brown,* 2015].

Top-down studies, focusing on large transportation networks, raise awareness of potential climate-change impacts, adaptation costs and discuss strategies for adaptation. A top-down assessment of climate-change costs for the U.S. road network found that an annual mean global temperature increase of 1.5°C by 2050 could increase the cost of maintaining the current road service by $785 million. These costs vary by region and time period. Pavement design changes using binder upgrades were found to cost more than increases in pavement resealing frequency [*Chinowsky et al.,* 2013]. Another top-down study analyzed GCM temperature output for 2071 through 2100 under a high-emissions and a lower-emissions scenario on the European road network [*Bizjak et al.,* 2014]. They found that the forecasted annual maximum temperature change,

ranging from 2.3° C to 3.4° C, will cause pavement rutting increases. They concluded that water tables may drop due to increased evaporation associated with higher temperatures, but coastal roads at low elevations may experience local SLR-induced groundwater rise. Temperature increases will shorten the fully frozen period that typically accommodates heavier winter loads [*Bizjak et al.,* 2014], but could also decrease maintenance costs by reducing the pavement resealing frequency when moderate-frost areas transition to low-frost areas [*Chinowsky et al.,* 2013].

Climate-change projection uncertainties make predictions of local pavement-life reduction and adaptation strategies difficult [*Mallick et al.,* 2016]. GCM uncertainty and natural variations can be reduced by analyzing output from an ensemble of models as opposed to one or two [*Deser et al.,* 2012; *USGCRP,* 2017; *Wilby and Harris,* 2006]. The World Climate Research Program's framework, the Climate Model Intercomparison Project (CMIP) simplifies this process [*Taylor et al.,* 2012]. Scenario uncertainty is a more difficult challenge because it depends, among other things, on future reductions of greenhouse gas emissions. Future reality may follow the high-emissions, intermediate-high, intermediate-low, or none of these scenarios. While pavements are typically designed for 20 years, they remain in service for much longer through maintenance and rehabilitation. Uncertainty in choosing the appropriate scenario(s) may lead road-infrastructure engineers to choose worst-case design recommendations to minimize risk [*Haasnoot et al.,* 2013; *Kwakkel, Haasnoot et al.,* 2016]. The high costs associated with worst-case design are often prohibitive and, consequently, may not be the best approach for road-infrastructure adaptation [*Brown et al.,* 2012]. Mallick et al. (2016) present a framework for assessing climate-change impacts on pavements using CMIP5 model output [*Reclamation,* 2016; *Taylor et al.,* 2012], a pavement system dynamics model [*Mallick et al.,* 2014], and Monte Carlo analysis. Using this methodology, the climate-parameter change rate can be determined,

pavement models can predict pavement performance under climate-change scenarios, and the risk of pavement failures or rehabilitation frequency can be determined for various emissions scenarios [*Mallick et al.,* 2016].

Pavement management typically consists of 10-year planning cycles, 20-year design cycles and 60-year pavement management periods. This planning, design, and management framework may allow for a dynamic or staged approach to adaptation planning that is either pavement design-cycle based, or performance based [*Kirshen, Caputo et al.,* 2014; *Kwakkel, Haasnoot et al.,* 2016]. A staged, adaptive, flexible approach where implementation of an adaptation strategy is tied to an environmental/climate change or another threshold may avoid over-investment in an overly robust strategy. A staged-adaptation approach requires a performance evaluation of many pavement structural designs under a wide range of possible climate futures [*Haasnoot et al.,* 2013]. This may be achieved using a bottom-up approach that begins with the assessment of asset vulnerabilities over a wide range of environmental/climate conditions as opposed to the top-down approach that begins with choosing one or more scenarios for evaluation.

1.4.2 Hybrid Bottom-Up/Top-down Approach

Studies employing the bottom-up or the hybrid bottom-up/top-down (hereafter called "hybrid") approaches to climate adaptation for road infrastructure are sparse in the literature; however, these approaches have been used in water resources, streamflow, and coastal zone management [*Bhave et al.,* 2014; *Brown et al.,* 2012; *Butler et al.,* 2015; *Groves and Lempert,* 2007; *Kwadijk et al.,* 2010; *Ray and Brown,* 2015; *Taner et al.,* 2017]. Bottom-up approaches seek to determine an asset's sensitivity to possible changes in environmental/climate variables and can be accomplished without using GCMs. In climate-change adaptation planning, however,

downscaled GCMs are essential for identifying plausible environmental/climate changes and the timing of these changes. This realization has led to the hybrid approach [*Taner et al.,* 2017].

The hybrid approach combines stochastic asset-performance assessment (bottom-up) with climate-change scenarios (top-down). Initially, it tests the asset's performance under many environmental/climate states using an exploratory modeling approach where various adaptation actions can be assessed and compared for many climate-parameter combinations [*Brown et al.,* 2012; *Herman et al.,* 2015; *Kwadijk et al.,* 2010; *Kwakkel, Haasnoot et al.,* 2016; *Kwakkel, Walker et al.,* 2016; *Ray and Brown,* 2015; *Taner et al.,* 2017]. The approach involves local stakeholders early in the process who identify critical infrastructure, current management practices, and stakeholder objectives. Stakeholders also may propose adaptation strategies for evaluation [*Bhave et al.,* 2014; *Butler et al.,* 2015] that may be based on proven solutions to current local problems [*van Aalst et al.,* 2008]. Downscaled GCMs are then introduced to identify the timing of plausible climate-related risks and to formulate an asset-specific adaptation plan [*Brown et al.,* 2012].

Kwakkel et al. (2016) compare bottom-up and hybrid approaches including Robust Decision-Making (RDM) [*Groves and Lempert,* 2007; *Lempert and Collins,* 2007], decision scaling [*Brown et al.,* 2012; *Ray and Brown,* 2015; *Taner et al.,* 2017], and Dynamic Adaptive Policy Pathways (DAPP) [*Haasnoot et al.,* 2013]. RDM is a bottom-up approach that identifies adaptation strategies that perform well over a wide range of climate futures [*Groves and Lempert,* 2007; *Lempert and Collins,* 2007]. The RDM approach uses computer simulation models to evaluate hundreds of future climate states to identify the robust strategies, the performance of which are relatively independent of some uncertainties. This method can also identify uncertainties

most important to the management decision [*Groves and Lempert,* 2007; *Kwakkel, Haasnoot et al.,* 2016; *Lempert et al.,* 2013].

The decision scaling hybrid approach seeks to identify environmental/climate conditions that are relevant to asset-specific adaptation decisions [*Brown et al.,* 2012]. It consists of the following steps: (1) identify the performance metrics, asset design alternatives, and a system model; (2) perform a climate stress test that systematically explores how the asset performs across a wide range of possible climate conditions; and (3) analyze climate information including historical climate data and GCM projections to quantify the risks associated with adaptation alternatives [*Ray and Brown,* 2015; *Taner et al.,* 2017]. For example, low risk alternatives are not sensitive to historical climate and projected future climate. Moderate risk alternatives are not sensitive to historical climate but are sensitive to projected future climate, and high-risk alternatives are sensitive to both historical climate and projected future climate [*Ray and Brown,* 2015]. This approach is illustrated with a hydropower project in Sub-Saharan Africa [*Taner et al.,* 2017]. In this study, 12 hydropower design capacities were evaluated relative to a performance metric based on the levelized cost of energy. A climate stress test was then performed to evaluate the performance of the 12 design capacities under a large domain of possible precipitation and temperature combinations. Following the climate stress test, an analysis of the CMIP5 model ensemble [*Taylor et al.,* 2012] output for two emissions scenarios was used to quantify the risks and rank the design alternatives [*Ray and Brown,* 2015; *Taner et al.,* 2017]. This analysis was used to determine the best design capacity for the 35-year project lifetime from 2016 through 2050 [*Taner et al.,* 2017].

Some assets are more well suited to a staged approach. These assets typically have limited budgets and can accommodate change within their lifespan. The DAPP approach introduces

a methodology for step-wise adaptation over time. This approach utilizes the concept of an "adaptation tipping point", or the point at which the existing performance strategy no longer achieves the objectives under future climate conditions [*Kwadijk et al.,* 2010]. The adaptation plan under the DAPP approach recommends short-term actions to be implemented followed by long-term options. When the tipping point is reached, a new adaptation strategy must be implemented to maintain acceptable performance for less favorable future climate conditions [*Haasnoot et al.,* 2013; *Kwadijk et al.,* 2010; *Kwakkel, Haasnoot et al.,* 2016]. A study of long-term water management planning under climate change in the Netherlands illustrates this concept [*Kwadijk et al.,* 2010]. The approach begins with identifying the asset's performance objectives and performance metrics. The Maeslant Barrier is closed to protect Rotterdam Harbor and the tidal river against flooding when the sea level from storm surge reaches a predetermined point. When the barrier is closed there are navigation restrictions and, consequently, local authorities have identified a maximum acceptable closing frequency of once per year. As sea level rises the barrier will close more often to prevent flooding. The restriction of once per year is a tipping point that must lead to a new adaptation strategy. Another tipping point occurs when the sea level is projected to exceed the height of the barrier and the flood-protection objectives can no longer be met. GCMs are used to estimate the timing of these adaptation tipping points [*Kwadijk et al.,* 2010].

The hybrid approach offers a systematic and quantitative methodology for identifying asset vulnerabilities important to decisionmakers under many possible climate futures [*Groves and Lempert,* 2007]. Through this process, stakeholders are equipped with new knowledge of their asset's performance sensitivity to climate stressors [*Ray and Brown,* 2015]. Climate scenarios are then introduced to determine the likelihood and timing of critical changes with respect to

asset performance. More comprehensive information on how the asset will respond to future climate will result in local stakeholder buy-in for adaptation planning and greenhouse gas reductions as certain thresholds for performance will become apparent [*Groves and Lempert,* 2007]. The bottom-up/top-down adaptation approach also has some challenges. First, it relies heavily on computer simulations of asset performance over a wide range of climate parameters. Many asset performance models, including those related to pavement performance, are calibrated to local climate conditions and may not provide accurate results outside the calibrated range [*AASHTO,* 2008; *Groves and Lempert,* 2007; *Tanquist,* 2001]. In addition, the bottom-up/top-down approach requires more computational time to evaluate asset performance under many possible climate states rather than testing asset performance under the small number of climate states associated with chosen scenarios. This can limit the number of climate parameters and adaptation options evaluated in the analysis. This approach also couples the analysis to a single decision defined by the chosen performance metric which may limit the relevance of the study [*Groves and Lempert,* 2007].

1.5 DISSERTATION THESIS STATEMENT AND OBJECTIVES

The thesis statement of this research is: SLR-induced groundwater (GW) rise and temperature increases will have significant impacts on the service life of coastal-road infrastructure, but adaptation planning can decrease the costs of these impacts.

The main objectives of the research are:

1. Identify the magnitude and areal extent of groundwater rise caused by SLR and create a groundwater-rise vulnerability map of NH's coastal roadways

2. Determine the magnitude of pavement service-life reduction associated with SLR-induced groundwater rise at five case-study sites
3. Evaluate adaptation strategies to mitigate coastal-road pavement damage from SLR-induced groundwater rise at two case-study sites using a top-down approach
4. Investigate seasonal and long-term changes to pavement life with temperature rise caused by climate change using a hybrid bottom-up/top-down approach
5. Develop a general adaptation framework for designing a climate-ready road
6. Demonstrate the adaptation methodology for groundwater and temperature rise at a case-study site in coastal NH
7. Compare the top-down and hybrid adaptation plans

The traditional top-down, or scenario-based, approach is used in Chapters 3 and 4 to examine SLR-induced groundwater rise impacts and adaptation strategies for coastal-road infrastructure. A hybrid approach is introduced in Chapter 5 to assess seasonal and long-term pavement vulnerabilities from climate-change induced temperature rise. Lessons learned from the literature and previous chapters are brought together in Chapter 6 to develop a general adaptation framework for designing a climate-ready road. This framework is then demonstrated at a coastal evacuation route in southeastern NH. Adaptation strategies developed using the top-down and hybrid approaches will be compared.

CHAPTER 2 - MODELING GROUNDWATER RISE CAUSED BY SEA-LEVEL RISE IN COASTAL NEW HAMPSHIRE

2.1 INTRODUCTION

The northeastern United States is expected to experience SLR greater than the global average due to factors such as changing ocean circulation patterns in the northwest Atlantic Ocean and land subsidence from glacial isostatic adjustment [*Ezer and Atkinson,* 2014; *Kopp, Robert E. et al.,* 2014]. The National Oceanic and Atmospheric Administration (NOAA) assessed a large body of SLR studies and produced scenarios of global mean SLR from 1992 ranging from 0.2 to 2 m by the end of the century [*Parris et al.,* 2012]. The low scenario is based on an extrapolation of the historical record. The high scenario is based on a combination of estimated thermal water expansion from the Intergovernmental Panel on Climate Change (IPCC) AR4 global SLR projections (IPCC, 2007) and an estimate of the maximum amount of glacial and ice sheet loss by the end of the century. NOAA recommends that the highest scenario be used to plan for infrastructure where there is little tolerance for risk [*Parris et al.,* 2012].

While increased surface-water flooding due to storm surge and tides is commonly recognized as a significant consequence of SLR, modeling studies have shown that groundwater will also rise with SLR in coastal areas [*Bjerklie et al.,* 2012; *Cooper, H. et al.,* 2015; *Habel et al.,* 2017; *Hoover et al.,* 2017; *Masterson,* 2004; *Masterson and Garabedian,* 2007; *P. Oude Essink et al.,* 2010; *Rotzoll and Fletcher,* 2013; *Walter et al.,* 2016]. The historical SLR signal has also been detected in groundwater. Groundwater rose by 2.1 mm/year from 1950 to 2001 in a

monitoring well 300 m from the coast on Cape Cod, which is slightly less than the 2.6 mm/year SLR recorded at the Boston tide gauge (1921 to 2000) [*Masterson and Garabedian,* 2007].

In the northeastern United States, groundwater rise from SLR is anticipated to occur farther inland than tidal flooding on Cape Cod [*Masterson and Garabedian,* 2007; *Walter et al.,* 2016] and in New Haven, Connecticut [*Bjerklie et al.,* 2012]. In Honolulu, Hawaii, the combined area of inundation from tidal water and groundwater rise caused by SLR was twice that of tidal water alone [*Rotzoll and Fletcher,* 2013]. Flooding associated with SLR-induced groundwater rise is expected to cause problems at the Homestead Air Reserve Base in Miami-Dade County, Florida. [*Cooper, H. et al.,* 2015]. Rising groundwater is predicted to have serious consequences for ecology and water quality in the barrier islands off the Maryland and North Carolina coasts [*Manda et al.,* 2015; *Masterson et al.,* 2014].

Several SLR-induced groundwater rise studies have investigated coastal aquifers where the bedrock is more than 100 m deep [*Masterson and Garabedian,* 2007; *Walter et al.,* 2016] or porous [*Cooper, H. et al.,* 2015; *Habel et al.,* 2017; *Rotzoll and Fletcher,* 2013] and the transmissivity, or the rate of groundwater flow through the geologic materials, is high. New Hampshire's (NH) coastal region was chosen for this study for its complex hydrogeology, extensive rivers and stream network, fresh and saltwater wetlands, estuaries and marine environments. Its geology is representative of the glaciated northeast with variations in topography and relatively thin unconsolidated glacial deposits overlying fractured metamorphic and igneous bedrock [*Ayotte and Toppin,* 1995; *Lyons et al.,* 1998; *Mack,* 2009; *Medalie and Moore,* 1995; *Stekl and Flanagan,* 1992]. While heterogeneous glacial deposits were also simulated in New Haven, Connecticut, the coastal NH deposits are thinner than the 75 m thick glacial meltwater and glaciolacustrine deposits found in New Haven [Bjerklie *et al.,* 2012].

Groundwater rise characterization is important because it has the potential to impact both natural and built systems in coastal regions. Rising groundwater has been shown to reduce pavement life in coastal-road infrastructure [*Knott et al.,* 2017], reduce the effectiveness of onsite wastewater treatment systems [*Habel et al.* 2017; Manda *et al.*, 2015], and infiltrate wastewater collection systems (Flood and Cahoon, 2011). Freshwater wetlands and salt marshes occur where groundwater is near or above the ground surface and are highly vulnerable to changing groundwater levels [*Lorah and Olsen*, 1999; *Masterson et al.*, 2014; *Wilson et al.*, 2012]. Salt-marsh ecology is dependent on the interaction between fresh groundwater and tidal surface water [*Harvey and Odum*, 1990; *Hemond and Fifield*, 1982]. Rising groundwater from SLR can expand or drown wetland ecosystems, change salinity within salt marshes, and change the type and distribution of wetland vegetation [*Moffett et al.*, 2012].

2.1.1 Objectives

The objectives of this study are to (1) determine the magnitude and inland extent of groundwater rise from SLR, (2) define the groundwater-rise zone (GWRZ), the area where groundwater is predicted to rise with SLR, (3) investigate the variability of projected groundwater rise with distance from the coast, (4) explore relationships between groundwater rise and depositional environments, and (5) demonstrate how this methodology can be used to identify potential impacts to freshwater and saltwater wetlands.

2.1.2 Study Area

The focus of this study is the NH coastal region (Figure 2-1).

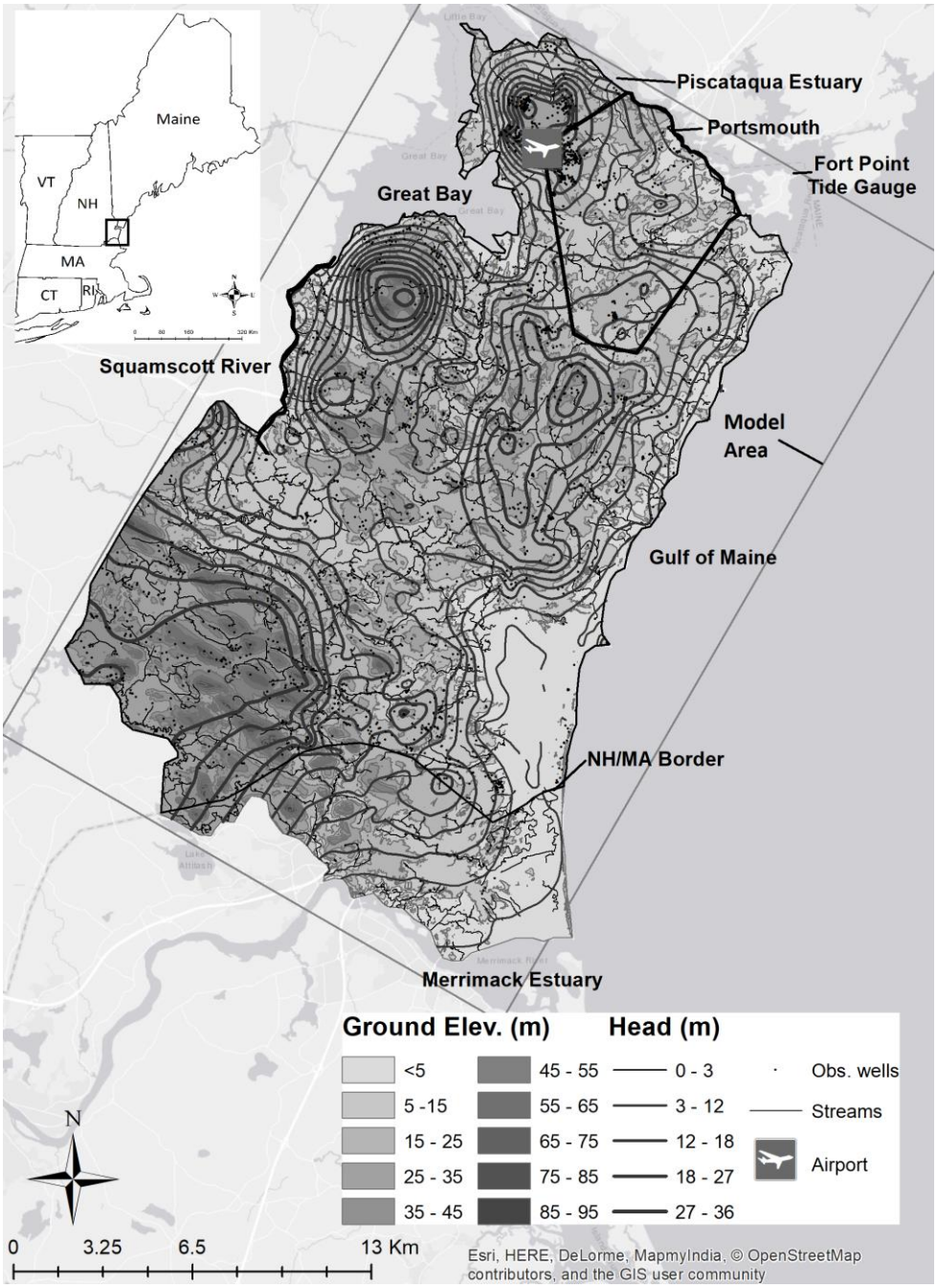

Figure 2- 1. Study area in New Hampshire's coastal region. The rectangular area is the groundwater model domain and the coastal boundaries are shown. Shading illustrates the land-surface elevation and observation wells are indicated. Groundwater piezometric head contour lines are illustrated with thick to thin lines indication high to low head. The inset shows the location within the New England region of the United States.

A regional groundwater-flow model (Mack, 2009) is used to simulate SLR-induced groundwater rise in coastal NH. The model boundaries simulate natural hydrologic boundaries and, consequently, a small section of Massachusetts (MA) is simulated to include the Merrimack Estuary as the southernmost boundary. The geography, hydrogeology, depositional environments of coastal NH are described below.

2.1.2.1 Geography

The modeled area encompasses approximately 488 km^2 of a coastal region with 410 km^2 in NH and 78 km^2 in MA. The NH coastal region consists of all or a part of 13 NH towns. The region includes coastal and freshwater wetlands, rivers and streams, estuaries, and beaches [*Mack,* 2009]. It is bounded by the Piscataqua Estuary and the Maine border to the north, Great Bay and the Squamscott River to the west, the Merrimack Estuary in MA to the south, and the Gulf of Maine to the east (Figure 2-1). There are approximately 64 km of shoreline including the Gulf of Maine, Piscataqua Estuary, and Great Bay within the study area. Land surface altitude is greater than 90 m above the North American Vertical Datum of 1988 (NAVD88) in the southwestern part of the coastal region, less than 15 m over areas in the south-central and northeastern parts of the region, and at sea level along the coast [*NH Coastal Lidar,* 2011].

2.1.2.2 Hydrogeology

NH's coastal region is characterized by thin glacial and marine sediments with topography that generally follows the bedrock surface [*Mack,* 2009]. Fine-grained till and marine silts and clays and coarse-grained stratified drift make up the surficial geology overlying crystalline metamorphic rock of sedimentary origin and igneous bedrock [*Lyons et al.,* 1998; *NH State Geologist,* 2004]. The surficial deposits, mapped by the United States Geological Survey (USGS) [*Moore,* 1990; *Stekl and Flanagan,* 1992] are typically less than 12 m thick in the region with

deposits of up to 21 m thick beneath Pease International Airport in the northern portion of the study area [*Mack,* 2009]. The coarse stratified-drift sediments, consisting of sands and gravels, are the most permeable with hydraulic conductivities ranging from 15 to more than 61 m/d with lower values ranging from 0.6 to 4.6 m/d in the fine-grained sands [*Ayotte and Toppin,* 1995; *Mack,* 2009; *Medalie and Moore,* 1995]. These sediments form unconfined aquifers bounded above by the water table and below by bedrock. Groundwater flows from areas of high groundwater altitude toward the natural discharge areas in streams, Great Bay and the Piscataqua estuary to the north, the Gulf of Maine to the east, and the Merrimack River to the south (Figure 2-1). Streams and wetlands are typically hydraulically connected to the groundwater and affect local groundwater-flow patterns [*Mack,* 2009].

2.1.2.3 Depositional Environment

Seven depositional environments are identified in the surficial geology (NH State Geologist, 2004, MassGIS, 2004). (1) Beach deposits consist of well-sorted sand and are located on the eastern shoreline bordering the Gulf of Maine. (2) Estuarine deposits are primarily salt marshes bordering the Gulf of Maine, Piscataqua estuary and Great Bay. (3) Anthropogenic deposits are coarse-grained fill materials used in landfills and the base layers of roads. (4) Glaciomarine deposits consist of deltaic, wave-formed and wave-modified marine delta deposits. Fine-grained clayey-silt and sand deposits are found adjacent to protected waterbodies such as Great Bay and wetland areas, while the coarse-grained materials are found further inland. Undifferentiated facies are found in the northern part of the study area. (5) Glacial till is poorly-sorted material consisting of fine-grained silts and clays and coarse sands and gravels with low hydraulic conductivities [*Ayotte and Toppin,* 1995; *Moore,* 1990]. (6) Palustrine are the freshwater

wetland deposits; and (7) alluvial deposits consist of alluvium and stream terrace deposits (NH State Geologist, 2004).

2.1.2.4 New Hampshire Wetlands

In the NH coastal region, 25% of the land area is wetland with 15% freshwater and 10% saltwater wetlands. Saltwater wetlands are classified at estuarine and marine wetlands and freshwater wetlands are classified as freshwater emergent wetland, freshwater forested/shrub wetland, and freshwater pond [*U.S. Fish and Wildlife Service,* 2001]. Forested/shrub wetlands, emergent wetlands, ponds, lakes, and riverine wetlands are the primary freshwater wetland types in the region with freshwater forested/shrub wetlands dominating at 72% of all freshwater wetlands [*U.S. Fish and Wildlife Service,* 2001]. Wetlands in Portsmouth are representative of the larger NH coastal region. Wetlands make up 30% (12.5 km^2) of the land area in Portsmouth with 21% (8.8 km^2) freshwater wetlands and 9% (3.7 km^2) estuarine and marine wetlands. Forested/shrub dominate the freshwater wetlands at 73% (6.4 km^2) and the remainder consists of emergent wetlands and freshwater ponds at 24% (2.1 km^2) and 3% (0.2 km^2), respectively. [*U.S. Fish and Wildlife Service,* 2001]

2.2 METHODS

A numerical groundwater-flow model was used to investigate the effect of rising sea level on groundwater levels in the study area. The output from the groundwater model was analyzed to determine the areal extent and variation of groundwater rise within the GWRZ. The assumptions and limitations of this analysis are also presented.

2.2.1 Groundwater Model

Groundwater modeling is used to simulate SLR effects on groundwater levels, changing groundwater-flow patterns, and saltwater intrusion [*Masterson,* 2004; *Masterson and Garabedian,* 2007; *P. Oude Essink et al.,* 2010; *Pitz,* 2016; *Walter et al.,* 2016]. In this study, an existing USGS regional groundwater flow model of the NH coastal region was updated and modified to investigate SLR-induced changes in groundwater levels. A portion of northeast Massachusetts is also included in the model area to allow for the use of a natural hydrologic boundary, the Merrimack River, as a model boundary. A complete description of the model is presented in [*Mack,* 2009] and only a brief description of the updates to the model is presented here.

MODFLOW2005 [*Harbaugh,* 2005], a 3-dimensional finite-difference model, was used to solve the groundwater-flow equation for various sea levels. The model grid consists of 535 rows, 350 columns, and 5 layers with a uniform horizontal discretization of 61 m [*Mack,* 2009]. The top of the model is defined by land-surface topography derived from LIDAR digital elevation models (DEMs) [*NH Coastal Lidar,* 2011] and the top two layers simulate unconsolidated geologic deposits consisting of stratified drift, till, beach and wetland sediments. Differentiation between these sediments in the model was achieved by creating zones of aquifer properties [*Mack,* 2009]. This study focuses on layer 1 as the groundwater table primarily resides in this layer throughout the model. Layer 1 simulates surficial deposits ranging in thickness from 3 to 21 m consisting of fine-grained marine silts and clays, coarse-grained stratified drift, and wetland deposits. Layer 2 is a thin layer simulating till above the bedrock and layers 3 through 5 represent bedrock. The three bedrock layers are used to simulate bedrock well withdrawals from multiple depths. The grid is oriented with the northeast-southwest structural pattern of the bedrock and aligns with the coastline [*Mack,* 2009].

2.2.1.1 Model Input

Climate-sensitive parameters include aquifer recharge, streamflow and sea level [*Kopp, Robert E. et al.,* 2014]. Aquifer recharge is the infiltration of precipitation and/or surface water and its percolation through the unsaturated zone to the saturated zone of the soil profile [*Heath,* 1983]. Areal recharge rates used in the groundwater model were determined by the NH Geological Survey (NHGS) using the Dripps water balance model [*Dripps and Bradbury,* 2007]. This is a soil-water model that accounts for interception, evapotranspiration (ET), partitioning of run-off, soil infiltration or snow-pack storage, and soil-moisture partitioning. The input parameters, compiled by NHGS, include the following GIS-gridded data: flow direction, land cover/land use, Natural Resource Conservation Service (NRCS) soil groups, NRCS available soil-water capacity, snow cover, and initial soil moisture. The recharge model is run with daily time steps and allows runoff to move from one cell to another. The output is a GIS map of gridded (28 m x 28 m) annual recharge rates (Dripps and Bradbury, 2007). The areal recharge values used in the model range from 0 to 0.96 m/year with an average of 0.21 m/year and a standard deviation of 0.14 m/year.

Rivers, streams, and wetlands connected to streams are represented as head-dependent flux boundaries using the stream package in MODFLOW2005 [*Harbaugh,* 2005]. There are over 14,000 stream reaches in the model ranging in length from 3 to 150 m [*NH Hydrography,* 2006]. The width of each stream reach was estimated using high resolution aerial photographs in GIS [*Aerial Photos,* 2011; *Coastal NH,* 2013; *NH Hydrography,* 2006]. Stream stage at the beginning and end of each stream reach was determined from bare earth LIDAR DEMs [*NH Coastal Lidar,* 2011]. The streambed hydraulic conductivity was initially estimated using typical values for the area [*Mack,* 2009] and refined using Groundwater Vistas parameter estimation techniques

[*Rumbaugh and Rumbaugh*, 2011]. The focus of this study is the effect of SLR on groundwater levels and climate change induced changes in recharge and streamflow were not simulated in this analysis.

Model cells inundated at mean sea level (MSL) were designated as constant-head boundary cells [*Harbaugh et al.,* 2000; *Rumbaugh and Rumbaugh,* 2011] for each steady-state model run. For the current condition, these cells were assigned a constant head of 0.09 m below NAVD88, the altitude of MSL recorded at the Fort Point tidal station (Station ID: 8423898) located in New Castle, NH in the northeastern corner of the study area [*NOAA,* 2016]. Freshwater equivalent heads were used to simulate the freshwater/saltwater density effects [*Rumbaugh and Rumbaugh,* 2011].

Climate-insensitive parameters include ground-surface topography from LIDAR, hydraulic conductivity and aquifer layer thickness. LIDAR DEMs collected over approximately 2336 km^2 covering all coastal NH in 2011 were used to map the ground-surface topography. The DEM resolution is 2 m and the vertical accuracy is 30 cm at the 95-percent confidence level per the National Standard for Spatial Data Accuracy (NSSDA) based on a root mean square error (RMSE) of 15 cm [*NH Coastal Lidar*, 2011]. Hydraulic conductivity and aquifer thickness were regional values based on the surficial and bedrock geology [*Mack*, 2009]. Hydraulic conductivity was refined using MODFLOW parameter estimation techniques during the calibration phase. A summary of the model input parameters is presented in Table 2-1.

Table 2- 1. Summary and comparison of groundwater model input parameters between Mack (2009) and this study. The hydraulic conductivity (K) shown is horizontal K. In both studies, vertical K is typically one-tenth of the overburden horizontal K and equal to the bedrock horizontal K.

Description	Units	Mack (2009)	Knott et al.
Overburden Hydraulic Conductivity			
Fine-grained sediments	m/d	0.03	0.02
Sand and coarse-grained sediments	m/d	3.05	0.12 - 7.86
Wetlands	m/d	3.05	7.86
Till	m/d	0.30	0.3 - 0.5
Bedrock Hydraulic Conductivity			
Rx1 - Rye Complex, Breakfast Hill Granite	m/d	0.15	0.15
Rx2 - Kittery Formation	m/d	0.30	0.24
Rx3 - Eliot and Berwick Formations	m/d	0.03	0.03
Rx4 - Exeter Diorite	m/d	0.06	0.06
Stream Parameters			
Streambed Hydraulic Conductivity	m/d	0.76	0.02 - 1.52
Streambed Thickness	m	0.30	0.30
Stream Width	m	1.52	1.52 - 305
Areal Recharge	m/yr	0.3	0 – 0.96
Sea Level (relative to NAV88)			
Mean Sea Level (MSL)	m	-0.09	-0.09
0.3 m SLR	m	-	0.21
0.8 m SLR	m	-	0.71
1.6 m SLR	m	-	1.51
2.0 m SLR	m	-	1.91

Note: Bedrock formations are from Mack (2009)

Permitted drinking water withdrawals from the NH Department of Environmental Service (NHDES) were included in the model and were kept constant through all the simulations. A total of 219 active production wells were simulated: 36 withdrawing water from the unconsolidated deposits and 183 withdrawing water from the fractured bedrock. Production well withdrawal volumes were based on reported well yields, permitted volumes, or wellhead protection maximum rates depending on the availability of data. These withdrawal volumes were reduced to represent

actual withdrawal volumes based on communication with NHDES. Water withdrawals used in the model ranged from 0.2 m^3/day from the bedrock to approximately 309 m^3/day from the unconsolidated deposits in the eastern portion of the study area with an average of 47 m^3/day and a standard deviation of 78 m^3/day. Domestic withdrawals were simulated in layers 3 and 4 using the flow and head boundary (FHB) condition in MODFLOW and withdrawal returns in non-sewered areas were distributed back into model layer 2 (Mack, 2009).

2.2.1.2 Groundwater Measurements and Contour Mapping

Groundwater piezometric heads were compiled from the NHDES, NH Geological Survey (NHGS), United States Air Force, USGS, and NH Department of Transportation (NHDOT). Data from 2919 wells, 1645 installed in unconsolidated deposits above the bedrock (overburden) and 1274 in the bedrock, were used in this study. Piezometric heads, measured monthly or quarterly from 2011 to 2015, in 901 wells (827 in the overburden and 74 in the bedrock) were available from the Pease International Airport (Figure 2-1). These wells were surveyed to the National Geodetic Vertical Datum of 1929 (NGVD29) and groundwater heads were measured with an accuracy of 0.03 m [*Forbes,* 2015; *Holmes et al.,* 2001]. Groundwater heads measured over the remainder of the study area from 1970 through the present were acquired from 652 wells in the GEOLOGs (NHGS) database (622 in the overburden and 30 in the bedrock) and 1366 wells (196 in the overburden and 1170 in the bedrock) from the water-well inventory (NHDES).

GEOLOGs are a compilation of boring and well information from NHDES, NHDOT, and USGS. Groundwater heads in many wells were measured only one time, while others were monitored over time through 2009 [*Barker,* 2016]. Approximately 37% of the GEOLOG wells had been surveyed to NGVD29 or NAVD88 and the accuracy of the measured heads is 0.03 m. The remainder of the wells were either surveyed to a local datum or were not surveyed for elevation.

The water-well inventory contains boring and well information compiled by the NHDES from wells installed between 1984 and 2015 for domestic and industrial water supply, exploration, and testing. Depths to groundwater were recorded by drillers during installation, but the wells were not surveyed. The location of these wells is typically sketched on property maps. The piezometric heads in the saline coastal water bodies were assumed to be MSL as recorded at the NOAA tidal gauge at Fort Point, Newcastle, NH [*NOAA*, 2016] and were adjusted for density using freshwater equivalent heads [*Rumbaugh and Rumbaugh*, 2011].

A new regional database of groundwater information referenced to the common datum, NAVD88, was created from the compiled groundwater information. This database includes the station number, well location in NH State Plane coordinates, well depth, ground-surface elevation, screened interval, groundwater piezometric heads, and measurement date. Heads referenced to NGVD29 in the source data were converted to NAVD88 using VERTCON [*National Geodetic Survey*, 2016]. Piezometric heads from the wells that were not surveyed to NGVD29 or NAVD88 were estimated from LIDAR ground-surface elevation and the measured water depth in the well. The vertical accuracies of the heads estimated from GEOLOGs and the water-well inventory are 0.6 m and 1.0 m, respectively. A groundwater piezometric head contour map was constructed from groundwater observations in the overburden to examine the existing groundwater flow regime. These contours are shown on Figure 2-1.

2.2.1.3 Calibration

The model was calibrated to average groundwater levels from 1970 to 2014 in 3156 wells (target observations). Groundwater levels representative of the low recharge condition were used from wells with seasonal observations. The automated calibration procedure from Groundwater Vistas [*Rumbaugh and Rumbaugh*, 2011] was used. This procedure determines the model

parameters that produce the best fit to these target observations using inverse calibration methods. It employs Marquardt's modification to the Gauss-Newton nonlinear least-squares parameter estimation technique [*Levenberg*, 1944; *Marquardt*, 1963]. Plots of the observed groundwater heads and the residual (the difference between computed and observed values) versus the computed heads are presented in Figure 2-2.

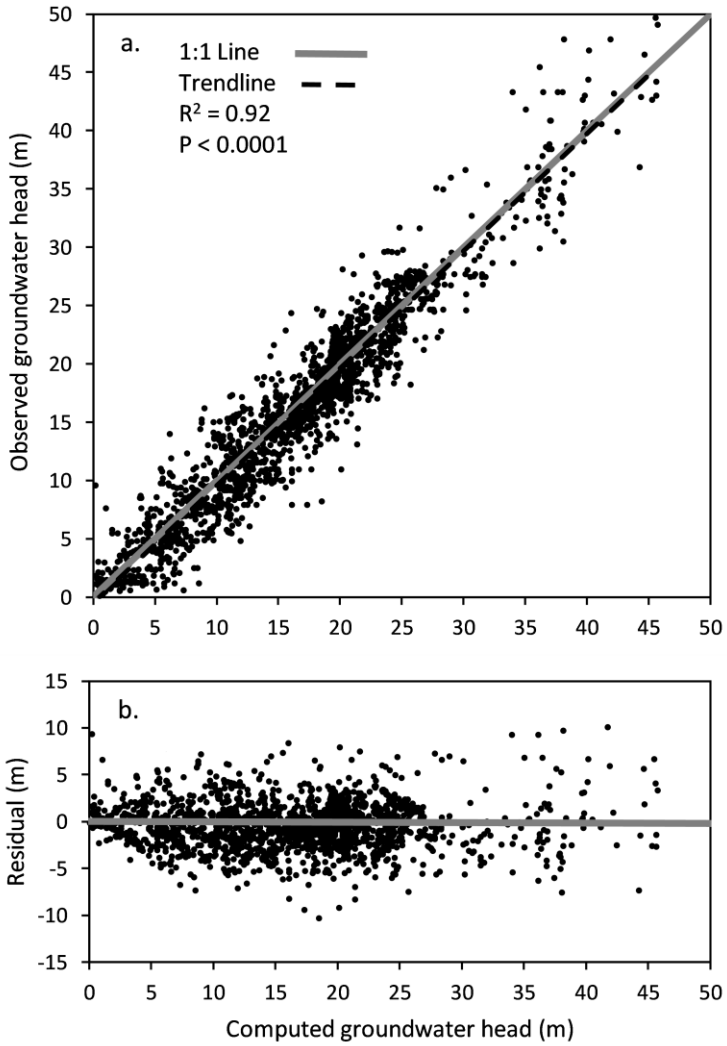

Figure 2- 2. Model calibration results: (a) observed groundwater piezometric heads in unconsolidated deposits versus computed groundwater heads, and (b) groundwater-head residuals (computed minus observed heads) versus computed groundwater heads.

For layer 1 of the model, the range of observed piezometric heads over the entire modeled region is 53.6 m. The root mean square error (RMSE) of the fit is 2.4 m, or 4.5% of the observed range (scaled RMSE). Typically, the scaled RMSE should be less than 10% for a good calibration [*Rumbaugh and Rumbaugh,* 2011]. The residual mean is -0.4 m and the absolute residual mean, a measure of the average error in the model, is 1.8 m. Differences between the computed and observed groundwater heads are due to groundwater measurement errors and uncertainties in the hydrogeologic properties of the heterogeneous geologic materials and fractured bedrock. In the northern part of the study area near the Pease International Airport where the groundwater measurements are the most accurate, the range of observed piezometric heads is 24.9 m. The RMSE is 1.7 m, or 6.7% of the observed range, the residual mean is -0.1 m, and the absolute residual mean is 1.3 m.

Streamflow, measured in 14 streams during a period of streamflow recession [*Mack,* 2009], were compared with the calculated base flow to streams. Groundwater flux from the aquifer to the stream at each reach upstream of the gaging station is summed to determine the simulated base flow at each gaging station. The comparison between observed and simulated base flows is presented in Figure 2-3.

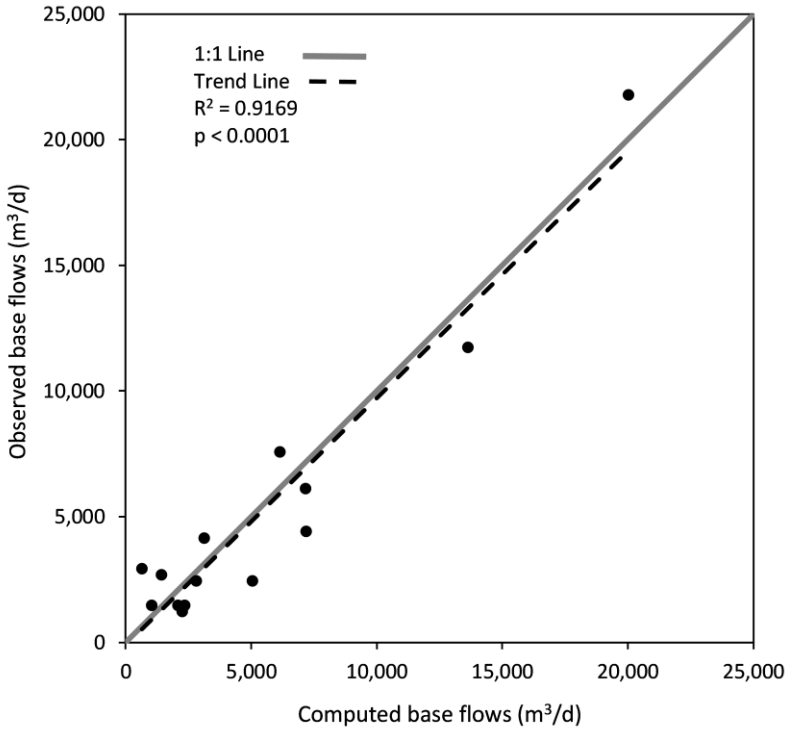

Figure 2- 3. Measured stream base flow versus computed groundwater discharge to streams in the model area. The base flow for the Winnicut River is the September mean flow from 2001 through 2016. All other base flows were measured in October 2004.

Observed base flows range from 0.014 to 0.252 m^3/s and the RMSE of the simulated flows is 0.018 m^3/s.

While the accuracy of the model is not sufficient to predict the groundwater head at any individual well or location, the simulations are useful in identifying future changes in regional groundwater-flow patterns and relative groundwater response to SLR. A comparison of the baseline simulated head contours and the average-observed head contours demonstrates that the groundwater model provides an accurate representation of the regional groundwater-flow patterns and discharge areas. The regional model is useful for identifying the GWRZ, as well as trends and uncertainties in SLR-induced groundwater rise. Coupled with LIDAR DEMs, areas

with shallow groundwater that are at risk from groundwater rise can be identified for detailed vulnerability studies and adaptation planning.

2.2.1.4 SLR Scenarios

The NH Hazards and Risks Commission's NOAA-derived SLR scenarios for coastal adaptation planning [*Kirshen, Wake et al.,* 2014; *Parris et al.,* 2012] were used in this research. SLR of 0.3, 0.8, 1.6 and 2 m corresponding to the high emission scenario in early-century (2030), mid-century (2060) and the end of the century (2090 and 2100), respectively, were simulated using the groundwater model. Each projected rise in sea level was added to the current MSL and then used as the coastal boundary condition for the steady-state simulations (Table 2-1). The model was run to calculate groundwater heads for the current condition and the four SLR scenarios. This is a conservative analysis of SLR-induced groundwater rise as it considers only the change in hydraulic head at the coast. It does not include the inland migration of the shoreline.

2.2.2 Analysis Methods

The model output utilized in this analysis is piezometric head corresponding to the phreatic surface (or water table) in the surficial layer and groundwater flow to discharge areas. Groundwater rise was calculated by subtracting the computed groundwater heads at MSL from the computed heads for each SLR scenario. Distributions of simulated groundwater rise within 1 km distance intervals from the coast were generated. The 1 km distance interval is a commonly used distance metric and encompasses a large enough sample of modeling results (61 x 61 m grid cell size) for statistical analysis. In addition, groundwater discharge to streams and coastal discharge areas was calculated and compared between the MSL condition and the SLR scenarios.

The transmissivity of the unconsolidated deposits, or the groundwater rate of flow per unit width, depends on the hydraulic conductivity of the materials and thickness of the deposits [*Bear*, 1979]. The depositional environment, identified in the commonly available surficial geology data layer [*NH State Geologist*, 2004], is one way to categorize these properties. Distributions of simulated groundwater rise within each depositional environment were calculated.

Wetland-area expansion and water depth increases were investigated and compared with projected seawater (marine surface water) inundation in the City of Portsmouth (Figure 2-1). This was a simple mapping analysis and was not intended to be a detailed investigation of these complex ecosystems. Wetland-area expansion was investigated by mapping the difference between the simulated wetland area at MSL and the predicted groundwater inundation (GWI) area (land inundated by groundwater rise) with SLR. The simulated wetland areas at MSL were determined by subtracting the computed groundwater heads at MSL from the LIDAR DEMs resulting in a depth to groundwater. Areas with groundwater at or above the ground surface were identified as wetland areas. Model findings were analyzed relative to the National Wetlands Inventory [*U.S. Fish and Wildlife Service*, 2001]. SLR-induced groundwater rise was mapped within existing wetland areas identified in the National Wetlands Inventory [*U.S. Fish and Wildlife Service*, 2001] to estimate the water-depth change that may occur in these ecosystems. Distributions of groundwater rise were compared among the following wetland types: estuarine and marine wetland, freshwater emergent wetland, freshwater forested/shrub wetland, and freshwater pond.

2.2.3 Assumptions and Limitations

The model is a regional groundwater-flow model in an area where the surficial geology is heterogeneous and typically thin (less than 30 m). Fractured bedrock is modeled as part of the flow regime. Ground-surface topography, areal recharge, water withdrawals, hydrogeologic properties, surface water, and SLR were used as inputs and the model was run in steady state. These inputs have uncertainties including errors associated with measuring the parameter, parameter variability in space and time, complex interactions between surface water and groundwater, insufficient data density, and an uncertain climate future. Consequently, the model should not be used to predict groundwater piezometric head at individual wells or locations but can be used to investigate regional groundwater flow patterns and relative trends with projected SLR.

The density effects of saltwater were included in this analysis using equivalent freshwater heads, but salt transport was not explicitly modeled. The location of the freshwater/saltwater interface in the bedrock is not well known, but is believed to be close to the coastline based on salinity measurements in a small number of domestic water-supply wells [*Mack,* 2009]. Regional inland migration of the freshwater/saltwater interface in the bedrock is not expected to be extensive with SLR due to low bedrock hydraulic conductivity and bedrock structure orientation parallel to the coast [*Mack,* 2004]. Equivalent fresh-water heads provide a good approximation of the density effects on piezometric heads in the shallow aquifer near the coast [*Mack,* 2004; *Rumbaugh and Rumbaugh,* 2011].

Steady-state simulations were used to assess the long-term effect of SLR on average groundwater levels. Seasonal or annual variation in recharge rates caused by climate change were not considered. In the northeast, the groundwater is typically highest in the early spring when the aquifer recharge from rainfall and snowmelt is maximum and evapotranspiration is

small [*Mack,* 2009]. Precipitation and temperature are expected to increase in the northeast with climate change [*Hayhoe et al.,* 2015] affecting groundwater levels through changes in aquifer recharge [*Bjerklie et al.,* 2012; *Mack,* 2009]. Groundwater withdrawals were also assumed to be constant throughout the study period. Mack (2009) investigated the effect of increased drinking water demands and found minor lowering of groundwater levels, most apparent near the water supply wells. This study's objective is to investigate the effect of SLR on groundwater levels and all other input parameters were held constant in the simulations. Long-term changes in recharge and groundwater withdrawals will affect long-term groundwater levels in the region.

The model calibration uses data from multiple years, but primarily represents periods of low recharge. Additional data collection and model calibration will be needed to generate higher resolution and transient groundwater rise projections required for adaptation planning in individual towns or municipalities within the study area.

2.3 RESULTS

This research demonstrates that groundwater will rise with SLR in coastal geologic environments typical of the glaciated northeast. The distribution of groundwater rise with distance from the coast and within different depositional environments is presented. GWI areas are compared with tidal-water inundation areas in Portsmouth, NH and consequential changes in freshwater and saltwater wetland hydrology is discussed. The results presented here represent groundwater rise caused by SLR only. Future groundwater levels will also be affected by changes in annual and seasonal recharge rates, influenced by precipitation and evapotranspiration changes, and future groundwater withdrawals in the region.

2.3.1 SLR Effects on Groundwater

In the NH coastal region groundwater rise caused by 2 m of SLR is projected to extend farther inland than projected mean higher high water (MHHW) inundation (Figure 2-4).

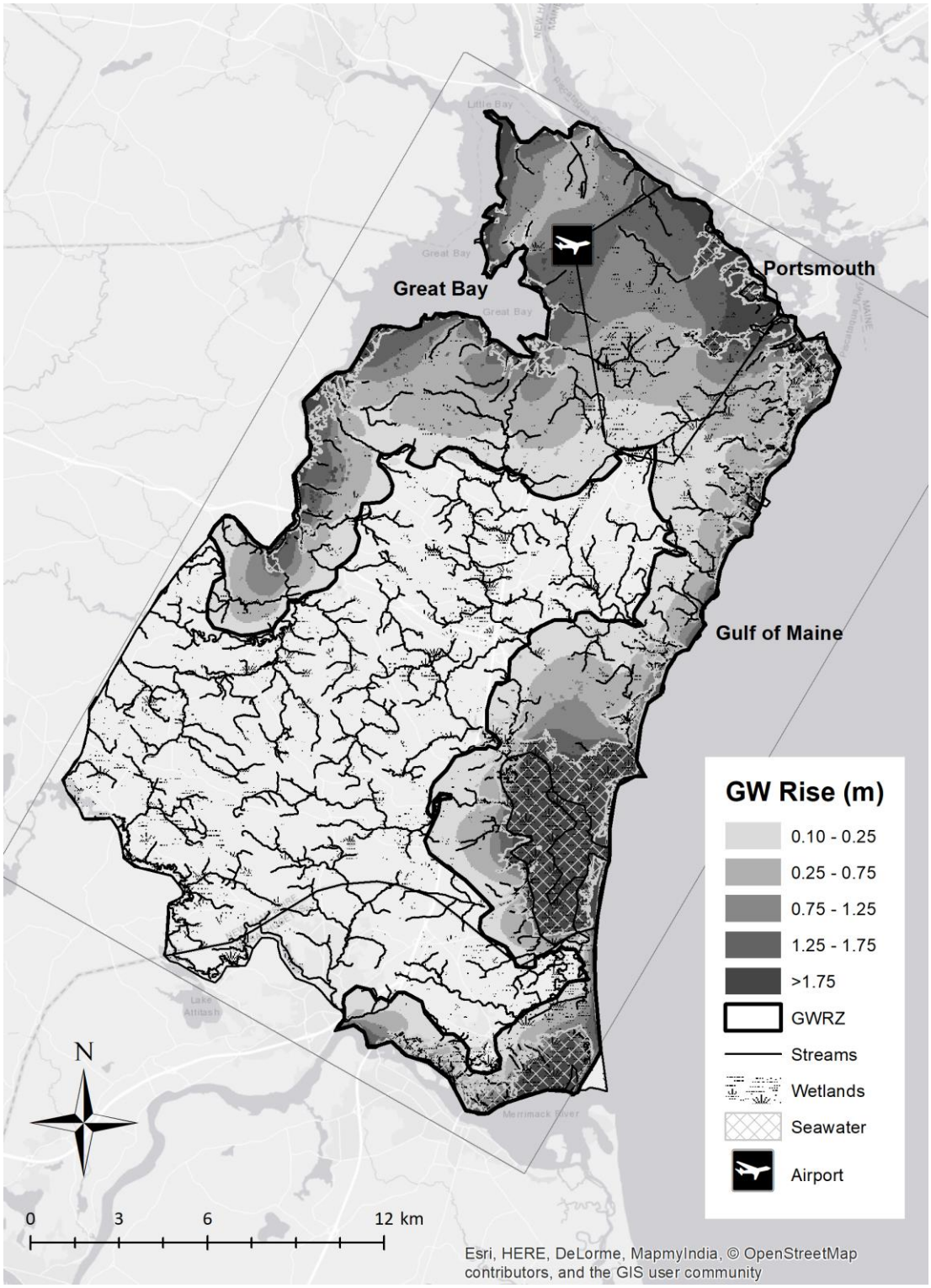

Figure 2- 4. Groundwater-rise zone (GWRZ) and mean higher high water (MHHW) seawater inundation simulated with 2 m of SLR. The shading indicates the magnitude of projected groundwater rise.

The farthest extent of projected MHHW inundation is approximately 1 to 1.5 km while groundwater rise up to 0.2 m is predicted to occur more than 4 km inland in some locations. The magnitude of groundwater rise and inland extent varies along the coastline. The analysis predicts 0.75 to 1.25 m groundwater rise 2 to 3 km from the shoreline with 2 m of SLR primarily in the northern part of the study area where groundwater rise is controlled by tidal-surface waterbodies on three sides (Figure 2-4). Projected MHHW with 2 m of SLR is predicted to extend inland from the coast less than 0.8 km in this region.

SLR-induced rising groundwater is projected inundate the land surface in some areas. Where the vadose-zone thickness is currently less than the projected groundwater rise, GWI may occur. Tidal surface water and groundwater are projected to inundate approximately 3.7 km^2 or 9% of Portsmouth land area with 2 m of SLR. GWI contributes 48% of the total inundation (1.8 km^2) and is projected to flood areas up to 3.5 km inland from the coast in Portsmouth.

Groundwater rise is dampened near streams (Figure 2-4) as increased gradients between the two systems drive more groundwater discharge to streams. The net groundwater discharge to surface water in the study area is approximately 3.1 m^3/s with 73% of the net groundwater discharge going to streams and 27% to coastal discharge areas (lands flooded with tidal waters at MSL). For all scenarios, SLR was found to increase gradients between groundwater piezometric head and stream stage increasing groundwater discharge to streams. However, increased tidal water piezometric head at the coast reduces groundwater discharge to coastal wetlands. In addition, inflow from marine surface water to coastal groundwater is projected to increase. For example, with 2 m of SLR, the net groundwater discharge to streams increases from 73% to 83% of the total discharge with a corresponding decrease in groundwater discharge to coastal discharge areas. This represents a 0.3 m^3/s increase in net groundwater discharge to streams compared to

the MSL condition. Inflow from marine surface water to coastal groundwater is projected to increase approximately 0.1 m^3/s or 52% relative to the MSL inflow.

2.3.1.1 Groundwater Rise with Distance from the Coast

Groundwater rise, simulated for the four SLR scenarios, was evaluated at 1 km distance intervals from the shoreline and the results are presented in Figure 2-5. The ratio of mean groundwater rise to SLR is consistent across the SLR scenarios analyzed and is projected to be approximately 66% between 0 and 1 km, 34% between 1 and 2 km, 18% between 2 and 3 km, 7% between 3 and 4 km, and 3% between 4 and 5 km of the coast (Figure 2-5). By the end of the century, the mean groundwater rise ranges from more than 1.3 m between 0 and 1 km to less than 0.1 m between 4 and 5 km from the coast (Figure 2-5d).

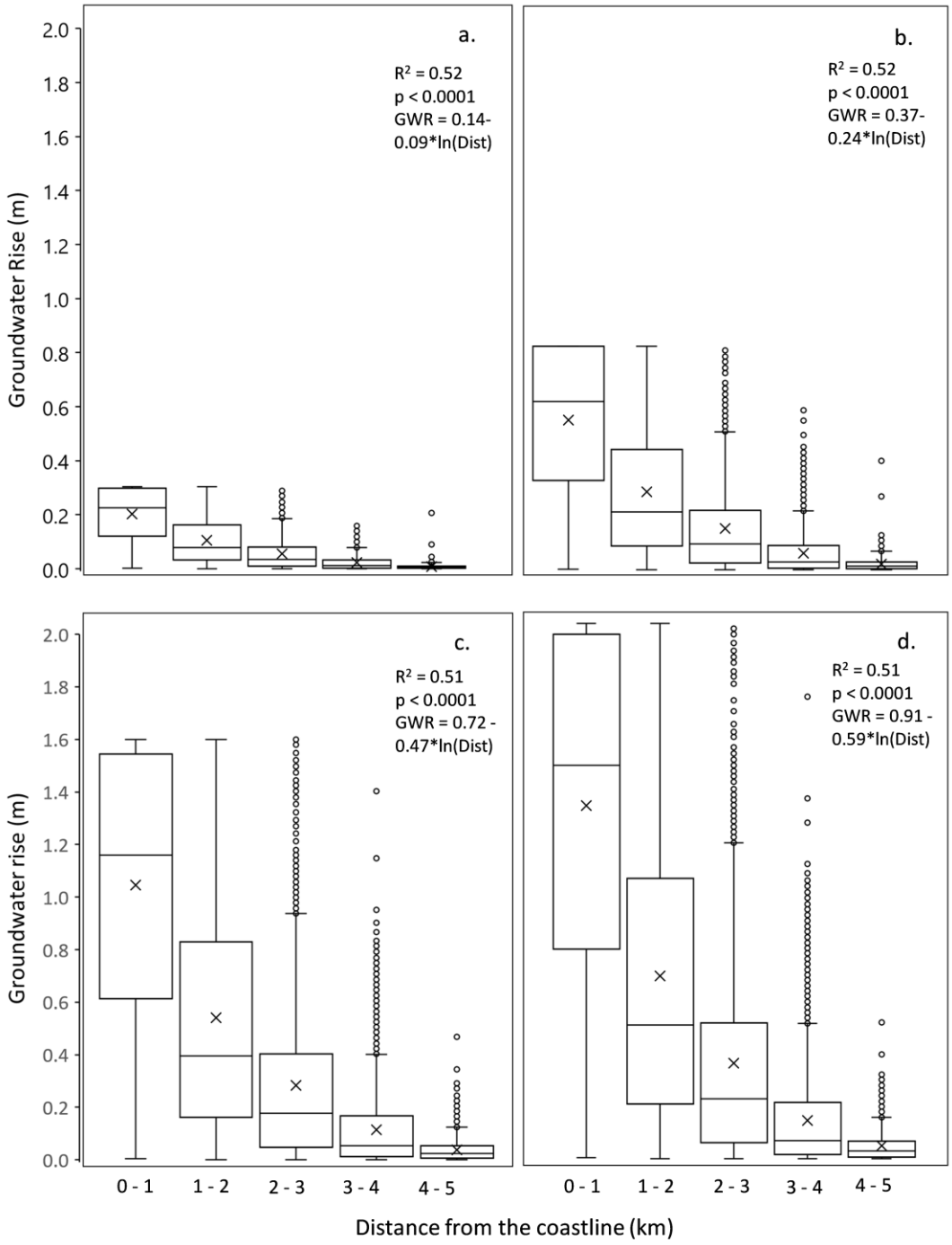

Figure 2- 5. Simulated groundwater rise versus distance from the coast for the four SLR scenarios: (a) 0.3 m, (b) 0.8 m, (c) 1.6 m, and (d) 2 m. Each box shows the mean (x), median, interquartile range, and outliers for each 1.0-km distance interval from the coast. The R^2 and p-values are from a linear fit of groundwater rise and the natural logarithm of the distance.

Distance from the coast explains approximately 50% of the variability in groundwater rise (R^2 = 0.51 to 0.52). While groundwater rise decreases with distance from the coast ($p < 0.001$), the remaining variability due to other factors is as important. Maximum groundwater rise at the coast equals the SLR magnitude and exceeds 1.8 m as far as 2 to 3 km inland with 2 m of SLR in some locations. In contrast, 25% of the area within 0 to 1 km of the coast is projected to experience groundwater rise less than 0.8 m.

The probability of finding various levels of groundwater rise within each distance interval was determined. With 2 m SLR, approximately 85% of land area within 1 km of the coast is projected to experience more than 0.5 m of groundwater rise and 50% is projected to experience more than 1.5 m rise. Within 2 km of the shoreline, there is a 50% chance of groundwater rise greater than 0.1 m by year 2030, 0.4 m by mid-century, and 0.9 m by the end of the century. With 2 m SLR, 25% of the land area between 2 and 3 km from the coast is predicted to experience more than 0.5 m groundwater rise. Projected groundwater rise greater than 0.5 m drops to 5% between 3 and 4 km of the coast and zero beyond 4 km. Based on this information and the results presented in Figure 2-5, the landward boundary of the SLR-induced GWRZ occurs between 4 and 5 km from the coast.

2.3.1.2 Groundwater Rise and Surficial Geology

The depositional environment controls on groundwater rise within 4 km of the coast for the 0.8 and 2 m SLR scenarios are quantified in Table 2-2. The mean groundwater rise is significantly different among all the depositional environments except between the palustrine and alluvial deposits according to the Tukey-Kramer HSD test ($p < 0.0001$). The relationship is also characterized by large variability around the mean as indicated by the standard deviation (std. dev.) and coefficient of variance (CV) (Table 2-2).

Table 2- 2. Summary of groundwater-rise statistics in the study area depositional environments at mid-century and end-of-century. The relative groundwater rise is the same for 0.8 m and 2 m sea-level rise.

	Mid-Century (0.8 m SLR)			End of Century (2 m SLR)			Relative GW Rise
Depositional Environment (% of area within 4 km of the coast)	Mean GW Rise (m)	Std. Dev. (m)	CV (%)	Mean GW Rise (m)	Std. Dev. (m)	CV (%)	Mean GW Rise (% of SLR)
Marine (2%)	0.67	0.19	28	1.62	0.46	28	81%
Estuarine (13%)	0.45	0.33	74	1.08	0.81	75	54%
Anthropogenic (1%)	0.37	0.24	65	0.90	0.59	65	45%
Glaciomarine (53%)	0.28	0.23	82	0.69	0.57	83	35%
Glacial till (27%)	0.26	0.25	97	0.63	0.62	99	32%
Palustrine (4%)	0.10	0.08	73	0.25	0.19	77	13%
Alluvial (<1%)	0.05	0.04	98	0.11	0.11	98	6%

As with distance from the coast, the mean groundwater rise to SLR ratio for each depositional environment is consistent regardless of the absolute magnitude of SLR, but large variations exist within the depositional environments.

The largest magnitude of groundwater rise occurs in the beach and estuarine depositional environments with mean groundwater rise relative to SLR of 81% and 54%, respectively. These deposits make up approximately 15% of the area within 4 km of the shoreline, are close to the coast, and experience direct marine surface-water influence on groundwater in beaches and dunes and coastal wetlands (estuarine). The interquartile range of relative groundwater rise in the beach sediments falls between 66 and 100% of SLR, while the estuarine depositional environment exhibits a large interquartile range of 12 to 100%.

Anthropogenic deposits make up slightly over 1% of the area and include fill used in coastal roadway construction and disposal sites. These deposits are predicted to experience a

mean relative groundwater rise of just under 50% with an interquartile range of 24 to 62% of SLR. Glaciomarine and glacial till deposits dominate the surficial geology of the region, making up approximately 53% and 27% of the area within 4 km of the coast, respectively. The mean glaciomarine and glacial till groundwater response are essentially the same, 35% versus 32% of SLR with standard deviations of 28 and 31% of SLR, respectively. The groundwater-rise differentiation between the major depositional environments (estuarine, glacial till, glaciomarine, and anthropogenic) increases from 0.2 m by mid-century to 0.4 m by the end of the century (Table 2-2). Palustrine deposits (freshwater wetlands) and alluvial deposits exhibit the lowest predicted mean groundwater rise.

2.3.2 Impacts of Rising Groundwater on Wetlands

Wetlands are areas where groundwater is near or above the ground surface and are, consequently, highly susceptible to changes in groundwater levels. The City of Portsmouth was chosen as a focus area to examine potential impacts of rising groundwater on wetlands. It occupies an area of 42.3 km^2 in the GWRZ and has freshwater and coastal wetlands representative of the coastal region (Figure 2-6). Freshwater and coastal wetlands currently occupy 8.8 km^2 and 3.7 km^2, respectively in Portsmouth and both are projected to be impacted by SLR either from marine surface-water inundation, GWI, or both. Projected MHHW seawater inundation and GWI-risk areas, where the groundwater-table (GWT) depth below land surface is less than 1 m, with 2 m SLR are presented in Figure 2-6. These vulnerable areas are typically low-lying lands located adjacent to existing wetlands. Freshwater wetland expansion from GWI is projected to begin slowly with a 3% increase by 2030, a 10% increase by mid-century, and a 19 to 25% increase by the end of century.

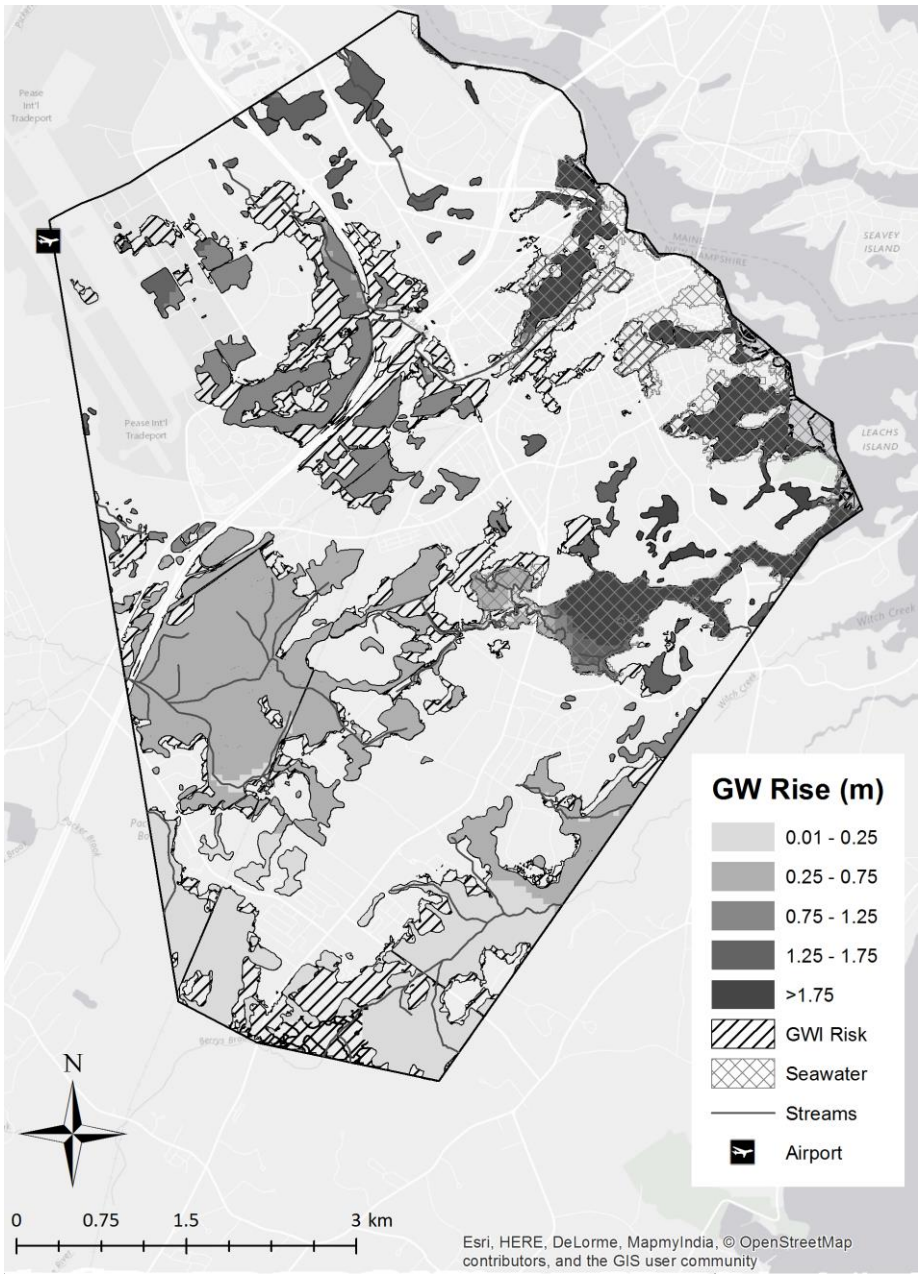

Figure 2- 6. Simulated groundwater rise in Portsmouth's marine and freshwater wetlands caused by 2 m of SLR. The shading indicates projected groundwater rise within existing wetlands defined by the National Wetlands Inventory (U.S. Fish and Wildlife Service, 2001). Areas of GWI risk (GWT < 1 m deep) are shown with black diagonal lines and projected MHHW seawater inundation is delineated with crosshatch.

The magnitude of SLR-induced groundwater rise, distance from the coast, land-surface topography, and wetland types are all important in determining the impact of SLR on wetlands.

By the end of the century, land projected to be flooded by marine surface water is 1.9 km^2 or 4.5% of Portsmouth, with approximately 3.6% of the freshwater wetlands near the shoreline projected to be inundated with seawater. GWI will more than double the inundated land, affecting 2.2 km^2 (5.2%) of the city. Approximately 1.8 km^2 (82% of the GWI area) will occur inland of the projected MHHW tidal inundation zone. The remaining 0.4 km^2 (18% of the GWI area) will occur beneath areas inundated by marine waters as possible new groundwater seeps in coastal wetlands.

Groundwater rise versus wetland type is presented in Figure 2-7. The projected mean groundwater rise is significantly different among all the wetland types analyzed except between the two dominant freshwater wetland types in the study area: forested/shrub and emergent wetlands. The marine and estuarine wetlands are projected to experience groundwater rise ranging from 0.2 to 0.8 m by mid-century and 0.5 to 2 m by end of century with a mean relative groundwater rise approximately 65% of SLR. The projected mean groundwater rise for the forested/shrub and emergent wetlands is 0.2 m by mid-century and 0.5 m by the end of the century (26% of SLR). The forested/shrub wetland distribution is skewed toward greater groundwater rise and exhibits more variation than the emergent wetlands. Freshwater pond wetlands make up less than 1% of Portsmouth but have the highest projected mean groundwater rise of the freshwater wetlands, 0.3 m by mid-century and 0.8 m by the end of the century (41% of SLR).

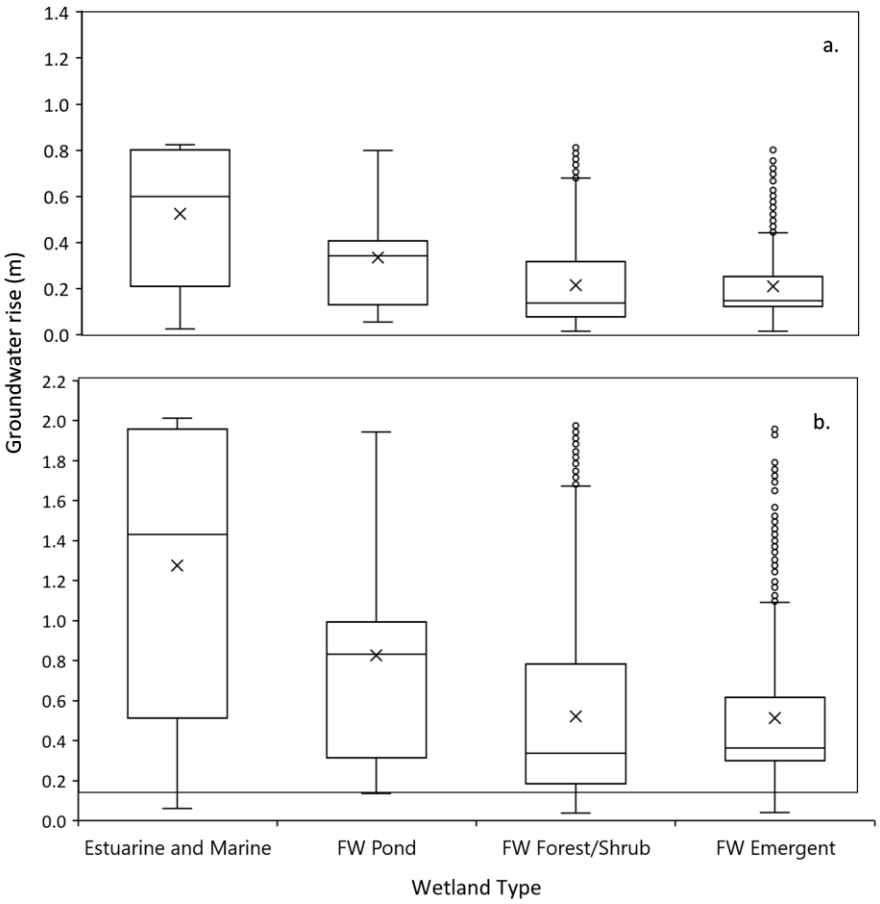

Figure 2- 7. Simulated groundwater rise caused by (a) 0.8 m and (b) 2 m of SLR versus wetland type: estuarine and marine wetlands, freshwater emergent wetlands, freshwater forest/shrub wetlands, and freshwater ponds in Portsmouth.

2.4 DISCUSSION

Many coastal vulnerability studies, used for adaptation planning, have used SLR mapping to show areas that will be flooded in the future [*Batouli and Mostafavi,* 2016; *Johnston et al.,* 2014; *Wu et al.,* 2009], and a few have included groundwater. Groundwater rise is predicted to be approximately 50% of SLR 3 km from the shoreline in New Haven, CT [*Bjerklie et al.,* 2012] and 6 km from the shoreline on Cape Cod [*Walter et al.,* 2016]. This study shows, in the northern part of the study area, relative groundwater rise equal to 50% of SLR is projected to occur within 2 to 3 km of the coast. This is more than twice the distance inland than MHHW surface-

water flooding projections (0.5 to 1 km) in this area. In addition, groundwater is predicted to rise in areas where no tidal inundation is anticipated, including the northwestern portion of the study area, due to tidal influences on the Great Bay and its contributing rivers as well as the tidally-influenced section of the Merrimack River at the study area's southern boundary.

Many of the previous studies used MODFLOW for 3-dimensional numerical modeling of the groundwater flow regime with SLR [*Bjerklie et al.,* 2012; *Habel et al.,* 2017; *Masterson and Garabedian,* 2007; *Masterson et al.,* 2014; *P. Oude Essink et al.,* 2010; *Walter et al.,* 2016], and others used a simpler approach to groundwater-elevation modeling assuming a linear groundwater response to SLR [*Cooper, H. et al.,* 2015; *Hoover et al.,* 2017; *Manda et al.,* 2015; *Rotzoll and Fletcher,* 2013]. Among the studies using MODFLOW, there are differences in approaches. In the study on Cape Cod, a migrating coastline and the freshwater/saltwater interface were both simulated [*Walter et al.,* 2016], while in Honolulu, a migrating coastline was simulated, but not the freshwater/saltwater interface [*Habel et al.,* 2017]. In New Haven, neither a migrating coastline nor the freshwater/saltwater interface were simulated [*Bjerklie et al.,* 2012]. Here, a similar approach to the New Haven study is used, representing SLR as a rising piezometric head at the coast without incorporating a migrating coastline. This results in a conservative estimate of the SLR-induced GWRZ. Freshwater/saltwater density effects at the coast were included as equivalent freshwater heads, but a moving freshwater/saltwater interface (salt transport) was not simulated. Recharge and drinking water withdrawals were assumed to be stationary.

Modeling a migrating coastline with SLR will move the groundwater signal farther inland especially in low, flat areas where surface tidal-water migration is projected to be large. Saltwater-intrusion modeling in the NH coastal region will improve estimates of groundwater rise in areas where the unconsolidated deposits are thick or where bedrock fractures allow for the

landward migration of the freshwater/saltwater interface. Saltwater-intrusion modeling also provides useful information on changing salinity distributions in coastal groundwater. Seasonal and annual recharge rates will change with rising temperatures affecting evapotranspiration, and changing precipitation patterns (Bjerklie *et al.*, 2012; Mack, 2009). In New Haven, a projected 12% increase in recharge was found to increase groundwater levels up to 0.3 m on top of SLR-induced groundwater rise (Bjerklie *et al.*, 2012). In coastal NH, simulated changes in seasonal precipitation and temperature patterns without SLR resulted in an earlier peak recharge in late winter with a longer low recharge period. This could lower base flows in streams and reduce freshwater discharge to the ocean. SLR coupled with decreased freshwater discharge to the sea could potentially result in saltwater intrusion into coastal aquifers (Mack, 2009).

SLR-induced groundwater rise is not spatially uniform. While this study shows a significant negative trend between groundwater rise and distance from the coast (low p-value), only half of the variation around the mean is due to distance from the coast. This variation results in low precision when using distance from the coast to predict SLR-induced groundwater rise at specific locations and mean values should be used with caution. Some generalizations can be made, however. Larger magnitudes of groundwater rise occur where groundwater is influenced by tidal waters on three sides and the unconsolidated deposits are the thickest (Figure 2-4) as in the northern part of the study area. In this area, the median relative groundwater rise is 62% of SLR (with an interquartile range of 42 to 82%) as opposed to areas with a linear coastline where the median relative groundwater rise is 19% of SLR (with an interquartile range of 11 to 40%). On Cape Cod, the median relative groundwater rise was found to range from 25 to 29% in the wider portion of the peninsula increasing to 46 to 50% farther out on the peninsula where the land mass between the two tidal water bodies thins [*Walter et al.*, 2016]. This suggests that the

potential impact of SLR-induced groundwater rise may be greater on peninsulas and islands than on straight coastlines.

In contrast, small magnitudes of groundwater rise are found in all distance intervals including very near the coast suggesting that distance from the coast, while important, is not the only factor dampening SLR-induced groundwater rise. Increased groundwater flow to surface-water discharge areas (palustrine and alluvial deposits) also dampens groundwater rise and may result in more stream base flow, freshwater wetland expansion, or greater water depth in wetlands. Net groundwater discharge to streams with 2 m of SLR increased from 73 to 83% of the total outflow resulting in a 14% increase in net discharge to streams and a 32% decrease in net outflow to coastal discharge areas. This is consistent with the findings of others [*Bjerklie et al.*, 2012; *Masterson and Garabedian*, 2007; *Walter et al.*, 2016]. On Cape Cod, the groundwater discharge to freshwater streams and wetlands increased from 49% to 61% of the total outflow with 1.8 m SLR [*Walter et al.*, 2016]. In New Haven, CT, groundwater rise caused by 0.9 m SLR was lower near a stream with a corresponding 34% increase in streamflow [*Bjerklie et al.*, 2012].

A relationship may exist between groundwater rise and depositional environments. Differences in the mean groundwater rise among the depositional environments investigated were found to be significant, except between palustrine and alluvial deposits, but the variation around the means is large. This limits the use of depositional environment as a precise predictor of SLR-induced groundwater rise, but some general observations can be made. The highest mean groundwater rise occurs in the beach and estuarine environments. The beach sediments consist of well-sorted beach sands with hydraulic conductivities that enable groundwater to respond uniformly to changes in sea level. The estuarine environment consists of a variety of organic and

inorganic sediments with wide ranging hydraulic conductivities and complex hydrology, including tidal inflows and outflows coupled with groundwater discharge. These characteristics most likely contribute to the large variability of projected groundwater rise. The next highest mean groundwater rise is predicted to occur in the anthropogenic sediments with the highest groundwater rise occurring along roads crossing the estuarine and beach sediments.

The hydraulic properties and thickness of the geologic materials may affect the propagation of groundwater rise. In coastal NH, the unconsolidated deposits are on average 12 m thick with the thickest deposits, 21 m, occurring in the northern part of the site. SLR-induced groundwater rise is projected to propagate the farthest inland in this area where the depositional environment is dominated by coarse-grained glaciomarine sediments. With hydraulic conductivities ranging from 0.1 to 61 m/d, the transmissivities range from 2.1 to 1,300 m^2/d. Transmissivity was found to be a dominant factor in determining the GWRZ in the Dutch delta region of the Netherlands where groundwater rise is projected to propagate 10 km from the coast in thick (210 to 300 m) unconsolidated deposits [*P. Oude Essink et al.,* 2010]. More study is needed to quantify the relationship between aquifer transmissivity and SLR-induced groundwater rise.

Rising groundwater impacts on natural and built surface features depend on the vadose-zone thickness. Areas in the GWRZ where the current groundwater depth is less than the expected groundwater rise have the potential for GWI and performance reduction in subsurface or surface infrastructure. In coastal NH, the mean vadose-zone thickness is 3.6 m with an interquartile range of 0 to 4.9 m. In the GWRZ, the mean vadose-zone thickness is 2.8 m with an interquartile range from 0 to 4.1 m. On Cape Cod, the vadose zone is thick, approximately 11 m on average [*Walter et al.,* 2016] while on Maryland barrier islands the vadose zone is thin, typically less than 1 m [*Masterson et al.,* 2014]. Rising groundwater can be impactful in places like

the Waikiki area in Honolulu or Miami/Dade county, Florida where the vadose zone is thin, and a high population density exists near the coast [*Cooper, H. M. et al.,* 2013; *Habel et al.,* 2017]. In Waikiki, 42% of the study area (13 km^2) has a vadose zone thickness less than 1.3 m. Habel *et al.* (2017) projected that 1.0 m of SLR will cause GWI in 23% of the study area within 2.5 km of the coast possibly impacting 86% of the active cesspool sites [*Habel et al.,* 2017]. An earlier study in urban Honolulu found 1.0 m of SLR inundated 10% of a 1 km wide coastal zone with GWI contributing more than half (58%) of the total inundation (surface water and groundwater) [*Rotzoll and Fletcher,* 2013]. By comparison, in Portsmouth where the mean vadose-zone thickness is 2.8 m, GWI is projected to occur in 7% of the area within 3.5 km of the coast (25 km^2) with 2 m of SLR. Surface water and groundwater are projected to inundate approximately 9% of Portsmouth (42.3 km^2) with GWI contributing 48% of the total inundation.

The current study projects that freshwater wetlands will expand from rising groundwater and, in some cases, be flooded by seawater due to SLR. Studies that considered wetland impacts from SLR and SLR-induced groundwater rise [*Cooper, H. et al.,* 2015; *Masterson et al.,* 2014] indicate that expansion as well as transitions between wetland types can be expected. While not all wetlands in Portsmouth are expected to expand, all are expected to experience groundwater rise. Freshwater and saltwater wetland vegetation are sensitive to the duration of root-zone saturation, directly related to groundwater levels and vadose-zone thickness, and the consequential ecohydrological zonation (Moffett *et al.,* 2012; Rheinhardt and Fraser, 2001). In addition, salinity changes can affect wetland ecosystem health. Masterson *et al*. (2014) found the freshwater lens above the saltwater shrinks and the vadose zone thins with SLR-induced groundwater rise, increasing both the salinity and duration of root-zone saturation. These groundwater changes have serious consequences for ecosystem extent and function (Masterson *et al.,* 2014). Overall,

changes in wetland structure will likely change their function in flood control, nutrient attenuation, biodiversity, fisheries production and recreation (Birol *et al.,* 2009; Barbier *et al.,* 2011; Linhoss *et al.,* 2015; Walters and Babbar-Sebens, 2016). Wetland expansion also has implications for wetlands-protection policy, surface and groundwater quality, and infrastructure. Regional models such as the one used in the study are not adequate to investigate detailed changes in specific wetland hydrology. They can, however, identify potentially vulnerable freshwater and marine wetlands for more detailed study.

2.5 CONCLUSIONS

This study combined groundwater modeling, marine surface-water mapping, groundwater and surface-water observations, LIDAR DEMs, and SLR scenarios to quantify SLR-induced groundwater rise in coastal NH. The modeling demonstrates that groundwater rise solely due to increased piezometric head at the coast will extend more than three to four times farther inland than projected tidal (MHHW) impacts. In much of the area within 2 km of the coast, SLR-induced groundwater rise will be at least half of the SLR. The ground-surface inundation from SLR-induced groundwater rise will double the projected inundation areas from tidal-surface water alone.

The groundwater-rise magnitude and areal extent is influenced by the geometry of the coastline, distance from the coast, geologic depositional environments, and the regional stream network. Groundwater underlying peninsulas, islands, and coastlines with extensive inlets will be the most affected by SLR. Marine and estuarine depositional environments are projected to have the highest groundwater rise and anthropogenic fill deposits are also at risk. In contrast, groundwater rise near streams is dampened where increased gradients between groundwater and surface

water result in more groundwater discharge to streams.

SLR-induced groundwater rise will increase the surface area of some coastal and freshwater wetlands and increase the water depth within existing wetlands in the GWRZ. Some freshwater wetlands will be inundated with rising marine surface water, while others, further inland, may expand. All wetlands in Portsmouth are in the GWRZ and are projected to experience groundwater rise; however, not all will expand. Wetland expansion will occur where adjacent lands have vadose-zone thicknesses less than the magnitude of projected groundwater rise. Information on groundwater rise can be used by wetland protection professionals and land-use planners to establish new wetland buffer zones, possibly elevation-based, to accommodate future changes in wetland area and location.

In areas within the GWRZ where the current groundwater depth is within the range of projected groundwater rise, underground assets will be vulnerable to damage or reduced performance. Coastal-road pavements will weaken when rising groundwater moves into the supporting base layers (Knott *et al.*, 2017). On-site wastewater treatment system performance will be reduced when rising groundwater intersects the treatment trenches (Manda *et al.*, 2015). Basements of historic structures may flood regularly with groundwater, compromising their structural integrity. Groundwater infiltration of wastewater collection systems with rising groundwater can damage and/or reduce the efficiency of wastewater treatment systems (Flood and Cahoon, 2011). In addition, long-term groundwater rise should be considered when remediating contaminated sites. The methodology and insights presented in this study can be used by land-use managers, transportation departments, and environmental protection professionals to identify coastal infrastructure and natural resources vulnerable from SLR-induced groundwater rise for detailed adaptation planning.

Future work may include incorporating a migrating coastline with SLR, modeling saltwater intrusion, and investigating the combined effects of SLR and seasonal fluctuations of groundwater levels. Climate change is projected to produce long-term changes in temperature and precipitation, both important factors affecting groundwater recharge. A study of the combined effects of SLR and long-term changes in recharge and groundwater withdrawal rates should also be investigated to improve the accuracy of future groundwater-level predictions.

CHAPTER 3 - ASSESSING THE EFFECTS OF RISING GROUNDWATER FROM SEA-LEVEL RISE ON THE SERVICE LIFE OF PAVEMENTS IN COASTAL ROAD INFRASTRUCTURE

3.1 INTRODUCTION

Coastal areas worldwide are becoming more developed. Roads, constructed to service the built environment along the shore, are increasingly at risk from SLR, more intense coastal storms and storm surge [*Moser et al.,* 2014]. While the shoreline in many locations may be fortified in the future to protect property from coastal storms, access roads in coastal communities are vulnerable from rising groundwater caused by SLR. Sea level in coastal New Hampshire (NH) is projected to rise 3.9 to 6.6 feet (1.2 to 2.0 meters) by the year 2100 [*Kirshen, Wake et al.,* 2014]. Groundwater is expected to rise with rising sea level not only along the coast but at significant distances inland [*Bjerklie et al.,* 2012]. In some locations rising groundwater caused by SLR will intersect the unbound layers of coastal road infrastructure, weakening the pavement structure. Pavement design criteria is currently based on historical information that assumes the environmental parameters are stationary or, on average, not changing with time. Recent advances in climate change science have shown that the climate is, in fact, no longer stationary. Transportation engineers, concerned that the pavement design criteria of the past are no longer valid, are looking for new guidance in designing and restoring pavement systems. Anticipated changes in groundwater levels will change the frequency, duration, and severity of road failures as well as the time and cost of their repair.

SLR can cause erosion and storm-surge damage, flood coastal communities and damage coastal infrastructure [*Melillo et al.,* 2014]. The causes of SLR are 1) thermal expansion of ocean

waters, 2) water transfer between glaciers and oceans, 3) vertical land movement, 4) shifts in the Earth's magnetic field, and 5) ocean dynamics [*Parris et al.,* 2012]. There is uncertainty in the sea-level-rise projections partly because it is unknown how quickly global economies will reduce greenhouse gas emissions and the ice loss dynamics from the Greenland and West Antarctica ice sheets are not well understood. A study linking global SLR to global temperature projected global SLR ranging from 2.5 to 6.2 feet (0.76 to 1.9 meters) over the period of 1990 to 2100 [*Vermeer and Rahmstorf,* 2009]. NOAA assessed a large number of SLR studies and produced scenarios of global mean SLR ranging from 0.7 to 6.6 feet (0.2 to 2.0 meters) by the end of the century [*Parris et al.,* 2012]. The lowest scenario is an extrapolation of the historical record and the highest scenario is based on the IPCC AR4 global SLR projections combined with an estimate of the maximum amount of glacial and ice sheet loss by the end of the century. They recommend the highest scenario be used to design infrastructure where the tolerance for risk is small [*Parris et al.,* 2012]. In coastal NH sea level rose 5.3 inches (13.5 cm) from 1927 to 2001 which is close to global mean SLR. The New Hampshire Hazards and Risks Commission have adopted the NOAA scenarios for coastal adaptation planning [*Kirshen, Wake et al.,* 2014].

In coastal areas, groundwater flows from recharge areas to discharge areas along the shoreline. As sea level rises, the groundwater levels near the coast also rise until a new equilibrium is established between aquifer recharge and groundwater discharge to the sea. Due to the long timeframes associated with the effects of climate change and SLR, scientifically-based mathematical models are used to simulate future changes. Groundwater modeling is a useful tool for projecting changes in groundwater levels driven by SLR [*Pitz,* 2016]. The effect of 3 feet (0.9 meter) of SLR on groundwater levels in New Haven, Connecticut was investigated by Bjerklie et al. [*Bjerklie et al.,* 2012] of the US Geological Survey using MODFLOW-2000, a

three-dimensional groundwater-flow model [*Harbaugh et al.,* 2000]. The simulations produced the same 3-foot (0.9-meter) increase in the groundwater level immediately along the coast. The effects of SLR on groundwater were also seen at significant distances inland where the original groundwater levels were 17 to 24 feet (5.2 to 7.3 meters) above mean sea level. Similar results have been published from research conducted on Cape Cod [*Masterson,* 2004], the barrier islands of Maryland [*Masterson et al.,* 2014], and Florida [*Cooper, H. et al.,* 2015]. A study conducted in urban Honolulu, Hawaii found the combined area of inundation from both rising groundwater and surface water was twice that of surface water inundation alone [*Rotzoll and Fletcher,* 2013].

Pavement performance is sensitive to parameters influenced by climate, specifically temperature and the moisture content of pavement sublayers [*Elshaer, Ghayoomi et al.,* 2015]. Higher temperatures reduce the stiffness (strength) of the asphalt layer and increased moisture content reduces the stiffness of the underlying unbound layers[*Mallick and El-Korchi,* 2013]. As groundwater rises with SLR, groundwater will intersect the unbound layers in some locations weakening the pavement structure. Increasing the groundwater level in field tests in Sweden produced a 20-percent increase in strain and had more effect on the stiffness of the pavement structure than either temperature or load [*Salour et al.,* 2014]. In addition, the useful life of a pavement structure decreases with an increase in the percentage of time the unbound soils are saturated [*Cedergren,* 1988]. The structure of the pavement, including layer thicknesses and material types as well as the nature of the subgrade, also influences the structural response to changes in moisture content [*Elshaer, Daniel et al.,* 2015; *Salour et al.,* 2015].

This research investigates the effects of groundwater rise from SLR on the service life of pavements in coastal road infrastructure. A groundwater-flow model and current groundwater

observations are used to identify roads that will be vulnerable from rising groundwater caused by SLR. Analysis of pavement profiles with changing groundwater levels using multi-layer elastic theory demonstrates that the service life of pavement systems is reduced as groundwater rises. This interdisciplinary approach provides a methodology for addressing future vulnerabilities of coastal-road infrastructure from groundwater and provides a framework for adaptation planning.

3.2 MATERIALS, METHODS, AND DATA

3.2.1 Study Area

The study area is 160 square miles in the coastal region of New Hampshire (NH) where there is approximately 18 miles (29 km) of shoreline. It is a hydrologically diverse area with coastal and freshwater wetlands, rivers and streams, estuaries, and beaches [*Mack,* 2009]. The study area is bounded by the Piscataqua tidal river in the north, Great Bay and the Squamscott River in the west, the Merrimack River in the south and the Atlantic Ocean in the east (Figure 3-1). Thirteen communities are located within the study area with a combined population of approximately 88,100 [*U.S. Census Bureau,* 2016]. Portsmouth is a city in the northern part of the study area with a population of approximately 21,500 and an international airport. The road network consists of local roads, local connectors, regional corridors, statewide corridors, and an interstate highway [*NHDOT,* 2016]. The locations of the pavement profiles chosen for analysis are identified in Figure 3-1.

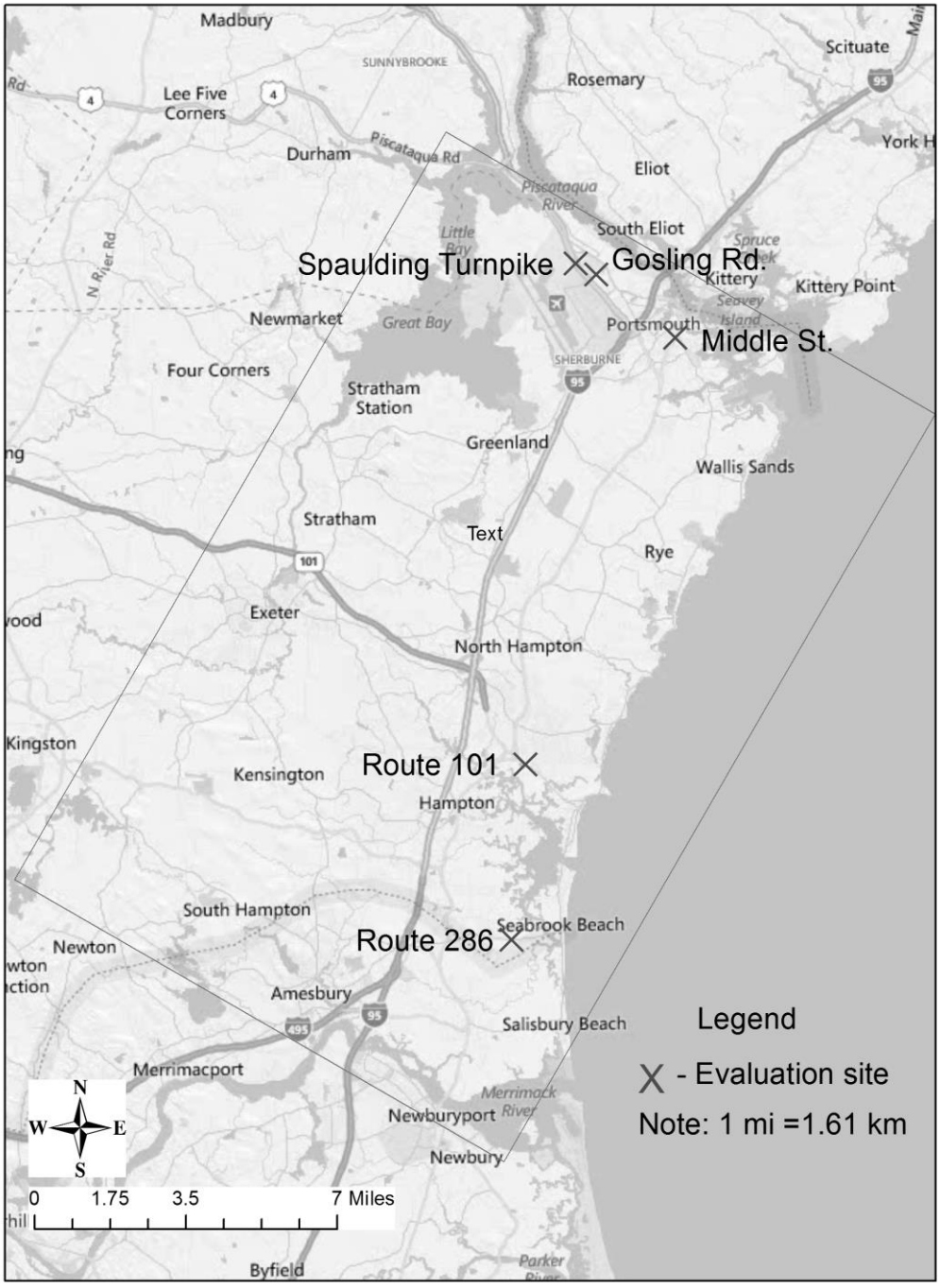

Figure 3- 1. Study area in coastal New Hampshire.

3.2.2 Groundwater Data

Current groundwater elevations were compiled from several sources including the NH Department of Environmental Services (NHDES), NH Geological Survey (NHGS), United

States Airforce, and the Town of Seabrook. Average groundwater elevations in a total of 1983 wells, installed in the unconsolidated deposits above the bedrock, were used to construct a groundwater elevation contour map with an interval of 2 feet (0.6 meters). The most accurate groundwater data used in this study were obtained from wells installed over the period of 1955 through 2014 at the Portsmouth International Airport at Pease located in the northeastern section of the study area. These wells were typically surveyed to a common datum and groundwater levels have been measured monthly or quarterly in recent years [*Forbes,* 2015]. Groundwater elevations over the rest of the study area were obtained from GEOLOGs (NHGS) and the water well inventory (NHDES). GEOLOGs are a compilation of boring and well information from NHDES, NH Department of Transportation (NHDOT) and the US Geological Survey (USGS). Groundwater level measurements from this data set are available from the early 1900s to the present. Many of these wells were measured only one time, while some were monitored over time. The water well inventory is a database of boring and well information compiled by the NHDES from wells installed for domestic and industrial water supply, exploration, and testing. Groundwater levels in this dataset were recorded by drillers during installation and are the most uncertain. The piezometric head along the shore was assumed to be mean sea level.

3.2.3 Groundwater Modeling

An existing USGS groundwater-flow model of coastal NH [*Mack,* 2009] was updated and modified to investigate the effect of SLR on groundwater levels. USGS MODFLOW-2005 was used to solve the groundwater flow equation [*Harbaugh,* 2005] with sea-level as a boundary condition. LiDAR datasets, areal recharge, water withdrawals, hydrogeologic properties, and SLR were used as inputs and the model was run in steady state. Mean sea level and groundwater

observations were used for calibration. A complete description of the groundwater model is presented in Mack [*Mack,* 2009]. The updated version of the model used in this analysis is described in Knott et al.[*Knott et al.,* 2018a].

3.2.3.1 Groundwater Model Input and Output Parameters

MODFLOW has several input parameters that are estimated prior to running the simulations. All have uncertainties including errors associated with measuring the parameter, parameter variability in space and time, complex interactions between parameters, insufficient data density, and an uncertain future.

Input parameters that are sensitive to climate include recharge and sea level. Recharge is the infiltration of precipitation and/or surface water and its percolation through unsaturated soils to the saturated zone [*Heath,* 1983]. Areal recharge rates were determined by the NHGS using a soil-water model that accounts for interception, evapotranspiration (ET), run-off partitioning, soil infiltration or snow-pack storage, and soil-moisture partitioning [*Dripps and Bradbury,* 2007]. Sea-level is modeled in MODFLOW as a constant-head boundary condition which can be modified for each steady-state simulation [*Rumbaugh and Rumbaugh,* 2011]. The interaction between groundwater and streams is also simulated in the model. Increased piezometric head in groundwater driven by sea-level rise may result in more groundwater discharge to streams [*Bjerklie et al.,* 2012; *Masterson,* 2004].

Input parameters that are insensitive to climate include aquifer properties, such as hydraulic conductivity, aquifer layer thickness, and ground-surface elevation. The geology in the model domain consists of glacial deposits approximately 40-feet thick overlying fractured bedrock [*Mack,* 2009] and the ground-surface elevation was determined using bare-earth LiDAR data [*NH Coastal Lidar,* 2011]. Current land use (NHGS) and drinking water withdrawals

(NHDES) are also included in the model but not varied with time. For this study, it is assumed that all of the input parameters remain constant except mean sea-level which is varied according to several sea-level rise projections.

MODFLOW generates groundwater elevations (head), fluxes, drawdowns and concentrations at each grid cell [*Harbaugh,* 2005]. The output parameter of interest for this study is groundwater head (elevation).

3.2.3.2 Sea-Level Rise Scenarios

Sea-level rise projections of 1.0 foot (0.30 meters), 2.7 feet (0.82 meters), 5.2 feet (1.6 meters) and 6.6 feet (2.0 meters) corresponding to the high emission scenario in early-century (2030), mid-century (2060) and the end of the century (2090 and 2100) were simulated using the groundwater model (Figure 3-2) [*Parris et al.,* 2012]. The current mean sea level in coastal NH is 0.3 feet (0.09 meters) below the North American Vertical Datum of 1988 (NAVD88). The projected rise in sea level for each of the four scenarios was added to the current mean sea level and then used as the sea-level boundary condition for the steady-state groundwater model. The model was run five times to generate groundwater elevation contours for the current condition and the four sea-level rise scenarios.

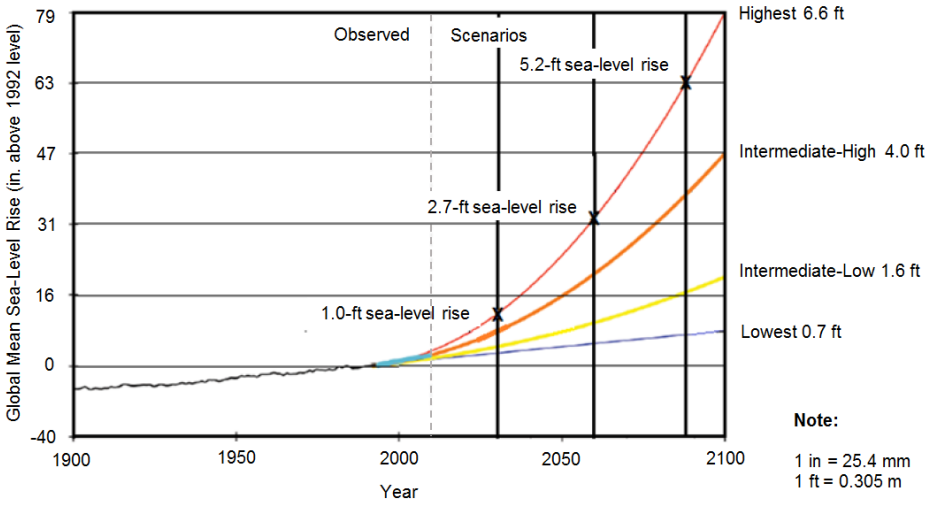

Figure 3- 2. Global mean sea-level-rise scenarios relative to 1992 from the National Climate Assessment [*Parris et al.,* 2012].

In addition to sea-level, precipitation and temperature are expected to rise in the northeast with climate change [*Hayhoe et al.,* 2006] affecting groundwater levels through aquifer recharge. The interactions between precipitation, runoff, and evapotranspiration are complex and have a strong seasonal signature. In the northeast, the groundwater is typically the highest in the early spring when the aquifer recharge from rainfall and snowmelt is maximum and evapotranspiration is small [*Mack,* 2009]. In this study, the groundwater model is run in steady-state to assess the long-term effect of sea-level rise on average groundwater levels and does not consider seasonal or annual variation in recharge rates caused by climate change.

3.2.4 Identification of Roads for Analysis

Coastal roads that will be vulnerable with groundwater rise from sea-level rise were chosen for pavement analyses based on three criteria: 1) functional classification from NHDOT, 2) location where groundwater is predicted to rise with sea-level rise, and 3) road sections where the current groundwater is less than 10 feet (3.0 meters) below the ground surface. The functional classifications are turnpike, statewide corridor, regional corridor, and local roads. Areas where groundwater is expected to rise with sea-level rise were identified using a GIS layer of predicted groundwater rise calculated using the groundwater model. Sections of roads where groundwater is currently less than 10-feet below the ground were identified by subtracting the current groundwater elevation from the LiDAR bare-earth ground-surface elevation [*NH Coastal Lidar,* 2011].

Five evaluation sites were chosen for pavement analysis; the locations of which are identified in Figure 3-1. They are Spaulding Turnpike, Route 101 (statewide corridor), Route 286 (regional corridor), Gosling Road (local) and Middle St. (local). Spaulding Turnpike and Gosling Road are located in Newington, NH. Spaulding Turnpike is a 33.2-mile (53.4 km) divided highway in eastern NH and its pavement evaluation site is located approximately 0.9 mile (1.4 km) from the Piscataqua River, a tidal river to the northeast. Gosling Road is a local road running perpendicular to Spaulding Turnpike and provides access to the Portsmouth International Airport at Pease. The evaluation site is located 0.8 mile (1.3 km) from the Piscataqua River. Route 101 (Exeter-Hampton Expressway) is an evacuation route from Hampton Beach, a popular tourist area. The evaluation site is located 1.7 miles (2.7 km) from the Atlantic Ocean and is adjacent to a saltmarsh in the Hampton-Seabrook estuary. Route 286 is a short east-west highway located in Seabrook, NH and Salisbury, Massachusetts. It is also an evacuation route away from the Atlantic shoreline. The Route 286 evaluation site is located approximately 1.3 miles (2.1 km) from the coast and is within 400 feet (122 meters) of a saltmarsh. Middle Street (Route 1) is a major local road in a densely-populated section of Portsmouth. This evaluation site is located approximately 0.6 mile (1.0 km) from a Piscataqua inlet to the southeast.

3.2.5 Pavement Performance Evaluation

3.2.5.1 Pavement Profiles and Material Properties

Typical pavement profiles were constructed for each of the five sites. The nature and thickness of the asphalt and base layers were determined from construction plans available from NHDOT [*NHDOT*, 2016]. The nature and thickness of the subgrade layers were determined from nearby boring logs from the GEOLOG database (NHGS). A Unified Soil Classification System

(USCS) soil group [*ASTM*, 2011] was assigned to the geologic layers in each boring based on soil descriptions recorded by drillers during well installation. Each lithographic layer was then assigned an AASHTO soil classification symbol based on the "Guide Sheet 1- General relationship of systems used for classifying soil samples" [*Natural Resources Conservation Service (NRCS)*, 2016].

The material properties for the five sites with current (average) groundwater levels are presented in Table 3-1. The location of the groundwater table within the pavement profile is at the interface between unsaturated and saturated soils (Table 3-1). The soil beneath the groundwater table is fully saturated and the unsaturated soil above the groundwater table is assumed to be at optimum moisture content used for pavement design. Typical values of resilient modulus and Poisson's ratio of unbound materials were assigned to each lithographic layer according to its AASHTO soil classification. These values were obtained from the Mechanistic-Empirical Pavement Design Guide (MEPDG) [*AASHTO*, 2008] level 3 inputs.

Table 3- 1. Input parameters for multi-layer elastic analysis at five study sites with current groundwater levels

Road & Tier Classification	Material Layer Type		AASHTO Class	Resilient Modulus (psi)	Poisson's Ratio	Thickness (in)	Current GWL
Spaulding Turnpike	Asphalt	HMA	na	400,000	0.35	7.5	Unsat.
	Base	Crushed stone	A-1-a	40,000	0.35	10	
	Subbase	Gravel	A-1-b	38,000	0.35	18	
	Subgrade	Fill	A-1-b	26,500	0.35	32	▼
				13,250	0.35	15	Saturated
		Sand, silt	A-2-4	12,250	0.25	24	
		Silt	A-4	8,250	0.25	48	
		Sand	A-3	8,250	0.30	24	
		Gravel	A-1-a	14,750	0.35	20	
		Bedrock	na	725,000	0.20	infinite	
Route 101 (Statewide Corridor)	Asphalt	HMA		400,000	0.35	5	Unsat.
	Base	Crushed gravel	A-1-a	40,000	0.35	16	
	Subgrade	Clay, sand	A-6	14,500	0.20	39	▼
				7,250	0.45	367	Saturated
		Till	A-2-7	10,250	0.25	53	
		Bedrock	na	725,000	0.20	infinite	
Route 286 (Regional Corridor)	Asphalt	HMA		400,000	0.35	5.5	Unsat.
	Base	Crushed gravel	A-1-a	40,000	0.35	16	
	Subgrade	Sand	A-3	16,500	0.30	1	▼
				8,250	0.30	105	Saturated
		Sand & gravel	A-1-b	13,250	0.35	294	
		Clay	A-7-6	5,750	0.45	180	
		Till	A-2-7	10,250	0.25	12	
		Bedrock	na	725,000	0.20	infinite	
Gosling Road (Local)	Aspahlt	HMA	na	400,000	0.35	4	Unsat.
	Base	Crushed gravel	A-1-a	40,000	0.35	24	
					0.35		▼
	Subbase	Sand	A-3	14,500	0.30	8	Saturated
	Subgrade	Silt	A-4	8,250	0.33	40	
		Gravel	A-1-a	14,750	0.35	24	
		Sand, silt	A-2-4	12,250	0.25	24	
		Till	A-2-7	10,250	0.25	infinite	
Middle St. (Local)	Asphalt	HMA	na	400,000	0.35	8	Unsat.
	Base	Crushed gravel	A-1-a	40,000	0.35	8	
	Subgrade	Gravel, sand, silt	A-2-4	24,500	0.25	31	▼
				12,250	0.25	34	Saturated
		Bedrock	na	725,000	0.20	infinite	

Note:
1 in = 25.4 mm
1 psi = 6.89 kPa
na = not applicable
▼ = water table

Typical resilient modulus values at optimum moisture content are used for the unbound materials above the water table and typical resilient modulus values at full saturation are used for the unbound materials below the water table. The ratio of resilient modulus at full saturation to resilient modulus at optimum moisture content (M_{Rsat}/M_{Ropt}) is assumed to be 0.5 for the unbound materials in this analysis based on guidance from the MEPDG [*AASHTO*, 2008]. While the dynamic modulus of the asphalt layer fluctuates with temperature and seasonal frequency, the

steady-state analysis does not consider seasonal variability. The average dynamic modulus is assumed to be constant at the 20°C value used for design from Cornell typical values [*Cornell University*,]. In addition, it is assumed that no fatigue and rutting distresses are currently present in the test sections of the roadway.

3.2.5.2 Multi-Layer Elastic Analysis

Multi-layer elastic analysis KENLAYER computer software [*Huang*, 2003] was used to determine changes in the pavement response to loading resulting from rising groundwater from sea-level rise in the five pavement profiles under interlayer full bond and full slip conditions. Loading was kept constant at 9000 pound (4086 kg) single axle single tire with a contact radius of 4.89 inches (12.4 cm). As groundwater rises in the soil profile with each sea-level rise scenario, the lithologic layer in which the groundwater table resides is divided into an unsaturated section above the water table and a saturated section below the water table. The change in unbound material stiffness is modeled by reducing the resilient modulus under optimum moisture conditions (M_{Ropt}) to the resilient modulus under saturated conditions ($M_{Rsat} = 0.5M_{Ropt}$) and the thickness of the saturated portion of the layer is changed accordingly. The projected groundwater levels for the current conditions and the sea-level rise scenarios are presented for the five study sites in Figure 3-3.

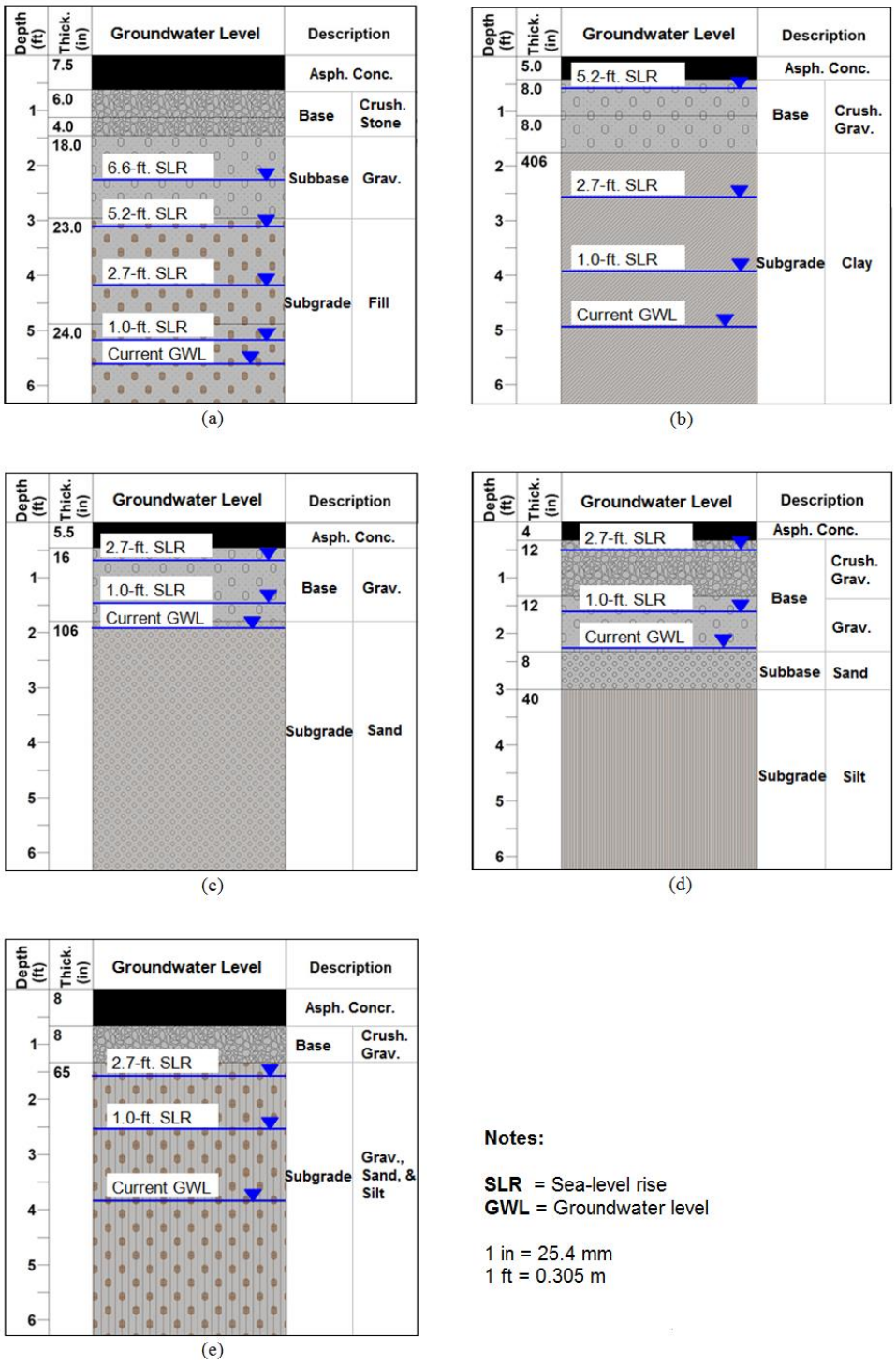

Figure 3- 3. Pavement profiles to a depth of 6 feet (1.8 meters) showing groundwater levels for the sea-level rise scenarios: (a) Spaulding Turnpike, (b) Route 101(statewide corridor), (c) Route 286 (regional corridor), (d) Gosling Road (local), (e) Middle Street (local).

Horizontal tensile strain was calculated at the bottom of the asphalt concrete layer and vertical compressive strain was calculated at the top of the subgrade layer for the various groundwater levels predicted in the sea-level rise scenarios. Strain was converted to number of cycles to failure (N_f) for fatigue cracking and rutting using equations developed for dense-graded asphalt mixtures by Minnesota Department of Transportation [*Timm et al.,* 1999]. The number of cycles to fatigue failure was calculated using the following equation:

$$N_f = 2.83 \times 10^{-6} \left[\frac{10^6}{\varepsilon_t}\right]^{3.148} \quad (3.1)$$

where,

N_f = number of load applications to fatigue cracking in 10% of the wheel path area

ε_t = horizontal tensile strain at the bottom of the asphalt layer (microstrain)

The number of cycles to rutting failure was calculated using the following equation:

$$N_f = 1.00 \times 10^{16} \left[\frac{1}{\varepsilon_v}\right]^{3.87} \quad (3.2)$$

where,

N_f = number of load applications to limit rutting

ε_v = vertical compressive strain at the top of subgrade (microstrain)

The changes in N_f for fatigue and rutting resulting from rising groundwater were evaluated using the ratio of N_f at the predicted groundwater level to the N_f at the current groundwater level.

3.3 DISCUSSION OF RESULTS

3.3.1 Rising Groundwater with Sea-Level Rise

Results from the groundwater modeling show that the effects of sea-level rise on groundwater will extend further inland than the effects of surface-water flooding [*Knott et al.,* 2018a]. Surface-water inundation is predicted to occur approximately one mile (1.6 km) from the coast [*Rockingham Planning Commission,* 2015] while up to 4 feet (1.2 meters) of groundwater rise from sea-level rise is predicted to occur at distances approximately 2 miles (3.2 km) from the coast [*Knott et al.,* 2018a]. The magnitude of groundwater rise is not uniform and linear with distance from the coast. It depends on the local hydrogeology, the proximity of groundwater discharge areas such as streams or wetlands, distance from the coast, and groundwater pumping. The impact of rising groundwater on the service life of pavements also depends on the local (current) depth to groundwater and the pavement structure.

Groundwater rises with sea-level rise at all the study sites for all of the sea-level rise scenarios (Figure 3-3). However, not all sections of roadways in the zone of groundwater rise will be equally impacted. In four out of the five locations, groundwater will inundate the road surface before the end of the century with the high emissions scenario. The Middle Street (local) site is closer to the coast and will experience more groundwater rise from sea-level rise than the Gosling Road (local) site, yet groundwater will intersect the pavement structure at the Gosling site sooner than at the Middle Street site. The roads in the zone of rising groundwater that are most at risk from the impacts of sea-level rise are the ones with current groundwater levels less than 3 feet (0.9 meters) from the road surface.

The vertical structure of the pavement has a significant effect on the vulnerability of the road to groundwater rise from sea-level rise. The Spaulding Turnpike and Gosling sites are only

0.5 mile (0.8 km) apart but have very different vulnerabilities from sea-level rise. Spaulding Turnpike consists of multiple layers of fill, subbase and base material. The road surface is approximately 7 feet (2.1 meters) above the natural soils and 5.6 feet (1.7 meters) above the current groundwater in contrast to Gosling Road where the road surface is 3 feet (0.9 meters) above the natural soils and 2.3 feet (0.7 meters) above the current groundwater. The groundwater will not enter the subbase of the pavement structure in this section of Spaulding Turnpike until the area experiences more than 5 feet (1.5 meters) of sea-level rise, projected to occur late in the century. However, the groundwater is already in the base layers of Gosling Road and any groundwater rise with sea-level rise will serve to weaken the unbound materials of the pavement structure.

The groundwater flow regime is also important in determining coastal road vulnerabilities from sea-level rise. A comparison of Route 286 (regional corridor) and Route 101 (state corridor) illustrates this difference. Both roads are similar in their distance from the ocean. They run perpendicular to the coast across wetlands and are evacuation routes from coastal properties. However, the current groundwater elevation at the Route 286 site is approximately 5 feet (1.5 meters) higher than the groundwater elevation at the Route 101 site. Groundwater discharge to the Taylor River keeps groundwater levels lower at the Route 101 site. In addition, groundwater pumping for public water supply, located northwest of the Route 101 site, lowers the groundwater levels in this area.

3.3.2 Multi-Layer Elastic Analysis

The results of the multi-layer elastic analysis are presented as the ratio of the number of cycles to failure (N_f) at the predicted groundwater level to the number of cycles to failure (N_f) at the current groundwater level for the four sea-level rise scenarios (Figure 3-4). This ratio is

considered representative of a worst-case service-life reduction as the groundwater will not be at the predicted level for the entire life of the pavement. In all profiles, the N_f for fatigue cracking is less than the N_f for rutting; consequently, fatigue cracking controls the service life of the pavement structure. The height of the bar in the Figure 3-4 is the average of the N_f ratio calculated under interlayer full bond and full slip conditions, assuming the reality will fall between the two extremes as shown with the error bars. When the groundwater is projected to flood the surface of the road, it is assumed that section will need to be rebuilt or raised. This situation is indicated in Figure 3-4 as not applicable (NA) for the analysis.

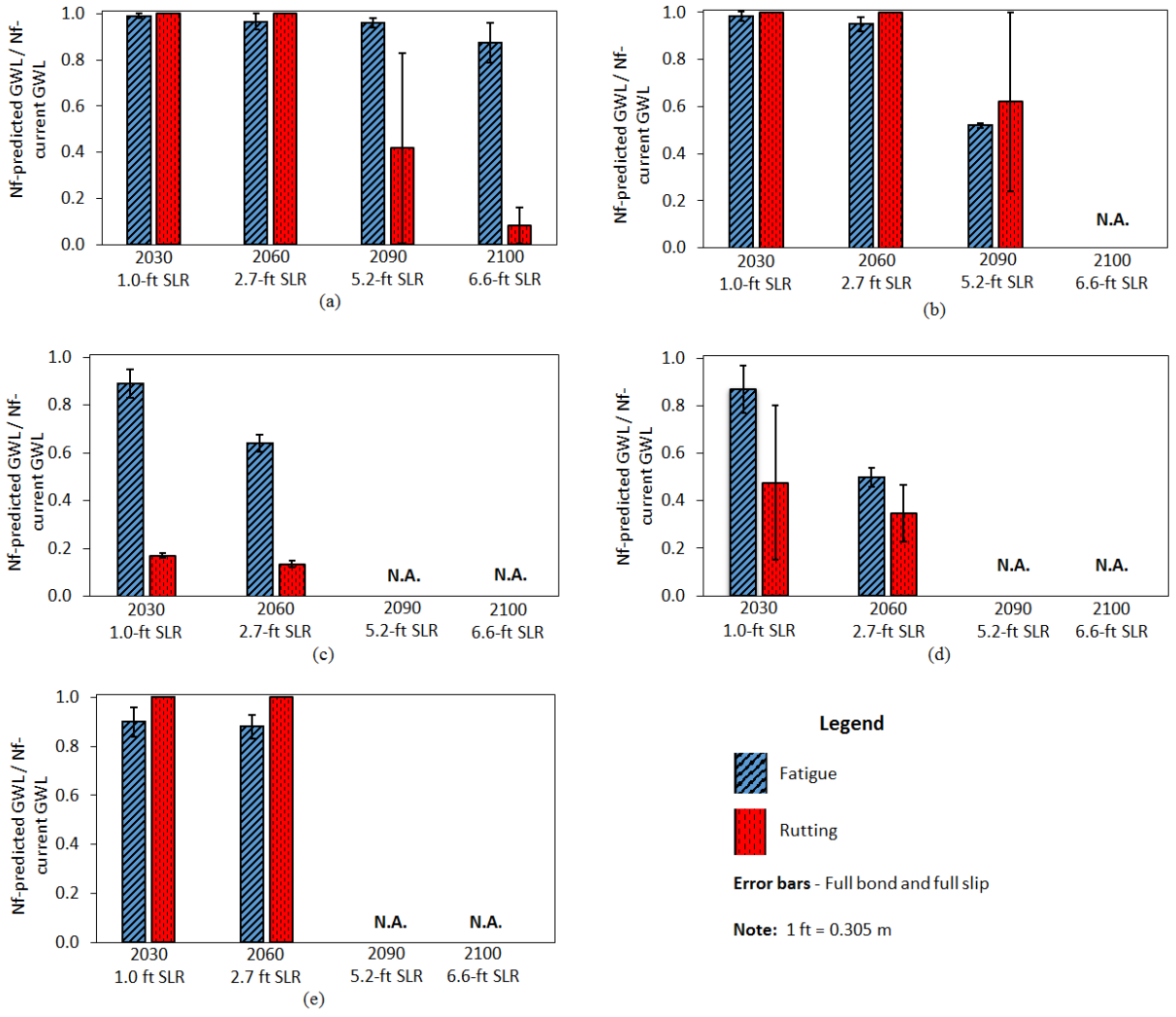

Figure 3- 4. Pavement service-life reduction from groundwater rise: (a) Spaulding Turnpike, (b) Route 101 (statewide corridor), (c) Route 286 (regional corridor), (d) Gosling Road (local), (e) Middle Street (local).

Spaulding Turnpike has a substantial pavement structure consisting of a thick asphalt concrete layer underlain by base and subbase layers. Service-life reduction is not predicted until 2090 with 5.2 feet (1.6 meters) of sea-level rise when the groundwater reaches the bottom of the subbase (Figure 3-3). The service life of the pavement, controlled by fatigue cracking, at Spaulding Turnpike is reduced relative to the current service life by 4 and 12 percent for 5.2 and 6.6 feet (1.6 and 2.0 meters) of sea-level rise, respectively. The fatigue life of the Route 101 pavement is reduced by 5 percent while the groundwater table is still in the clay subgrade with 2.7 feet (0.8 meters) of sea-level rise and 48 percent with 5.2 feet (1.6 meters) of sea-level rise when the groundwater moves into the base materials (Figures 3-3 and 3-4). Flooding of the road surface from groundwater occurs toward the end of the century.

Roads with groundwater currently near the ground surface (Figure 3-3) in the zone of groundwater rise will be affected the most. Route 286 and Gosling Road exhibit the largest service-life reduction and are projected to have structural damage much earlier than the other pavement evaluation sites. Again, fatigue cracking is the controlling factor for the structural failure of the pavement. The fatigue life of the pavement at the Route 286 site is predicted to be reduced by 11 and 36 percent with 1 foot and 2.7 feet (0.3 and 0.8 meter) of sea-level rise, respectively. The fatigue life of the pavement at the Gosling Road site is predicted to be reduced by 13 and 50 percent with 1-foot and 2.7 feet (0.3 and 0.8 meter) of sea-level rise, respectively. Shortly after 2060, the surface of both of these roads will be inundated from rising groundwater unless adaptation strategies to raise the road or lower the groundwater table are implemented.

The Middle Street site has the thinnest pavement structure of all the pavement profiles with a thick asphalt concrete layer that makes up 50 percent of the pavement thickness (Figure 3-3). The analysis reveals 10 and 17 percent reductions in fatigue life for 1.0 and 2.7 feet (0.3 and 0.8 meter) of sea-level rise with the groundwater table in the subgrade. Inundation of the pavement surface occurs between 2.7 and 5.2 feet (0.8 and 1.6 meters) of sea-level rise projected to occur between 2030 and 2060.

While fatigue cracking controls the pavement failure in all the profiles analyzed, significant reductions in rutting performance, dictated by vertical strain on the top of the subgrade, is observed in all of the pavement profiles as groundwater rises except at the Middle Street site (Figure 3-4). A comparison of Figures 3-3 and 3-4 reveals that reduction in rutting performance does not occur until the groundwater table nears the top of the subgrade and moves into the base layers of the pavement structure. At Middle Street the groundwater remains in the subgrade for the first two sea-level rise scenarios with no reduction in rutting performance occurring despite groundwater rising to within 2 inches (5 cm) of the base layer with 2.7 feet (0.8 meter) of sea-level rise. This contrasts with the nearly 60-percent reduction in rutting performance observed at Spaulding Turnpike when the groundwater approaches the subbase layer with 5.2 feet (1.6 meters) of sea-level rise. The thick asphalt concrete layer in relation to the total thickness of the pavement structure may have contributed to better rutting performance prior to inundation at this location. The potential for rutting failure increases more than 50 percent by 2030 with 1.0 foot (0.3 meter) of sea-level rise at the Route 286 and Gosling Road sites. This is important when considering other variables that may be affected by climate change such as the reduction of stiffness in the asphalt layer with rising temperatures and in the design of future pavements.

It was assumed in these analyses that the unbound materials above the water table were at optimum moisture content. If, in reality, the moisture content is above optimum under current conditions as in poorly drained fine-grained silts and clays, the initial N_f would be lower resulting in a smaller reduction in service life from rising groundwater in the ratio analysis. Conversely, if the initial moisture content is below optimum as in well-drained coarse-grained materials, groundwater rise will result in a larger reduction in the service life of the pavement. It was also assumed that the pavement was without distress under current conditions. If the pavement currently contains fatigue or rutting distresses and the condition of the pavement continues to deteriorate over time, the increased strains caused by loading under conditions of higher groundwater table will result in greater service-life reduction when compared with current conditions.

3.4 CONCLUSIONS

An interdisciplinary approach coupling groundwater modeling with multi-layer elastic analysis of pavement systems is used to assess the effect of sea-level rise on groundwater and coastal road infrastructure. The results of this study show that groundwater will rise with sea-level rise and provides a framework for determining which sections of roads will be most impacted.

The magnitude of groundwater rise with sea-level rise depends on the hydrogeology, the proximity of groundwater discharge areas, groundwater pumping, and distance from the coast. Pavements within the zones of predicted groundwater rise with current groundwater levels near the top of the subgrade will experience the most service-life reduction caused by rising groundwater. In addition, the surface of some sections of these roads will be inundated with groundwater by mid-century if adaptation strategies are not implemented. Roads with existing

groundwater levels deeper than 10 feet will likely not be impacted by rising groundwater under the current sea-level rise projections out to the end of the century.

For roads that are vulnerable, reductions of 5 to 17 percent in fatigue life are predicted as groundwater rises in the subgrade and increase to 50 percent as groundwater moves into the base layers of the pavement. Reductions in rutting life from 38 to 92 percent are predicted when groundwater moves from the subgrade into the base layers. Variations in the magnitude of service-life reduction are affected by the depth to groundwater, the pavement structure, and subgrade materials.

Groundwater information is available in many local communities from hydrogeological studies for water supply and groundwater assessment. The use of this interdisciplinary approach to inform pavement design and maintenance in coastal communities will reduce the costs of premature pavement failure caused by rising groundwater from sea-level rise and provide necessary guidance for targeted adaptation planning. Future work includes using this methodology to investigate the effects of other changing climate parameters, such as temperature and precipitation, in combination with changes in groundwater levels on pavement service life and to evaluate adaptation strategies for pavement resilience to climate change.

CHAPTER 4: ADAPTATION PLANNING TO MITIGATE COASTAL ROAD PAVEMENT DAMAGE FROM GROUNDWATER RISE CAUSED BY SEA-LEVEL RISE

4.1 INTRODUCTION

Sea-level rise (SLR) can cause erosion and storm-surge damage, flood coastal communities and damage coastal infrastructure [*Melillo et al.*, 2014]. Many studies have investigated SLR-induced surface-water flooding and storm surge on road infrastructure [*Johnston et al.,* 2014; *Wu et al.,* 2009] but few have investigated the effect of SLR-induced groundwater rise on coastal-road pavement systems. As groundwater rises, the unsaturated zone decreases [*Masterson et al.,* 2014] and groundwater will impact roads, septic systems, underground utilities, and foundations in areas where the groundwater is currently near the ground surface[*Walter et al.,* 2016].

The effect of rising groundwater on pavement performance has been investigated. Full-scale pavement tests conducted in Florida test pits found more than a 50% reduction in the resilient modulus of granular subgrade layers when the groundwater table rises 24 in. (61 cm) to the bottom of the base layer [*Ping et al.,* 2010]. A study of SLR and increased precipitation on roads along the Gold Coast in Australia found approximately 1.9 mi (3.0 km) (32%) of roadway will be at high risk of failure by 2070 when groundwater is predicted to be less than 3.3 ft (1.0 m) below the pavement surface [*Roshani,* 2014]. Similarly, SLR-induced groundwater rise was found to reduce coastal-road pavement life by 50% from fatigue-cracking distress and up to 90% from rutting distress when groundwater moves into the pavement base layers [*Knott et al.,* 2017].

Climate-change adaptation studies assess the vulnerability of assets, choose appropriate climate-change scenarios, identify adaptation strategies, and recommend actions that may be robust or flexible [*Kirshen, Caputo et al.,* 2014]. Studies have shown that some pavement

structures are more resilient to rising groundwater than others[*Elshaer et al.,* 2017b; *Salour et al.,* 2015], but to date, no studies have quantified the cost and benefits of strategies to mitigate pavement impacts from SLR-induced groundwater rise. The implementation of targeted adaptation actions to vulnerable coastal-road infrastructure will save money through damage avoidance [*Knott et al.,* 2017].

The objective of this research is to identify pavement structures that will preserve pavement service life in the face of SLR-induced groundwater rise. It provides a quantitative assessment of pavement strains for projected groundwater levels and compares service-life reductions in terms of fatigue and rutting across different pavement structures. Pavement construction costs and road-surface elevations are evaluated to determine cost-effective strategies to prevent premature pavement failure as rising groundwater weakens the pavement supporting layers and inundates the pavement surface. While rising temperatures may also weaken pavements [*Mallick and El-Korchi,* 2013], this investigation considers only the effects of SLR-induced groundwater rise on pavement service life. Fatigue cracking and rutting are evaluated independently, and it is assumed that no pre-existing distresses exist in the pavement evaluation sites. In reality, these distresses are coupled and exist to some degree in the pavement structure; consequently, pavement failure will likely occur sooner than predicted in this analysis. SLR-induced groundwater rise projections are limited to the SLR scenarios chosen for this study.

4.2 BACKGROUND

4.2.1 Study Area

The study area is 158 mi^2 (410 km^2) in the NH Seacoast region where there is approximately 18 miles (29 km) of shoreline [*Mack,* 2009]. The study area is bounded by the Piscataqua Estuary in the north, Great Bay and the Squamscott River in the west, the Massachusetts border

in the south and the Gulf of Maine in the east (Figure 4-1).

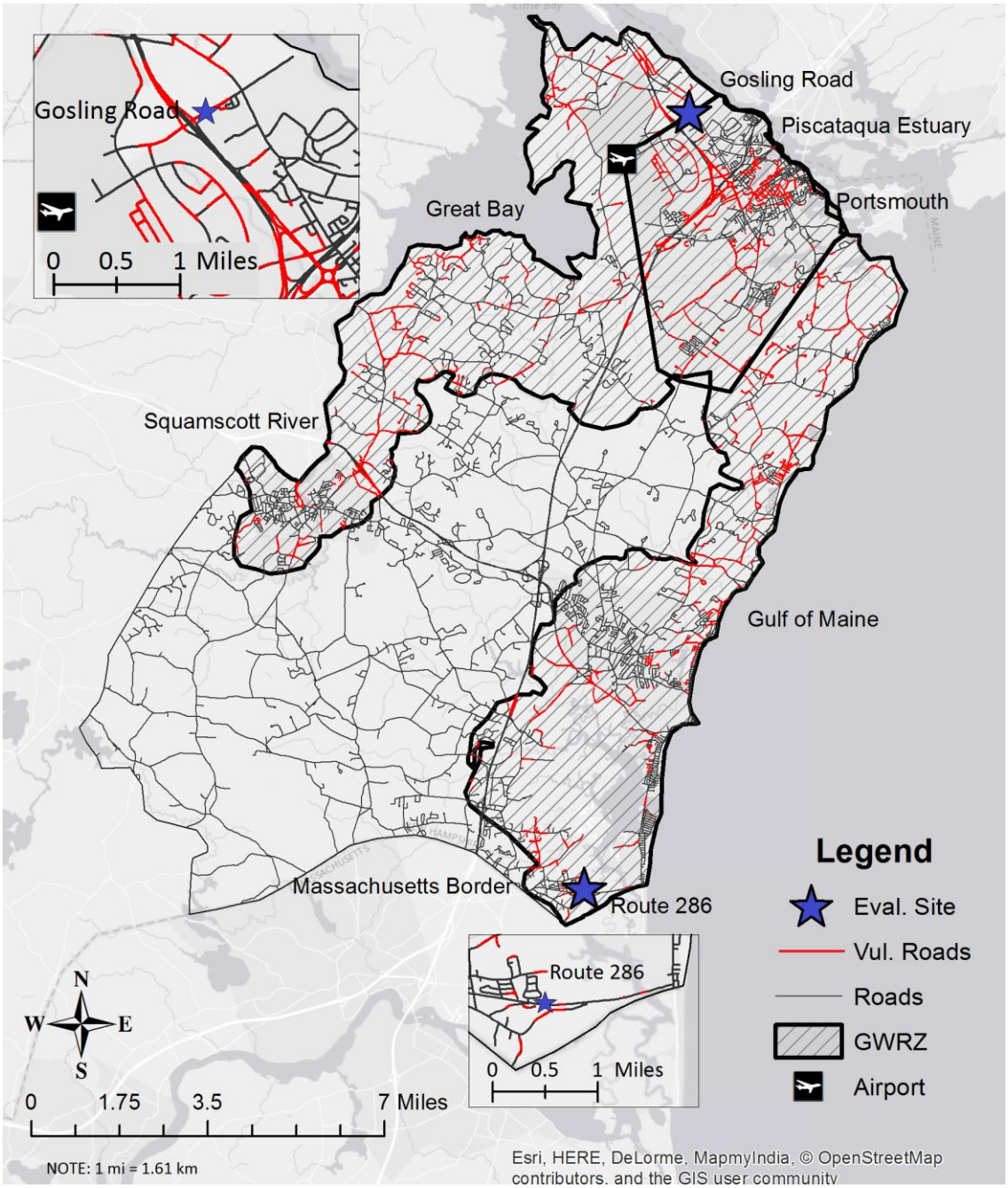

Figure 4- 1. Study area in coastal NH. The NH-GWRZ is the projected area of SLR-induced groundwater rise. Two case-study sites, Gosling Road and Route 286, were chosen for the evaluation of adaptation strategies.

4.2.2 Groundwater Modeling

Groundwater modeling, using USGS MODFLOW-2005[*Harbaugh,* 2005], was conducted to identify the NH groundwater-rise zone (NH-GWRZ) within the study area (Figure 4-1). This is the land area where groundwater is projected to rise with SLR [*Knott et al.,* 2017]. SLR scenarios of 1.0 ft (0.3 m), 2.7 ft (0.8 m), 5.2 ft (1.6 m) and 6.6 ft (2.0 m) in early-century (2030), mid-century (2060) and end of century (2090 and 2100) were simulated [*Parris et al.,* 2012]. Results demonstrate that groundwater rise will extend more than three to four times farther inland than surface-water impacts [*Knott et al.,* 2017]. Approximately 23% (146 mi, 235 km) of the region's roads, or 30% of NH-GWRZ roads, currently have groundwater less than 5.0 ft (1.5 m) below the road surface and are vulnerable for pavement damage. In addition, road-surface inundation is projected to occur in approximately14% (20 mi, 32 km) of these roads with 6.6 ft (2.0 m) SLR.

4.2.3 Case Study Sites

In a previous study, the pavement service-life reduction was determined at five pavement evaluation sites using simulated groundwater levels corresponding with the SLR scenarios. All pavements are projected to experience service-life reductions with groundwater rise, the magnitude of which depends on the location, local hydrogeology, and pavement structure [*Knott et al.,* 2017]. Two case-study sites, Route 286 and Gosling Road, were chosen for this study based on the projected service-life reduction and criticality with input from the NH Department of Transportation (NHDOT), regional planning commissioners, and the NH Department of Environmental Services (NHDES) (Figure 4-1).

Route 286 is an east-west 2-lane highway spanning Seabrook, NH and Salisbury, Massachusetts. It is an evacuation route from a popular tourist area along the Atlantic shoreline and the evaluation site is located approximately 1.3 mi (2.1 km) from the coast and within 400 ft (122 m) of a coastal wetland. Gosling Road, located in Newington, NH, is a 4-lane local road providing access to the Portsmouth International Airport at Pease and a local shopping mall. The evaluation site is located 0.8 mile (1.3 km) from the Piscataqua River.

4.3 MATERIALS, METHODS, AND DATA

4.3.1 Pavement Evaluation

4.3.1.1 Pavement Profiles and Material Properties

Pavement profiles were constructed with information from NHDOT construction plans [*NHDOT,* 2016] and boring logs from the NH Geological Survey and NHDES [*Knott et al.,* 2017]. The material properties for the existing pavement structure with the current groundwater table are presented in Table 4-1. The AC, base and subbase material resilient modulus values are estimated from AASHTO correlation charts [*Christopher et al.,* 2006] using NHDOT layer coefficients determined from field tests [*Janoo,* 1994; *NHDOT,* 2014]. Subgrade resilient modulus values were obtained from laboratory tests of subgrade soil types typically found in NH [*Janoo et al.,* 1999]. Poisson's ratio of unbound materials was assigned to each lithographic layer per its AASHTO soil classification [*Christopher et al.,* 2006]. The soil beneath the groundwater table is fully saturated and the unsaturated soil above the groundwater table is assumed to be at optimum moisture content used for pavement design. The ratio of resilient modulus at full saturation to resilient modulus at optimum moisture content (M_{Rsat}/M_{Ropt}) is assumed to be 0.5 for the unbound materials based on MEPDG guidance [*AASHTO,* 2008]. The AC dynamic modulus fluctuates with temperature but was assumed to be constant to isolate the effect of rising groundwater.

Table 4- 1. Material properties and input parameters for multi-layer elastic analysis at Route 286 and Gosling Road with saturation

Road & Tier Classification	Layer Type	Material	AASHTO Class	Resilient Modulus (psi)	Poisson's Ratio	Thickness (in.)	U/S
Route 286 (Regional Corridor)	Asphalt	HMA	na	325,000	0.35	5.5	U
	Base	Gravel	A-1-a	15,000	0.35	16	U
	Subgrade	Sand	A-3	3,800	0.30	1	U
				1,900	0.30	105	S
		Sand & gravel	A-1-b	19,250	0.35	294	S
		Clay	A-7-6	1,500	0.45	180	S
		Till	A-2-7	3,250	0.25	12	S
		Bedrock	na	725,000	0.20	infinite	S
Gosling Road (Local Road)	Asphalt	HMA	na	325,000	0.35	4	U
	Base 1	Crushed gravel	A-1-a	21,000	0.35	12	U
	Base 2	Gravel	A-1-a	15,000	0.35	12	U
	Subbase	Sand	A-3	4,500	0.30	8	S
	Subgrade	Silt	A-4	8,250	0.33	40	S
		Gravel	A-1-a	19,250	0.35	24	S
		Sand & silt	A-2-4	4,500	0.25	24	S
		Till	A-2-7	10,250	0.25	infinite	S

NOTE: 1 in. = 25.4 mm, 1 psi = 6.89 kPa, na = not applicable, U = unsaturated, S = saturated

4.3.1.2 Multi-Layer Elastic Analysis

KENLAYER computer software [*Huang*, 2003] was used to determine changes in pavement response to loading resulting from SLR-induced groundwater rise under full bond and full slip interlayer conditions. KENLAYER is based on multi-layer elastic theory that assumes each pavement layer is continuous, homogeneous, isotropic and linearly elastic. Loading was kept constant at 9000 lb (4086 kg) single axle single tire with a contact radius of 4.89 in. (12.4 cm) using the methodology presented in Knott et al. [*Knott et al.*, 2017]. The number of cycles to failure (N_f) for fatigue cracking and rutting were determined from the horizontal tensile strain calculated at the bottom of the AC layer and the vertical compressive strain calculated at the top of the subgrade using transfer functions developed by the Minnesota Department of Transportation [*Timm et al.*, 1999]. Pavement service-life reduction is represented by the ratio of the N_f for

the predicted groundwater condition (N_{fp}) to the N_f for the current groundwater condition (N_{fc}). After analyzing the existing structure, structures were modified and fatigue and rutting N_f's were calculated with the projected groundwater levels to determine viable adaptation strategies.

4.3.2 Adaptation Options

Adaptation options chosen for analysis were based on input from NHDOT and local planners. These include changes in layer thicknesses and base/subbase material types with the goal to meet or exceed a performance threshold. Increases in road-surface elevation with the new structure are considered beneficial by delaying road-surface inundation from surface water or groundwater. Route 286 crosses a coastal wetland and does not have many adjacent properties; consequently, it is possible to increase the road-surface elevation without major adjacent-road modifications. Gosling Road has adjacent properties, including a shopping mall, and a nearby overpass making increases in road-surface elevation impractical. In this analysis, adaptation options that raise the road surface at the Gosling Road site are not considered.

The adaptation options analyzed for Route 286 and Gosling Road are presented in Table 4-2. These options are not exhaustive but are used to illustrate the methodology.

Table 4- 2. Adaptation options analyzed for Route 286 (regional corridor) and Gosling Road (local road) in the order of increasing construction complexity

Description	AC Thickness (in.)	Base 1 Thickness (in.)	Base 1 Material	Base 2 Thickness (in.)	Base 2 Material	Subbase Thickness (in.)	Subbase Material
Route 286							
Existing structure	5.5	16.0	G	na	na	na	na
Increase AC thickness	6.0	16.0	G	na	na	na	na
	6.5	16.0	G	na	na	na	na
	8.0	16.0	G	na	na	na	na
	8.5	16.0	G	na	na	na	na
	9.0	16.0	G	na	na	na	na
Increase G thickness	5.5	20.0	G	na	na	na	na
	6.0	20.0	G	na	na	na	na
	5.5	24.0	G	na	na	na	na
	6.0	24.0	G	na	na	na	na
	5.5	28.0	G	na	na	na	na
Add RSB on top of G base	5.5	12.0	RSB	16.0	G	na	na
Add CS on top of G base	5.5	8.0	CS	16.0	G	na	na
	6.0	8.0	CS	16.0	G	na	na
	5.5	12.0	CS	16.0	G	na	na
	5.5	16.0	CS	16.0	G	na	na
Replace G base CG	5.5	20.0	CG	na	na	na	na
	5.5	24.0	CG	na	na	na	na
	5.5	28.0	CG	na	na	na	na
Replace G base with CS	5.5	20.0	CS	na	na	na	na
	5.5	24.0	CS	na	na	na	na
	5.5	28.0	CS	na	na	na	na
Replace G base with CG, add CS	5.5	12.0	CS	12.0	CG	na	na
	5.5	16.0	CS	12.0	CG	na	na
Gosling Road							
Existing structure	4.0	12.0	CG	12.0	G	8.0	S
Increase AC, decrease CG base	5.0	11.0	CG	12.0	G	8.0	S
	6.0	10.0	CG	12.0	G	8.0	S
Increase AC, replace CG base, decrease thickness	5.0	11.0	CS	12.0	G	8.0	S
	5.0	11.0	RSB	12.0	G	8.0	S
Keep AC thickness constant, replace base and subbase layers	4.0	12.0	CS	12.0	G	8.0	S
	4.0	12.0	CS	12.0	CS	8.0	S
	4.0	12.0	CS	12.0	CS	8.0	G
	4.0	12.0	CS	12.0	CS	8.0	CS

NOTE: AC= asphalt concrete, G = gravel, CS = crushed stone, CG = crushed gravel, RSB = reclaimed stabilized base; 1 in. = 25.4 mm

Pavement structures that meet the following performance threshold are considered viable adaptation strategies:

$$\frac{N_{fn}}{N_{fe}} \geq 1 \quad (4.1)$$

Where N_{fn}/N_{fe} is the relative pavement life, N_{fn} is the number of cycles to failure with the new pavement structure and projected groundwater levels, and N_{fe} is the number of cycles to failure with the existing pavement structure and existing groundwater level. The relative pavement-life ratios (N_{fn}/N_{fe}) calculated using the lowest N_f (worst case) of the two interface bond conditions (full bond and full slip) and the two distresses (fatigue cracking and rutting) are presented.

4.3.3 Adaptation Cost Analysis

Adaptation costs were calculated for each of the adaptation options. Costs included the NHDOT material, excavation, and construction costs required to enhance the existing structure to achieve the adaptation option. Material costs were estimated by converting the unit costs to cost/sq. yd.-in. and multiplying by the thickness of additional or replacement material. Excavation costs were estimated for structures requiring AC removal and base material replacement. Construction unit costs were estimated using machine operation and productivity values from Valle et al. [*Valle et al.,* 2017]. The unit costs [*NHDOT,* 2017] and the resilient modulus [*Christopher et al.,* 2006; *Janoo,* 1994; *NHDOT,* 2014] for the materials used in this analysis are presented in Table 4-3.

Table 4- 3. Material and construction costs for New Hampshire pavements [*NHDOT*, 2017] with resilient modulus

Description	Unit Costs ($/yd^2-in.)	Resilient Modulus (psi)
Material:		
Asphalt concrete (AC)	3.64	325,000
Crushed stone	0.60	31,000
Reclaimed stabilized base (RSB)	0.14	31,000
Stone for RSB	0.83	31,000
Crushed gravel	0.82	21,000
Gravel	0.66	15000
Sand	0.45	9,000
Construction costs:		
Asphalt concrete	11.23	
Base and subbase	1.17	
Excavation	0.20	

NOTE: $1.00/yd^2-in. = $0.47/m^2-cm, 1 psi = 6.89 kPa

The adaptation strategies meeting the performance threshold for both 1.0 and 2.7 ft SLR scenarios are presented with the costs to illustrate the most cost-effective adaptation options. The road-surface elevations corresponding with various pavement structures are also discussed with respect to future road-surface inundation.

4.4 DISCUSSION OF RESULTS

4.4.1 Pavement Service-Life Reduction – Existing Structures

The existing pavement structures and the simulated groundwater levels for the current condition and SLR scenarios are presented in Figure 4-2. The corresponding pavement service-life reductions caused by SLR-induced groundwater rise are also shown.

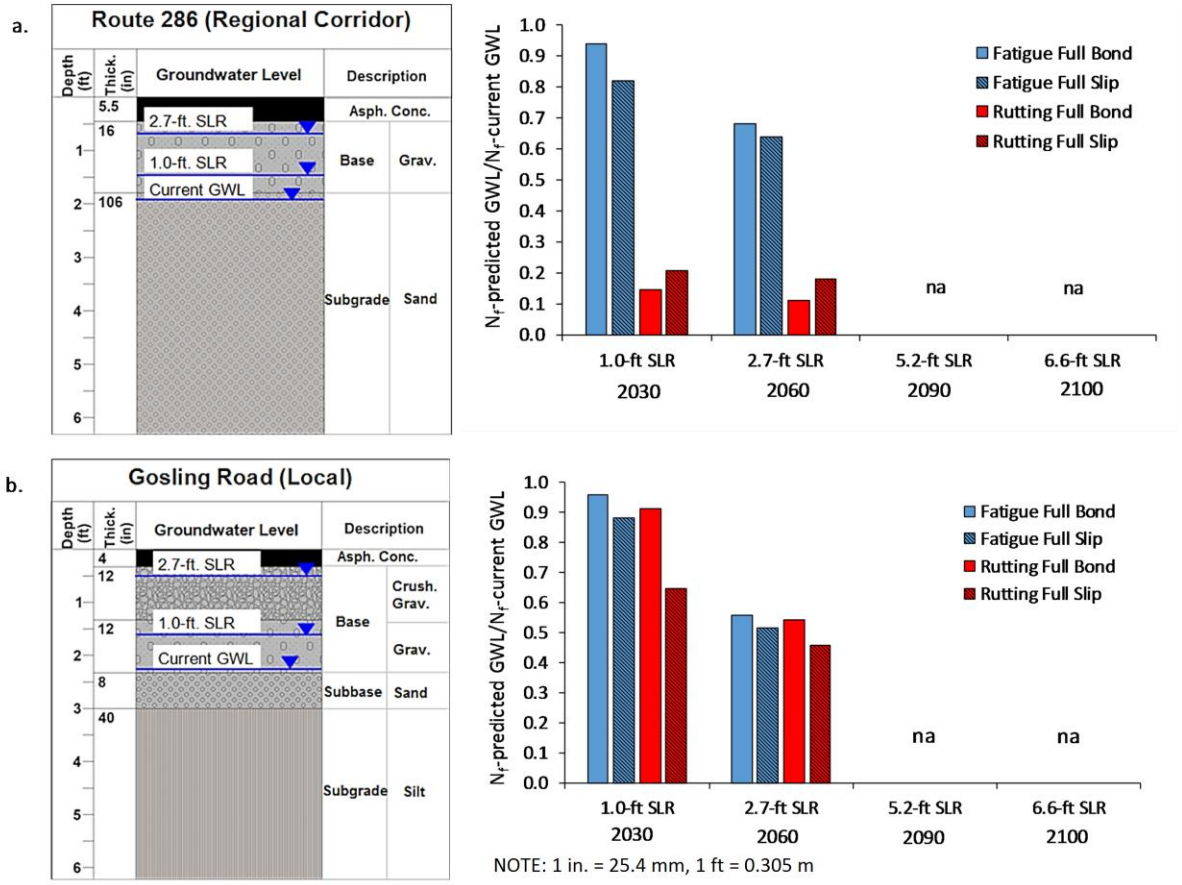

Figure 4- 2**.** Existing pavement structures to a depth of 6.0 ft (1.8 meters) and pavement service-life ratios (N_{fp}/N_{fc}) with SLR-induced groundwater rise: (a) Route 286 (regional corridor) and (b) Gosling Road (local road) [*Knott et al.,* 2017] (SLR = sea-level rise, GWL = groundwater level, na = road surface is flooded).

Groundwater rises into the pavement base layers at both case-study sites with 1.0 ft (0.3 m) and 2.7 ft (0.8 m) SLR and the road surfaces are projected to be flooded with groundwater inundation (GWI) between the years 2060 and 2090. Rutting controls pavement failure at the Route 286 evaluation site due to the relatively thin gravel base. In contrast, fatigue failure is the controlling factor at Gosling Road with a thin AC layer atop a more robust base and subbase structure. The controlling distress for pavement failure is indicated by the lowest N_f between rutting and fatigue. Route 286 is projected to experience approximately 80 to 90% service-life

reduction from rutting by 2030 with 1.0 ft (0.3 m) SLR as groundwater moves into the pavement base layer. Assuming a standard design life of 20 years with appropriate maintenance, this represents a service-life reduction of 16 to 18 years if adaptation strategies are not implemented. Gosling Road is projected to experience only slightly more than 10% service-life reduction from fatigue cracking with 1.0 ft (0.3 m) SLR increasing to approximately 45% with 2.7 ft (0.8 m) SLR predicted by 2060. Consequently, rising groundwater is projected to reduce the pavement service life by only 2 years by 2030 and 9 years by 2060 if adaptation strategies are not implemented. Rutting may become more of a factor at Gosling Road if the AC is weakened by rising temperatures associated with climate change.

Road-surface inundation is projected to occur at Route 286 in the mid-to-late 2070s with standing-water depth slightly less than 7 in. (15 cm) predicted with 5.2 ft (1.6 m) SLR by year 2090 increasing to 13 in. (33 cm) with 6.6 ft (2.0 m) SLR by end of century. GWI is projected to occur sooner (by year 2070) at Gosling Road with standing-water depth on the road surface approximately 13 in. (33 cm) by 2090 increasing to 21 in. (53 cm) by year 2100.

In summary, pavement-service life reduction from SLR-induced groundwater rise at the Route 286 site will occur sooner and be more severe than at the Gosling Road site because of the thin base layer in the Route 286 pavement structure. GWI, on the other hand, is projected to occur more than 5 years earlier at the Gosling Road site with greater standing-water depth than at the Route 286 site.

4.4.2 Adaptation Strategies and Costs

4.4.2.1 Route 286 (Regional Corridor)

Pavement analysis results for the Route 286 adaptation options are presented in Table 4-4. Only the groundwater levels for 1.0 ft (0.3 m) and 2.7 ft (0.8 m) SLR were considered in this analysis since GWI is projected with 5.2 ft (1.6 m) SLR and beyond. The options are ordered by increasing construction complexity with simple AC overlays the easiest to implement and base and subbase material replacement the most complex. Options meeting the performance threshold for both SLR scenarios have the N_f ratios highlighted in **BOLD**.

Table 4- 4. Route 286 adaptation options with the resultant pavement service life relative to the existing conditions represented by N_{fn}/N_{fe} for 1.0 ft and 2.7 ft SLR

AC Thick-ness	Base -1: Thick-ness and Mate-rial		Base -2: Thick-ness and Mate-rial		Road-Surface Elevation Increase	Control-ling Distress	Resultant Pavement Life (N_{fn}/N_{fe})		Adapta-tion Costs
(in.)	(in.)	Material	(in.)	Material	(in.)		1.0-ft SLR	2.7-ft SLR	$/yd^2
Existing structure									
5.5	16	G	0	na	0.0	Rutting	0.15	0.11	0.00
Increase AC layer thickness									
6.0	16	G	0	na	0.5	Rutting	0.20	0.16	7.44
6.5	16	G	0	na	1.0	Rutting	0.28	0.22	14.87
8.0	16	G	0	na	2.5	Rutting	0.69	0.59	37.18
8.5	16	G	0	na	3.0	Rutting	0.92	0.79	44.62
9.0	16	G	0	na	3.5	Rutting	**1.21**	**1.05**	52.06
Increase gravel base thickness									
5.5	20	G	0	na	4.0	Rutting	0.37	0.28	90.23
6.0	20	G	0	na	4.5	Rutting	0.49	0.37	97.67
5.5	24	G	0	na	8.0	Fatigue	**1.23**	0.83	97.59
6.0	24	G	0	na	8.5	Fatigue	**1.68**	**1.16**	105.02
5.5	28	G	0	na	12.0	Fatigue	**1.40**	**1.00**	104.94
Add reclaimed stabilized base on top of gravel base									
5.5	12	RSB	16	G	12.0	Fatigue	**1.41**	**1.29**	102.93
Add crushed stone on top of gravel base									
5.5	8	CS	16	G	8.0	Fatigue	**1.05**	0.90	97.09
6.0	8	CS	16	G	8.5	Fatigue	**1.42**	**1.24**	104.53
5.5	12	CS	16	G	12.0	Fatigue	**1.41**	**1.29**	104.20
5.5	16	CS	16	G	16.0	Fatigue	**1.86**	**1.77**	111.30
Replace gravel base with crushed gravel									
5.5	20	CG	0	na	4.0	Fatigue	**1.29**	0.81	125.95
5.5	24	CG	0	na	8.0	Fatigue	**1.59**	**1.01**	133.94
5.5	28	CG	0	na	12.0	Fatigue	**1.84**	**1.27**	141.93
Replace gravel base with crushed stone									
5.5	20	CS	0	na	4.0	Fatigue	**1.77**	**1.00**	121.54
5.5	24	CS	0	na	8.0	Fatigue	**2.24**	**1.33**	128.65
5.5	28	CS	0	na	12.0	Fatigue	**2.62**	**1.76**	135.75
Replace gravel base with crushed gravel and add crushed stone									
5.5	12	CS	12	CG	8.0	Fatigue	**2.53**	**1.21**	131.29
5.5	16	CS	12	CG	12.0	Fatigue	**2.84**	**1.67**	138.40

NOTE: AC = asphalt concrete, G = gravel, CS = crushed stone, CG = gravel, RSB = reclaimed stabilized base, na = not applicable; SLR = sea-level rise; BOLD = meets performance threshold; 1 in. = 25.4 mm, 1 ft = 0.305

The distress controlling pavement failure switches from rutting, in the existing structure, to fatigue cracking in all adaptation options with gravel-base thicknesses more than 20 in. (51

cm). An AC layer thickness of 9.0 in. (23 cm) or more with the existing 16 in. gravel base will provide enough protection for the weakened underlying layers with 1.0 and 2.7 ft (0.3 and 0.8 m) SLR projected to occur by 2030 and 2060, respectively. AC overlays less than 3.5 in. (9 cm) thick (with the existing base structure) will not prevent premature rutting failure with rising groundwater by year 2030. Pavement structures that meet the performance threshold without increasing the AC thickness include adding 12 in. (30 cm) crushed-stone atop the existing 16 in. (41 cm) gravel base or substituting 12 in. reclaimed stabilized base (RSB) supplemented with crushed stone to achieve the same adaptation result. In addition, options with a 28 in. (71 cm) gravel base, 24 in. (61 cm) crushed-gravel base, or 20 in. (51 cm) crushed-stone base will meet the performance threshold for both SLR scenarios.

The road-surface elevation is an important consideration for both case-study sites because the road surfaces are projected to be inundated between 2060 and 2080. Continuous road-surface flooding will render Route 286 useless as an evacuation route unless actions to raise the road are implemented. The increase in road-surface elevation is shown for each option in Table 4-4. Road-surface elevation increases of 3.5 in. (8.9 cm) and 12.0 in. (30 cm) are projected to delay GWI by 8 and 20 years, respectively. Viable adaptation options with road-surface elevation increases of 12 in. (30 cm) or more are those with granular base layers at least 28 in. (71 cm) thick.

The viable Route 286 adaptation options, i.e. those that exceed the performance threshold for both SLR scenarios, are presented with costs in Figure 4-3. The adaptation costs range from \$52/yd^2 to \$142/yd^2 (\$62/m^2 to \$170/m^2). A large cost increase from \$52/yd^2 to \$103/yd^2 (\$62/m^2 to \$123/m^2) occurs when the underlying base layers require modification and remains relatively constant at \$105/yd^2 (\$126/m^2) for next the four options.

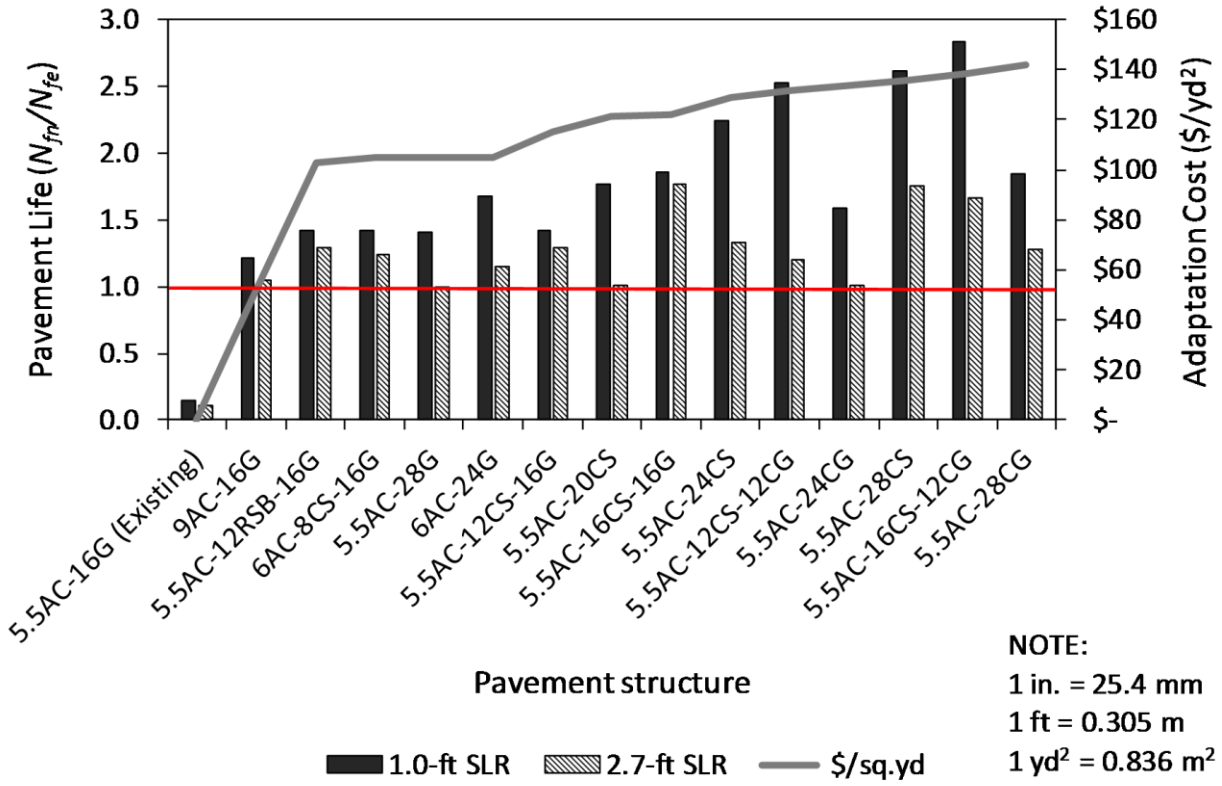

Figure 4- 3. Route 286 (regional corridor) adaption strategies meeting the performance threshold for 1.0 ft and 2.7 ft SLR with construction costs (thickness in inches, AC = asphalt concrete, G = gravel, CS = crushed stone, CG = crushed gravel, SLR = sea-level rise).

The least expensive option (9AC-16G) adds 3.5 in. (8.9 cm) of AC overlay to the existing pavement structure. This increases the designed (existing) pavement service life 20% with 1.0 ft (0.3 m) SLR and preserves the current service life to year 2060. It adds 3.5 in. (8.9 cm) additional elevation, delaying road-surface inundation by 8 years if the pavement is maintained and enhanced as groundwater rises. This option will not meet the performance criteria, however, if there is pre-existing rutting damage in the underlying layers. The existing pavement structure at Route 286 is projected to experience large service-life reductions from rutting distress with groundwater rise (Figure 4-2), so it is essential that adaptation actions be taken well before 2030 to prevent damage to the underlying layers. The current groundwater level at Route 286 is just

below the bottom of the base layer suggesting that this adaptation option, if chosen, should be implemented in the next renewal cycle to avoid the increased cost of rehabilitating the base layers.

When considering both the road-surface elevation and pavement life, the most cost-effective adaptation option (5.5AC-12RSB-16G) places 5.5 in. (13.0 cm) new AC atop 12 in. (30 cm) reclaimed stabilized base, all resting on the pre-existing 16 in. (41 cm) gravel layer. It increases the designed service life 40% and 30% with 1.0 and 2.7 ft (0.3 and 0.8 m) SLR, respectively. In addition, the road-surface elevation is increased 12 in. (30 cm), delaying inundation of the road surface until year 2100. This option has the best predicted performance of the four least-costly options and costs $\$103/yd^2$ ($\$123/m^2$), almost doubling the cost of the 9.0 in (23 cm) AC option. While expensive, it provides a stronger base, upon which AC overlays can be placed, extending the pavement life even further.

The most robust cost-effective option (5.5AC-16CS-16G) adds 16 in. crushed stone atop the existing 16 in. gravel layer. This option costs $\$122/yd^2$ ($\$146/yd^2$) and almost doubles the designed service life with 1.0 ft (0.3 m) SLR and increases it 80% with 2.7 ft (0.8 m) SLR. It also increases the road-surface elevation 16 in. (41 cm) making the evacuation route resilient to surface-water flooding and GWI beyond 2100.

4.4.2.2 Gosling Road (Local Road)

The Gosling Road pavement analysis results are presented in Table 4-5. The pavement surface was constrained to the existing elevation to accommodate adjacent properties. Fatigue cracking controls the pavement failure for the existing structure and all adaptation options considered at this location. Four options meet the performance threshold for the two SLR scenarios. Increasing the AC layer thickness from 4 to 5 in. (10 to 13 cm) while reducing the base layer

thickness to maintain the pavement surface elevation will provide enough protection for the weakened underlying layers with 1.0 and 2.7 ft (0.3 and 0.8 m) SLR. All pavement structures analyzed with 4 in. (10 cm) AC thickness, despite stiffening the base and subbase layers with crushed stone or crushed gravel, will suffer premature fatigue-cracking failure with rising groundwater between years 2030 and 2060.

Table 4- 5. Gosling Road adaptation options with resultant pavement service life relative to the existing condition represented by N_{fn}/N_{fe} for 1.0 and 2.7 ft SLR

AC	Base-1: Thickness and Material		Base-2: Thickness and Material		Subbase: Thickness and Material		Controlling Distress	Resultant Pavement Life (N_{fn}/N_{fe})		Adaptation Costs
(in.)	(in.)	Material	(in.)	Material	(in.)	Material		1.0-ft SLR	2.7-ft SLR	$/yd^2
Existing Structure										
4	12	CG	12	G	8	S	Fatigue	0.88	0.52	0.00
Increase AC layer while decreasing CG base layer										
5	11	CG	12	G	8	S	Fatigue	**1.62**	**1.17**	75.35
6	10	CG	12	G	8	S	Fatigue	**2.98**	**2.49**	90.42
Increase AC layer, replace CG base with stiffer material, and decrease thickness										
5	11	RSB	12	G	8	S	Fatigue	**2.04**	**1.35**	96.95
5	11	CS	12	G	8	S	Fatigue	**2.04**	**1.35**	97.04
Keep AC thickness constant and replace unbound layers with stiffer materials										
4	12	CS	12	G	8	S	Fatigue	**1.23**	0.63	83.94
4	12	CS	12	CS	8	S	Fatigue	**1.33**	0.73	107.61
4	12	CS	12	CS	8	G	Fatigue	**1.38**	0.76	123.88
4	12	CS	12	CS	8	CS	Fatigue	**1.43**	0.79	123.39

NOTE: AC = asphalt concrete, G = gravel, CG = crushed gravel, RSB = reclaimed stabilized base, CS = crushed stone, S = sand; SLR = sea-level rise; **BOLD** = meets performance threshold; 1 in. = 25.4 mm, 1 ft = 0.305 m

The viable Gosling Road adaptation options and costs are presented in Figure 4-4. The adaptation costs range from \$75/yd^2 to \$97/yd^2 (\$90/m^2 to \$116/m^2). The lowest-cost option removes 5 in. (13 cm) of surface material (AC and crushed-gravel base) and repaves with 5 in. (13 cm) of new AC. The underlying base and subbase materials remain untouched. It increases the designed pavement service life 60% with 1.0 ft (0.3 m) SLR and 17% with 2.7 ft (0.8 m) SLR. Replacing the base layers with various thicknesses of stiffer materials while keeping the AC layer thickness constant is more expensive and has no beneficial effect. The most robust adaptation option (6AC-10CG-12G-8S) has a projected pavement service life almost 3.0 and 2.5 times the designed service life at 1.0 ft (0.3 m) SLR and 2.7 ft (0.8 m) SLR, respectively. This option

thickens the AC layer from 4 to 6 in. (10 to 15 cm) while reducing the crushed gravel layer by 2 in. (5 cm). At \$90/yd^2 (\$108/m^2), it costs \$15/yd^2 (\$18/m^2) more than the low-cost alternative. If this adaptation option were implemented by 2020, with appropriate maintenance it should not fail from SLR-groundwater rise until the early 2070s when the road surface is projected to be flooded with GWI. The 1.0 ft (0.3 m) SLR annualized adaptation cost for the most robust option (\$1.52/yd^2-yr) is less than the annualized adaptation costs for the lowest-cost option (\$2.33/yd^2-yr) due the projected increase in pavement life.

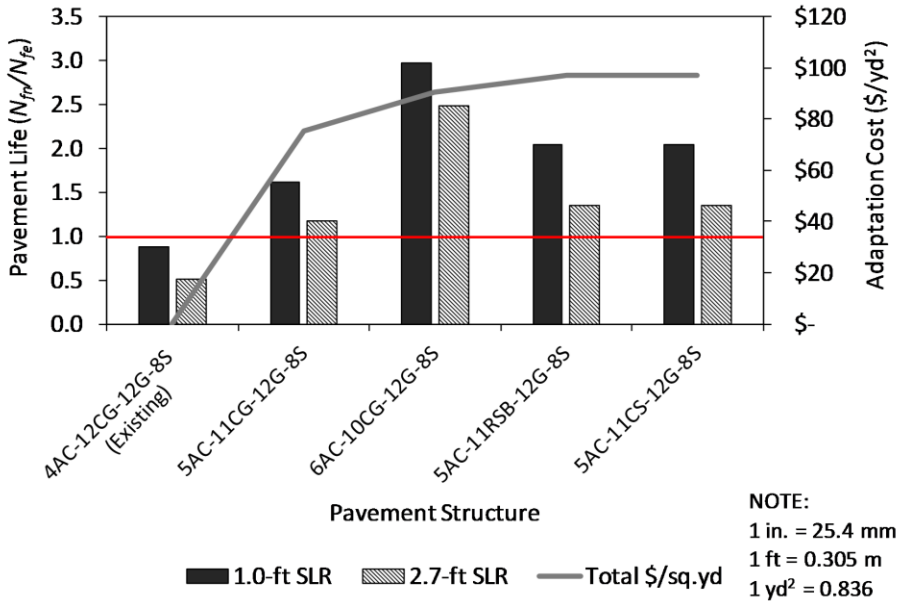

Figure 4- 4. Gosling Road (local road) adaption strategies meeting the performance threshold for 1.0 ft and 2.7 ft SLR with construction costs (thickness (in.), AC = asphalt concrete, G = gravel, CS = crushed stone, CG = crushed gravel, SLR = sea-level rise).

The analysis of adaptation options for Gosling Road assumes that it is not feasible to increase the road-surface elevation. If this constraint is relaxed, a 1, 4, and 12 in. (2, 10, and 30 cm) surface-elevation increase would delay GWI of the road surface by 2, 6, 18 years, respectively, beyond 2070. The costs of simply adding new asphalt overlays would be less than the

options requiring modification of the base layers, but adjacent property modifications (including a nearby overpass) would add to the overall cost of the adaptation project. Other adaptation options, beyond the scope of this study, might include active groundwater pumping to lower the groundwater table below the bottom of the pavement structure.

4.5 SUMMARY AND CONCLUSIONS

An interdisciplinary approach, coupling groundwater modeling and multi-layer elastic pavement analysis, has been used to assess various pavement structural designs that would be resilient in the face of SLR-induced groundwater rise. The groundwater model was used to define the NH-GWRZ and, coupled with lidar ground-surface elevations, used to identify vulnerable roads for four SLR scenarios projected out to year 2100. Approximately 23% (146 mi, 235 km) of roads in NH's Seacoast Region are at risk for premature pavement failure with 6.6 ft (2.0 m) SLR by 2100 if adaptation actions are not taken.

Two case-study sites, predicted to experience pavement service-life reduction, were investigated to determine the effectiveness of different adaptation options. A 2-lane regional connector and evacuation route, located near a coastal wetland, is predicted to experience pavement rutting-life reduction from groundwater rise in the coming decade, reaching 80% to 90% pavement-life reduction by 2030. Road-surface inundation is projected to occur by the mid-2070s. Adding 12 in. (30 cm) of reclaimed stabilized base atop the existing 16 in. (41 cm) gravel base was found to be the most cost-effective adaptation option to mitigate service-life reduction at this location. The 12 in. (30 cm) road-surface elevation increase delays pavement-surface flooding by approximately 20 years to the end of century. Applying AC overlays less than 3.5 in. (8.9 cm) thick in response to pavement distress will not protect this pavement structure from pre-mature

failure caused by SLR-induced groundwater rise.

An important 4-lane local road, providing access to a shopping mall and international airport is predicted to experience less service-life reduction, 10% by 2030 and 45% by 2060. Fatigue cracking, in contrast to rutting, controls pavement failure at this evaluation site because of a more robust underlying pavement structure; consequently, simply thickening the AC layer on top of the existing base layers is the most cost-effective adaptation option. Adjacent properties may render road-surface elevation increases infeasible at this location, in which case, it is possible to maintain the designed service life with rising groundwater by increasing the AC layer 1 to 2 in. with a corresponding reduction in crushed-gravel base thickness. The surface of the pavement is projected to be inundated with rising groundwater by the early 2070s.

Significant reductions in pavement service life with SLR-induced groundwater rise are predicted if no adaptation strategies are implemented. These reductions will potentially be more severe as the AC weakens with temperature increases caused by climate change. This investigation shows that when base layers are sufficient in material and thickness to protect the subgrade from rutting failure, increasing the AC layer thickness is sufficient to avoid the costs of premature failure from SLR-induced groundwater rise. Coastal roads with inadequate base layer thicknesses may experience premature rutting failure. It is recommended that the rehabilitation of these roads include projected SLR-induced groundwater rise and pavement temperature changes in design calculations to avoid the high costs of more frequent pavement failures. The adaptation options analyzed here were based on input from NHDOT and local planners, but it is unclear whether recommendations would be implemented. Considerations in addition to cost and performance, such as base-material availability and design practicality may also factor into implementation decisions.

Future work includes investigating the combined effect of climate-change-induced groundwater rise and increasing pavement temperatures on pavement service life over a broader range of climate scenarios. Future adaptation work will examine a staged response to groundwater and temperature rise where a series of shorter-term actions, such as rebuilding a more robust base, are implemented during major road maintenance projects and thicker AC overlays are applied in future steps.

CHAPTER 5 - SEASONAL AND LONG-TERM CHANGES TO PAVEMENT LIFE CAUSED BY RISING TEMPERATURES FROM CLIMATE CHANGE

5.1 INTRODUCTION

A key factor in a community's ability to be resilient with climate change is the integrity of the transportation network [*Muench and Van Dam,* 2015]. Given the long lifespan of roadways (50 to 100 years) transportation agencies should prepare for climate change in their long-term design strategies to avoid the costs of more frequent pavement maintenance, rehabilitation, and reconstruction [*Chinowsky et al.,* 2013; *Mallick et al.,* 2016]. Research on climate-change impacts to road infrastructure performance raises the possibility that the frequency and severity asphalt pavement damage will increase [*Meagher et al.,* 2012; *Mills et al.,* 2009].

Greenhouse gas emissions have caused an increase in global atmospheric and oceanic temperatures since the mid-20th century and the rate of warming is projected to increase through the 21st century and beyond [*USGCRP,* 2017]. The average annual temperature from 1986 to 2016 in the Northeast region is 0.79°C warmer than early in the century (1901 to 1960) [*Vose et al.,* 2017; *Vose et al.,* 2014]. Data analysis from 73 weather stations in New England and New York revealed a regional average 100-year temperature increase of approximately 1.1°C, which is more than the global average of 0.6°C over the same period [*Trombulak and Wolfson,* 2004]. The Northeast region is projected to continue this accelerated warming trend with a 2°C temperature rise predicted to occur 20 to 30 years sooner than the 2°C global mean temperature rise [*Karmalkar and Bradley,* 2017].

Pavement performance is sensitive to temperature and the variations and excess amounts of moisture in pavement sublayers [*Elshaer, Ghayoomi and Daniel,* 2017b; *Wang et al.,* 2016].

Higher temperatures reduce asphalt layer stiffness and strength [*Meyer et al.,* 2014] and increased moisture content reduces the stiffness of the underlying unbound layers [*Mallick and El-Korchi,* 2013]. Asphalt-layer stiffness is quantified by the temperature-dependent modulus of the hot mix asphalt (HMA). Higher temperatures reduce the asphalt-layer stiffness, primarily due to the properties of the viscoelastic asphalt binder [*Mallick and El-Korchi,* 2013]. Climate-change induced temperature changes were investigated in Australia where they found a 4°C increase in temperature resulted in a projected 4-year reduction in pavement life [*Kumlai et al.,* 2017]. Gudipudi et al. studied the impact of climate-change induced temperature increases on interstate highways in Arizona, Maine, Montana, and Virginia. They found daily temperature increases predicted to occur by mid-century (2040 to 2060) increased asphalt-layer fatigue cracking 2 to 9% and rutting 9 to 40% [*Gudipudi et al.*, 2017].

Rising temperatures also have the potential to change season length and seasonal average temperatures. Daniel et al. project a mid-century reduction in the frozen period in Maine and New Hampshire (NH) of at least 10 to 20% increasing to 30 to 40% by the end of century [*Daniel et al.,* 2017]. The temperature dependency of the asphalt-layer modulus makes pavement life vulnerable to changes in the seasons [*Orr and Irwin,* 2006]. Winter HMA modulus is approximately four to six times higher than typical summer modulus in northern portions of the United States [*Mallick and El-Korchi,* 2013; *Orr and Irwin,* 2006; *Tanquist,* 2001]. In addition, the underlying unbound materials are stronger and less susceptible to permanent deformation when the ground is frozen [*Swett,* 2007]. Departments of Transportation (DOTs) often allow heavier loads to travel on low volume roads during the freezing season and seasonal load restrictions are applied during spring thaw periods [*Daniel et al.,* 2017]. Researchers at the Minnesota Department of Transportation (MnDOT) have recognized the importance of modulus variations among

seasons and have incorporated them into MnDOT pavement design software MnPAVE [*Tanquist,* 2001; *Tanquist,* 2012].

Most previous studies have used the top-down (or scenario-based) approach; this uses climate-change scenarios [*de Bruin et al.,* 2009; *Kwadijk et al.,* 2010; *Smith et al.,* 2009] to identify potential future pavement-life reductions and promote enhanced, resilient pavement design *(1, 2, 4, 5).* This approach provides an understanding of pavement response but is limited by the temperatures (or scenarios) selected for the analysis. In contrast, the bottom-up (asset-based) approach focuses on an asset's response to a range of environmental parameters independent of climate-change scenarios. This approach has been used to assess climate-change impacts in hydrology-related projects including hydropower optimization *(23, 27)* and coastal zone management with sea-level rise *(26),* but not in pavement design. Because the bottom-up and top-down approaches both have strengths, integration of the two approaches achieves a more complete understanding of an engineered system's response to future climate change [*Kwakkel, Haasnoot et al.,* 2016; *Ray and Brown,* 2015; *Taner et al.,* 2017].

5.1.1 Research Objective and Approach

This research investigates the impacts of climate-change induced seasonal change and long-term impact on pavement life using a hybrid bottom-up/top-down approach. First, changes in season duration and seasonal average temperatures associated with 0.5°C incremental temperature rise are determined. Next, relationships between resilient modulus (M_R) and temperature from existing laboratory testing data are identified and used to predict changes in M_R. Layered-elastic analysis (LEA) is then used to predict pavement damage and seasonal contributions to total damage in a 2-lane regional connector in coastal NH with incremental temperature rise. A

top-down assessment using downscaled Global Climate Models (GCMs) is then superimposed to determine the timing of the effects [*Taner et al.,* 2017]. Finally, simple adaptation strategies to maintain design life with temperature rise are investigated.

Rutting and fatigue cracking are assumed to be the primary pavement structural distress mechanisms in this study. While other durability related pavement distresses will also be affected by climate change, flexible pavement design and rehabilitation activities are predominantly conducted in response to rutting, fatigue cracking, and thermal cracking. Thermal cracking distress is not expected to increase with warming temperature trends and therefore is not considered.

5.2 METHODOLOGY AND DATA

Statistically downscaled temperature data from GCMs were analyzed to determine representative daily average temperatures for four future 21-year periods in coastal NH. These projections were used to establish the temperature-rise limits and quantify changes in season duration and seasonal average temperatures. Resilient modulus (M_R) was analyzed as a function of temperature from existing laboratory testing data and seasonal multipliers were determined. MnPAVE software was used with temperature-dependent material properties and season lengths to determine changes in pavement life caused by 0.5°C incremental temperature rise from 0°C to the maximum temperature rise projected out to late-mid-century.

5.2.1 Temperature Projections

Identifying seasonal changes with temperature rise begins with evaluating daily average temperatures. Daily maximum and minimum temperatures for four 580 km^2 grids in coastal NH and northeastern MA were downloaded from the U.S. Bureau of Reclamation's Downscaled Climate and Hydrology Projections (DCHP) CMIP5 (Coupled Model Intercomparison Project

Phase 5) [*Reclamation,* 2016; *IPCC,* 2013]. The U.S. Department of Transportation (U.S. DOT) CMIP Climate Data Processing Tool [*ICF International,* 2016] was used to process output from up to 20 GCMs for each of three Representative Concentration Pathways (RCPs): RCP 4.5, 6.0 and 8.5. Daily temperature output from the multiple GCMs and the four spatial grids were averaged to produce daily average temperature projections for each RCP scenario. The GCMs and grid coordinates used in this analysis are presented in Appendix A.

Five 21-year periods were analyzed in this research: the observed and model baseline period (1979 to 1999), early-century (2000 to 2020), early-mid-century (2020 to 2040), mid-century (2040 to 2060), and late-mid-century (2060 to 2080). Representative daily average temperatures were determined by averaging over the 21 years in each period. In addition to the observed daily average temperatures, the three RCP scenarios and five 21-year periods result in a total of 15 combinations. Projected daily average temperature rise was determined for each RCP scenario by taking the difference between the model-ensemble average of the future representative daily average temperatures and the model-ensemble averages of the baseline daily average temperatures. The temperature-rise projections are presented in the results.

5.2.2 Pavement Evaluation

LEA was conducted using MnPAVE [*Tanquist,* 2012], a mechanistic-empirical pavement performance model created by MnDOT for pavement design. MnPAVE calculates seasonal contributions to pavement damage based on season duration, seasonal average temperatures, and seasonal changes to material properties. There are four input categories in MnPAVE: pavement structure, traffic, climate, and material properties [*Tanquist,* 2012].

5.2.2.1 Pavement Structure, Material Properties, and Traffic

The evaluation site pavement profile was constructed from NH Department of Transportation (NHDOT) construction plans [*NHDOT,* 2016] and boring logs from the NH Geological Survey and NH Department of Environmental Services [*Knott et al.*, 2017]. The pavement structure consists of 140 mm HMA, 406 mm gravel base, and 2692 mm sand [*NHDOT*, 2014]. The HMA binder grade is PG 58-34 and the M_R at 25°C is 1493 MPa [*Nemati et al.,* 2018]. The gravel base M_R is estimated to be 103 MPa from AASHTO correlation charts [*Christopher et al.,* 2006] and NHDOT layer coefficients [*Janoo,* 1994; *NHDOT,* 2014]. The sand subgrade M_R is estimated to be 62 MPa from tests conducted at the US Army Corps of Engineers Cold Regions Research and Engineering Laboratory (CRREL) [*Janoo et al.,* 1999]. MnPAVE [*Tanquist,* 2012] recommended values of Poisson's ratio were assigned to each lithographic layer, based on the AASHTO soil classification [*Christopher et al.,* 2006] and climatic inputs. The average groundwater depth is estimated from boring logs to be 700 mm beneath the pavement surface [*Knott et al.,* 2017]. The unbound material M_R is adjusted for moisture content using the methodology described in Elshaer [*Elshaer,* 2017]. In this methodology, the pavement layers are divided into sublayers and the matric suction is estimated from each sublayer-midpoint distance to the groundwater table. The degree of saturation is determined from the soil water retention curve (SWRC) for each soil type and used in the Witczak equation to calculate the M_R at the current moisture condition relative to the M_R at optimum moisture content [*Elshaer,* 2017; *Witczak, Houston et al.,* 2000; *Witczak, Andrei et al.,* 2000].

Traffic loading is described in terms of ESALs, defined in MnPAVE as one 80 kN dual tire axle with a 552 kPa tire pressure [*Tanquist,* 2012]. The average daily traffic at the pavement evaluation site is estimated to be 16,000, with 6% trucks, a truck factor of 0.24, lane distribution

factor of 1, an annual growth factor of 1.22%, and a design life of 20 years [*Seabrook Master Plan Steering Committee,* 2011]. Based on this information, 938,000 ESALs were used in the analysis.

5.2.2.2 Climate

Climate inputs to MnPAVE include five seasonal average air temperatures (fall, winter, spring 1, spring 2, and summer), season duration, and frost depth. Spring is divided into early spring (spr1) and late spring (spr2) to account for aggregate-base and subgrade-soil property changes during the spring thaw period [*Tanquist,* 2001]. The season definitions are presented in Table 5-1 [*Tanquist,* 2001].

Table 5- 1. Season definitions [*Tanquist,* 2001]

Season	Winter	Spring 1	Spring 2	Summer	Fall
Description	Layers are Frozen	Base Thaws; Subgrade is Frozen	Base Recovers; Subgrade Thaws	HMA Weak; Subgrade Recovers	HMA Recovers
Beginning	CFI > 90°C-days	CTI > 15°C-days	End of Spring 1	3-day T_{ave} > 17°C	3-day T_{ave} < 17°C
Ending	CTI > 15°C-days	28 days later	3-day T_{ave} >17°C	3-day T_{ave} < 17°C	CFI > 90°C-days

Note: CFI = Cumulative freezing index, CTI = Cumulative thawing index, T_{ave}=Daily aver-

The season duration and seasonal average temperatures for coastal NH were determined by applying the season definitions shown in Table 5-1 to the baseline and projected early-century, early-mid-century, mid-century, and late-mid-century daily average temperatures for the RCP 4.5, 6.0 and 8.5 scenarios. The cumulative freezing (CFI) and thawing (CTI) indices were calculated using MnDOT CFI and CTI equations and guidelines [*Minnesota Department of*

Transportation, 2014b]. The CFI and CTI begin with the first daily average temperature below freezing and above freezing, respectively. The seasonal average temperature increase was also calculated for the four future 21-year periods and the three RCP scenarios. The average maximum freezing depth for southeastern NH is estimated to be 1020 mm based on NH and MA observations [*FHWA*, 2008].

5.2.2.3 Temperature-Dependent Resilient Modulus

Temperature-induced changes in the HMA, unbound base, and subgrade M_R were estimated. The HMA M_R temperature adjustment was made using the FHWA Long Term Pavement Performance Program (LTPP) temperature adjustment factor [*FHWA*, 1998a]. This was applied to the HMA M_R measured at 25°C (1493 MPa) using the FWHA default slope parameter (-0.021). The asphalt temperature at one-third of the pavement thickness was calculated from air temperature using the Witczak equation [*Asphalt Institute*, 1982; *Shook et al.*, 1982; *Tanquist*, 2001].

The temperature-induced M_R changes for the unbound materials were estimated from M_R testing conducted on representative NH soil samples over temperatures ranging from -10 to 20°C by Janoo et al. (1999) at the CRREL [*Janoo et al.*, 1999]. The gravelly coarse sand (A-1-a) and fine sand (A-2-4) were used to represent the bank run gravel base and sand subgrade [*NHDOT*, 2014] in the pavement profile. The M_R variation for these soil types for temperatures below freezing is presented in Figure 5-1 [*Janoo et al.*, 1999]. Using the Shapiro-Wilk test [*Shapiro and Wilk*, 1965], the residuals for the bi-variate fit do not violate normality at the 0.05 significance level indicating a good fit for the two soil types.

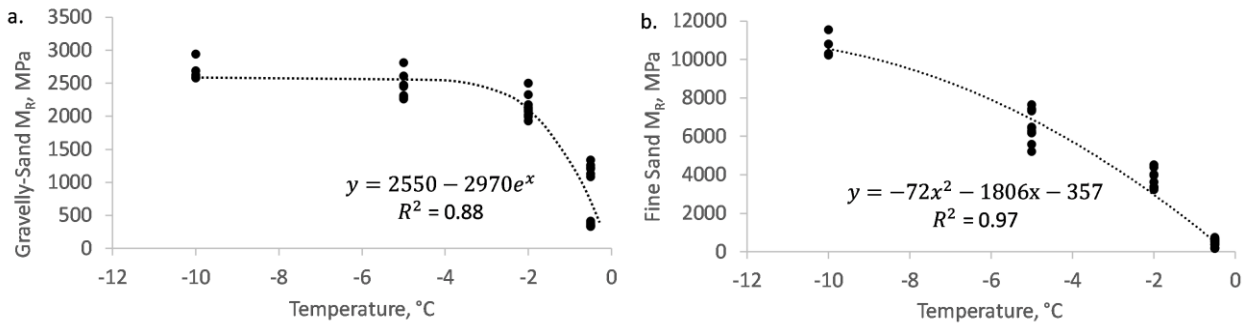

Figure 5- 1. Winter resilient modulus as a function of temperature for (a) gravelly coarse sand and (b) fine sand [*Janoo et al.,* 1999].

Table 5-2 presents the unbound material M_R values for a range of temperatures above freezing. The gravelly sand has a linear relationship between M_R and temperature. There is no significant difference between the mean M_R values (as indicated by t-tests) for the fine sand materials. These relationships were used to estimate the unbound material M_R with temperature rise.

Table 5- 2. Resilient modulus test results with temperatures above freezing for NH gravelly coarse sand and fine sand samples [*Janoo et al.,* 1999]

Material	Season	Temp. (°C)	Mean M_R (MPa)	Std. Dev. (MPa)	Lower 95% (MPa)	Upper 95% (MPa)	Passes t-test?
Gravelly Coarse Sand	Spring	0.5	286	21	260	311	Yes
		15	262	10	253	270	
		20	220	16	200	239	
	Summer to Fall	20	284	3	280	288	Yes
		0.5	315	6	309	322	
Fine Sand	Spring	0.5	51	7	47	55	No
		20	48	8	35	61	
	Summer to Fall	20	59	7	52	66	No
		5	55	9	48	62	
		0.5	52	8	45	58	

The effective M_R ($M_{R,eff}$) was also calculated using the AASHTO damage function [*AASHTO*, 1996]. Newer mechanistic-empirical approaches may have the ability to yield a better M_R equivalent, but the AASHTO damage function was chosen to be consistent with the Janoo et al. study [*Janoo et al.*, 1999]. The monthly ratio of $M_R/M_{R,eff}$ was determined and averaged over each season for the three RCP scenarios in each of the four future 21-year periods. These ratios were used as seasonal multipliers to determine the seasonal effect on unbound material stiffness as temperature rises.

5.2.2.4 Layered-Elastic Analysis

For each scenario and 21-year period, MnPAVE was run eleven times for an annual average temperature rise from 0 to 5°C in 0.5°C increments. Season duration, seasonal average temperature, and seasonal M_R for each layer were adjusted with temperature according to the established relationships. Pavement damage, defined as the number of ESALs divided by the predicted number of cycles to failure (N_f) (ESALs/N_f), was calculated for each incremental temperature change and the seasonal contribution to total damage was determined [*Tanquist*, 2012].

Preliminary adaptation strategies were evaluated. One strategy is to increase the layer thickness to maintain the design life despite the projected temperature rise. HMA and base-layer thicknesses were varied using MnPAVE to determine the thickness required to achieve a minimum 85% reliability (recommended for less than 1 million ESALs) for each incremental temperature rise [*Tanquist*, 2012]. Material costs were estimated for layer thickness increases [*NHDOT*, 2017].

5.3 DISCUSSION OF RESULTS

5.3.1 Projected Temperature Rise

Projected daily temperature rise from the baseline period (1979 to 1999) to 2080 ranges from 0 to 5°C as shown in Figure 5-2. The 95% confidence intervals in the projected annual average temperature rise are 0.7 to 0.8°C in early century, 1.3 to 1.6°C in early-mid-century, 2.0 to 2.8°C in mid-century, and 2.5 to 4.0°C in late-mid-century. Temperature rise varies by season with the maximum rise projected to occur in the winter and late summer seasons. The most variability in temperature rise among scenarios occurs in late winter/early spring and late fall. The temperature rise statistics are presented in Appendix A.

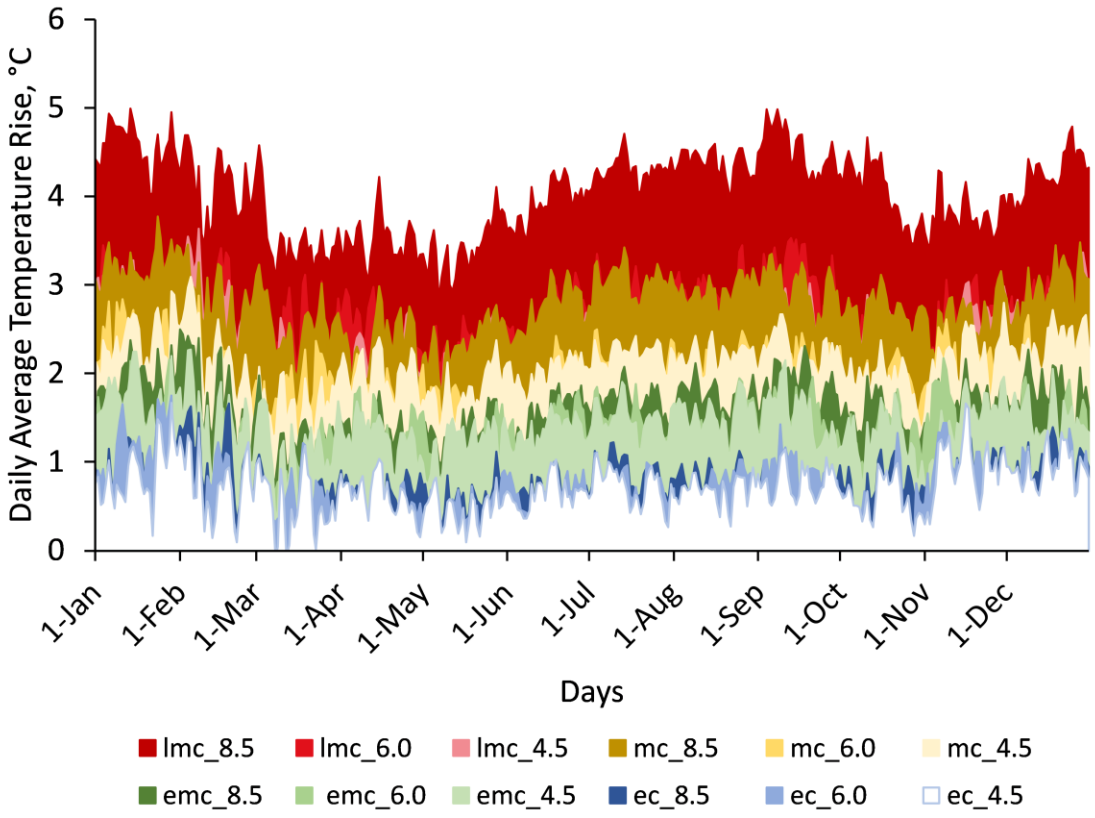

Figure 5- 2. Projected daily average temperature rise for four 21-year periods: early century (ec: 2000 to 2020), early-mid-century (emc: 2020 to 2040), mid-century (mc: 2040 to 2060), and

late-mid-century (lmc: 2060 to 2080) for RCP 4.5, 6.0 and 8.5 in coastal NH. Temperature rise is relative to the baseline daily average temperature from 1979 through 1999.

5.3.2 Projected Seasonal Changes with Temperature Rise

5.3.2.1 Season Duration

The change in pavement season length with annual average temperature rise is shown in Figure 5-3. Analysis of the linear-regression residuals using the Shapiro-Wilk test [*Shapiro and Wilk*, 1965] indicates a good fit for all seasons. There is a strong correlation between season duration and temperature rise (R^2 values > 0.8) for the fall, winter and summer seasons. Early spring is fixed at 28 days per the season definitions and late spring duration demonstrates a weak relationship with temperature rise. The fall season initially lengthens as the winter season decreases with temperature rise. When the annual average temperature rises more than 2.5°C, the winter season ceases to exist and is replaced by an expanded fall season. The fall season begins to shorten when temperature rise exceeds 2°C and summer continues to lengthen.

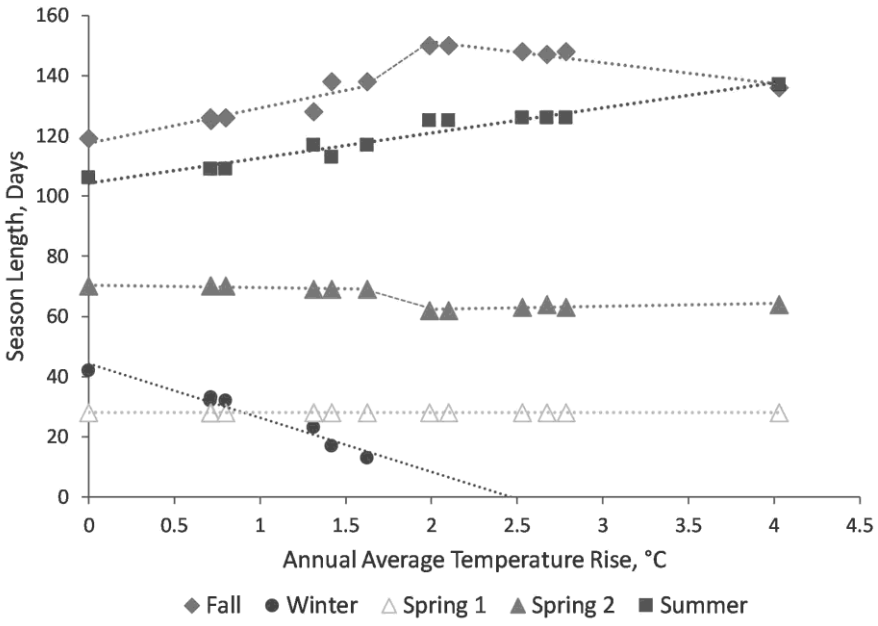

Figure 5- 3. Changes in season duration with average annual temperature rise. The five seasons are defined by projected cumulative freeze and thaw indices and 3-day average temperatures [*Tanquist,* 2001].

5.3.2.2 Seasonal Average Temperatures

Seasonal average temperatures also change with temperature rise. The seasonal average temperatures increase with annual average temperature rise in all seasons except fall. The average fall temperature initially decreases as fall replaces the shrinking winter season. At approximately 2°C temperature rise, the average fall temperature reaches a minimum and begins increasing with further warming. The winter average temperature exhibits the highest rate of seasonal temperature rise relative to the annual average.

5.3.3 Temperature-Dependent Resilient Modulus

The HMA modulus follows the seasonal temperature trends with temperature rise. The winter season at the pavement evaluation site currently has the highest HMA M_R at approximately 5200 MPa followed by early spring, fall, and late spring, respectively. Summer M_R is consistently lowest of all seasons at approximately 1400 MPa. The HMA loses stiffness continuously with temperature rise in all seasons except fall. The fall M_R increases initially corresponding with the fall seasonal temperature decline and reaches a maximum (3351 MPa) with 2°C temperature rise. It then declines with a gentler slope to 3031 MPa at 5°C temperature rise. The sharpest decline in HMA stiffness is projected to occur in winter, losing 14% between 0 and 2°C rise. Early spring M_R begins at approximately 4200 MPa declining at a steady rate of 186 MPa per degree temperature rise. Late spring M_R is closest to the annual average M_R beginning at approximately 2500 and 2600 declining to 1900 and 2100 MPa over 5°C of temperature rise, respectively. Summer M_R declines at a rate of 52 MPa per degree temperature rise.

Fine sand and gravelly coarse sand M_R to $M_{R,eff}$ ratios versus temperature rise are presented in Figure 5-4. Analysis of the bivariate-fit residuals indicates a good fit for both the fine sand and the gravelly-coarse sand for all seasons. The R^2 values for the relationships vary between 0.84 and 0.99 for the fine sand and between 0.81 and 0.96 for the gravelly coarse sand.

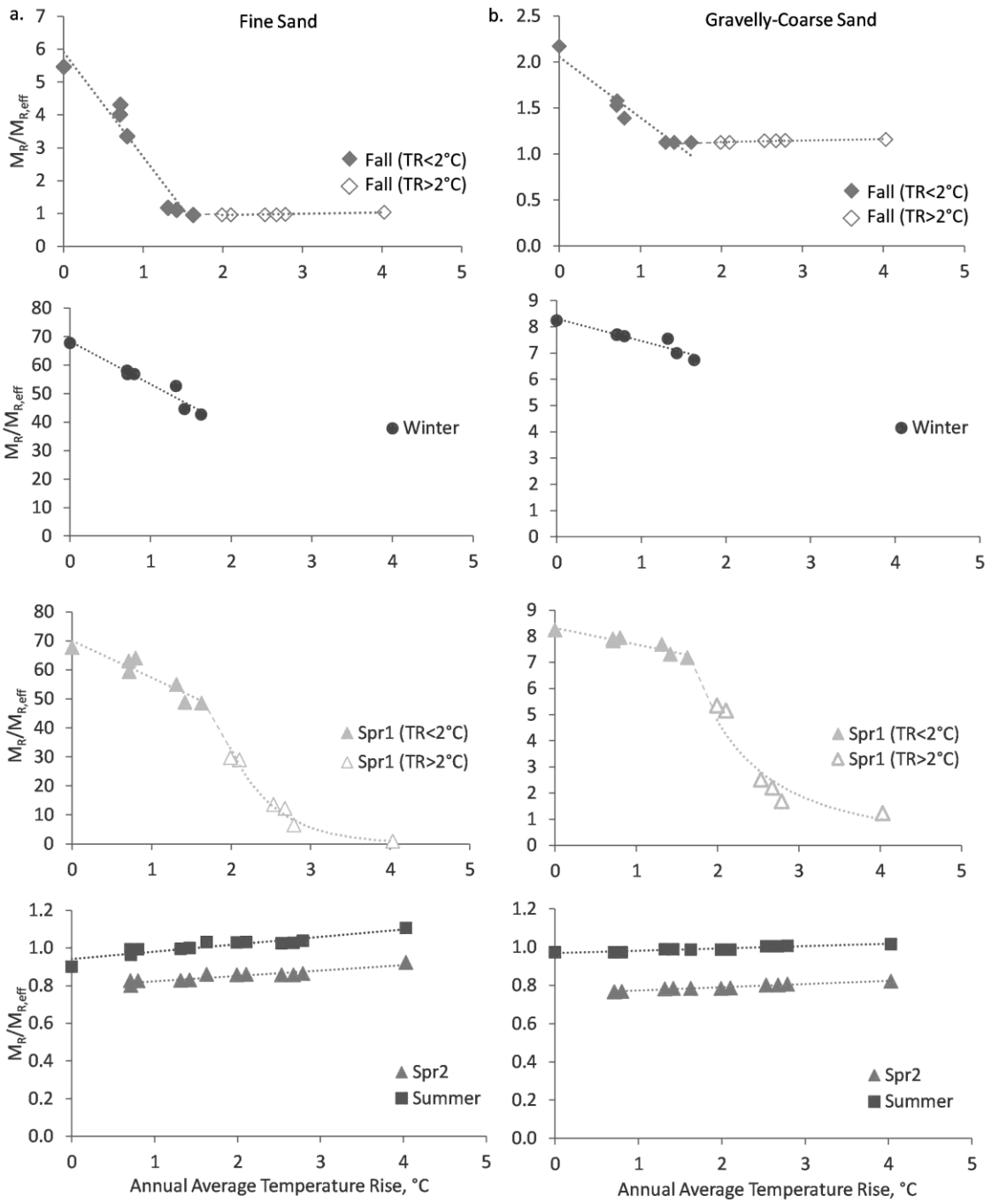

Figure 5- 4. Seasonal $M_R/M_{R,eff}$ for (a) fine sand and (b) gravelly coarse sand versus annual average temperature rise. Spr1 and Spr2 represent early and late spring, respectively; TR = temperature rise.

Fine-grained $M_R/M_{R,eff}$ ratios are greater than coarse-grained ratios and are an order of magnitude greater during the winter and early spring seasons. The $M_{R,eff}$ appears to be most representative of the late spring and summer seasons as $M_R/M_{R,eff}$ is approximately 1 in the summer and slightly less (0.8) in late spring. During the other seasons, the ratio is greater than 2 suggesting that the $M_{R,eff}$ is a conservative estimate for most of the year.

A negative linear relationship between $M_R/M_{R,eff}$ and temperature rise is projected during the winter season with a slightly positive relationship projected in the late spring and summer seasons. Fall and early spring exhibit non-linear responses to temperature rise. The fall ratio drops steeply with less than 2°C temperature rise and levels off to near 1 with increased warming. The decline in the ratio is more pronounced in the fine versus the coarse-grained materials, but both level off near 1 with temperature rise greater than 2°C. The most dramatic decline in $M_R/M_{R,eff}$ is predicted in the winter and early spring as temperatures warm above freezing. The pattern of decline is similar for the fine and coarse-grained materials, but the magnitude of change is less in the gravelly coarse sand. The ratio is predicted to drop below 1 in the fine-grained sediments with temperature rise greater than 4°C during the early spring.

Gravel base and sand subgrade M_R versus temperature rise at the pavement evaluation site are presented in Figure 5-5. The M_R is plotted on a log scale because of the large seasonal difference between frozen and thawed conditions. The summer M_R of the gravel base is close to the $M_{R,eff}$ at approximately 100 MPa and remains fairly constant with temperature rise. The winter M_R maintains a stiffness above 650 MPa until the winter season is projected to end. The early spring M_R matches the winter M_R up to 1.5°C rise and then drops to less than 100 MPa

when temperature rise exceeds 4°C. The late spring M_R, at 80 MPa, is the lowest of all the seasons, except early spring when the temperature rise exceeds 4.5°C.

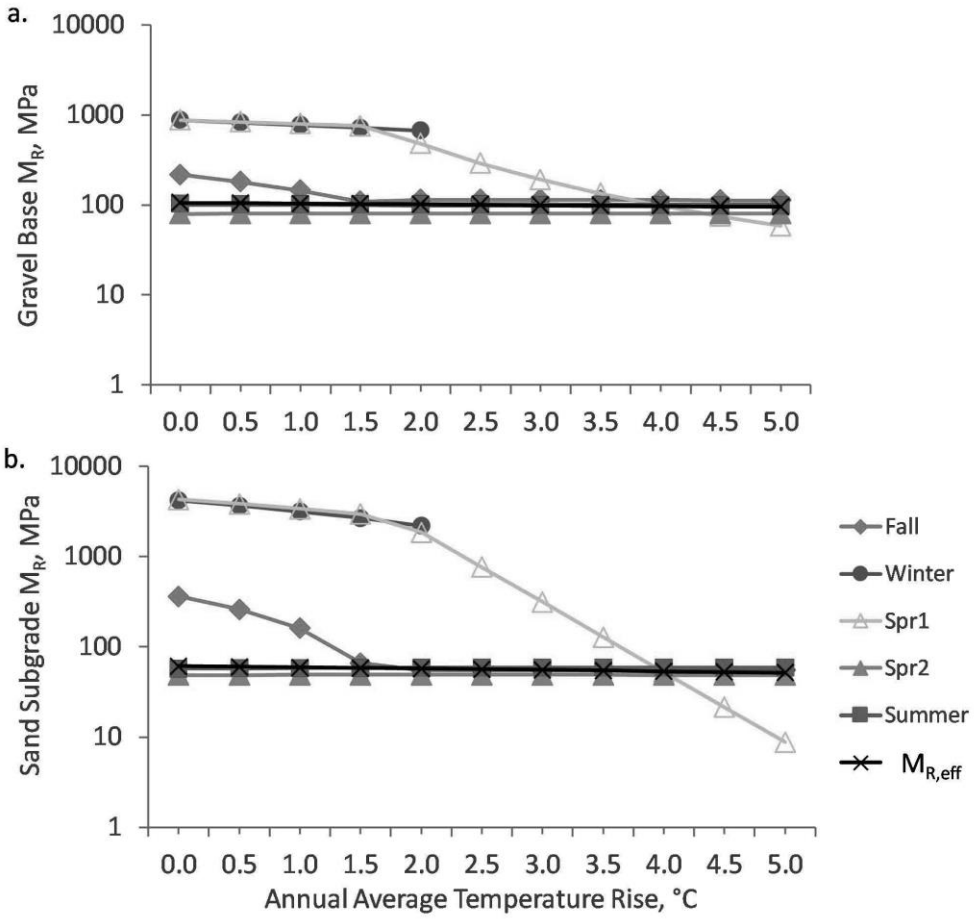

Figure 5- 5. Projected seasonal changes in M_R of (a) bank-run gravel base, and (b) sand subgrade with temperature rise at a regional connector in coastal NH.

The sand subgrade is more sensitive to temperature rise than the gravel base, especially in the winter, early spring and fall seasons. Winter and early spring M_R drops from approximately 4000 to 2000 MPa with up to 2°C temperature increase. Beyond 2°C rise, early spring M_R drops steeply to less than 10 MPa. The fall season M_R remains greater than 100 MPa with less than 1°C temperature rise and then drops to 55 MPa from 2.5 to 5°C temperature rise. The sand subgrade

M_R during late spring and summer remain relatively constant at just under 50 and 60 MPa, respectively. In contrast to the strong seasonal M_R change with temperature rise, both the gravel base and sand subgrade $M_{R,eff}$ remain relatively constant.

5.3.4 Seasonal and Long-Term Effects on Pavement Life

5.3.4.1 Seasonal Contributions to Pavement Damage

Total rutting and fatigue damage as well as the seasonal contribution to total damage at the pavement evaluation site are presented in Figure 5-6. The total fatigue damage is less than one, meaning that number of load repetitions to failure (N_f) due to fatigue is less than the expected ESALs for the simulated temperature rise, but more fatigue cracking can be expected in the future. Rutting controls the pavement failure at this site and the rutting N_f exceeds the expected ESALs when temperature rise exceeds 0.5°C.

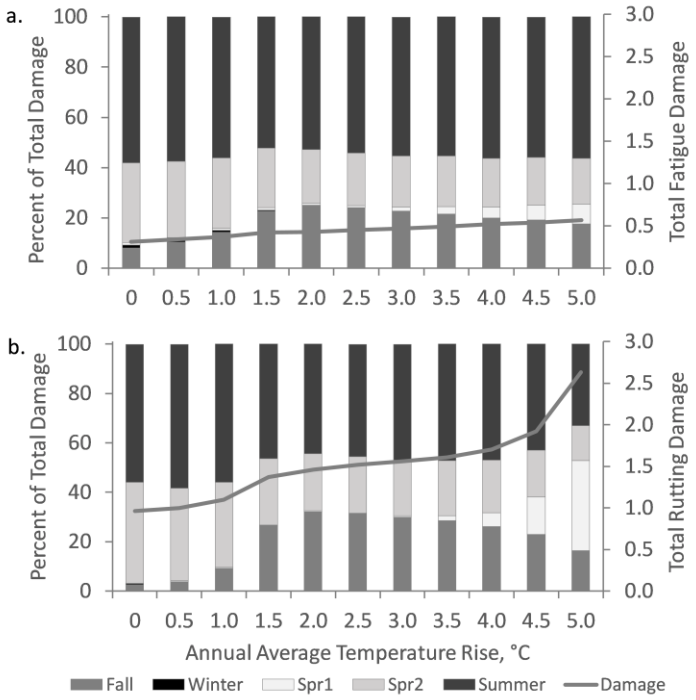

Figure 5- 6. Projected seasonal distribution of (a) fatigue damage and (b) rutting damage with temperature rise at the pavement evaluation site in coastal NH.

Seasonal contributions to both fatigue and rutting damage change with temperature rise, but the effect is more pronounced with rutting damage at this site. Summer and late spring contribute more than 90 percent of the total damage under current conditions. Rutting damage is distributed more evenly over late spring, summer, and fall between 1.5 and 3.5°C temperature rise. The changing fall season duration appears to influence the changing fall damage contribution with temperature rise. Winter damage is minimal, and the early spring contribution is negligible until temperature rises more than 3.5°C. Early-spring rutting damage becomes more important as temperatures rise above 3.5°C and dominates at the high end of the temperature-rise scale when projected total rutting damage increases sharply.

5.3.4.2 Adaptation

The layer thickness required to achieve at least 85% reliability with increasing annual average temperature rise is shown in Figure 5-7. The required HMA-layer thickness (holding the base-layer thickness constant) under current conditions is simulated to be 145 mm, approximately 4% higher than the existing thickness (140 mm). With a 5°C temperature rise, a 46% HMA thickness increase (from 140 to 205 mm) is required. The required base-layer thickness (holding the HMA thickness constant) under current conditions is 432 mm (6% thicker than the existing 406 mm thickness). The required thickness increases steeply to 508 mm with 2°C temperature rise, levels off between 2 and 3.5°C temperature rise and increases steeply again from 513 to 623 mm (53% increase) between 3.5 and 5°C temperature rise.

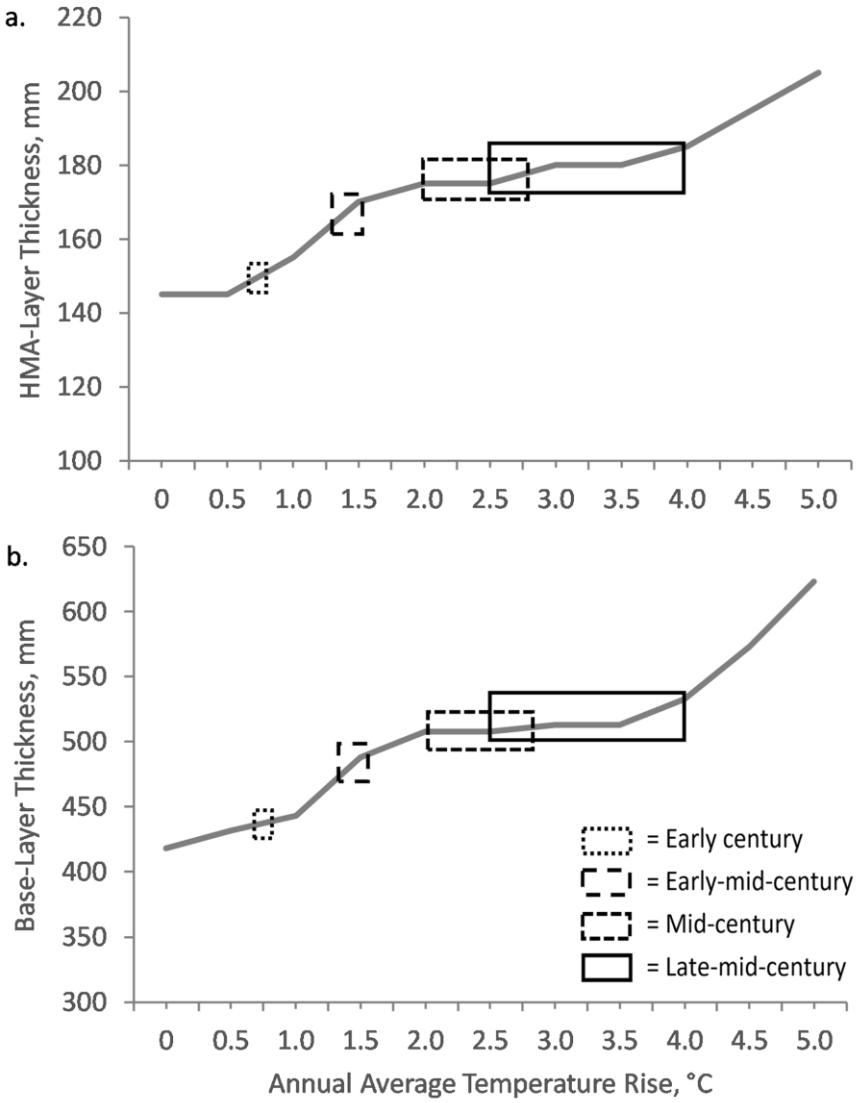

Figure 5- 7. Layer thickness required for pavement to achieve its design life with at least 85 percent reliability: (a) HMA-layer thickness required assuming 406 mm gravel base, (b) gravel-base-layer thickness required assuming 140 mm HMA. The boxes represent the 95% confidence interval of temperature rise projected during the period indicated.

The 95% confidence intervals for temperature rise from the RCP 4.5, 6.0 and 8.5 scenarios are shown with rectangles in Figure 5-7. The interval is less than 0.5°C up to 2040 but increases to 1.5°C in the late-mid-century period (2060 to 2080). The required HMA and base layer thicknesses are relatively insensitive within the mid-century period's temperature

indicating that differences among models does not result in projected differences in pavement management. In contrast, required layer thickness is much more sensitive to the potential range of the late-mid-century temperatures. If the base-layer thickness is left unchanged at 406 mm, the corresponding HMA thicknesses required to maintain 85% reliability are 150, 170, 178, and 185 mm for the four periods considered.

The corresponding HMA material costs are $40,000/km by early-mid-century and increase to $60,000/km by late-mid-century. If the HMA layer needs to be removed and replaced to rebuild a failing base layer, the required base-layer thicknesses are 437, 488, 510, and 533 mm, respectively. The corresponding gravel material-costs are $21,000/km by early mid-century and increase to $35,000/km by late-mid-century. Replacing the HMA layer would cost up to $350,000/km for 140 mm thick HMA material. In addition to these material-only costs, there will be substantial agency and user costs, such as project planning, design and construction quality-assurance costs, and user delays costs. Furthermore, the environmental impacts of increased greenhouse gas production due to increased pavement roughness and frequent maintenance needs will have potential to accelerate climate change and will result in other increased agency and user costs [*Valle et al.*, 2017]. This suggests that considering seasonal change and long-term temperature rise in pavement design and rehabilitation can help to avoid premature pavement failure, increased environmental impacts, and high road reconstruction costs.

5.4 SUMMARY AND CONCLUSIONS

Seasonal and long-term effects of climate-change-induced temperature rise on pavement life were investigated. Changes in pavement season length and seasonal average temperatures were determined at a pavement evaluation site in coastal NH using downscaled daily average

temperatures [*ICF International,* 2016; *Reclamation,* 2016] and MnDOT season definitions [*Tanquist,* 2001]. Pavement material M_R changes with incremental temperature rise were determined using M_R and temperature relationships from existing laboratory testing data [*Janoo et al.,* 1999]. $M_{R,eff}$ was determined using the AASHTO empirical pavement design damage factor approach following protocols used by NHDOT[*NHDOT,* 2014].

MnPAVE software [*Tanquist,* 2001]was used with the projected season durations, seasonal average temperatures and seasonal M_R values to calculate pavement damage and seasonal contributions to total damage for 0.5°C incremental annual average temperature increases from 0 to 5°C. Many pavement layer thicknesses were simulated to determine the thickness required to achieve 85% reliability with each 0.5°C temperature increase. Temperature rise projections for early century, early-mid-century, mid-century and late-mid-century were then superimposed on the pavement thickness and temperature rise curves to identify the timing of plausible temperature changes. The following conclusions have been reached:

- Pavement season length in coastal NH will change with climate-change-induced temperature rise. The summer season increases steadily at a rate of approximately 8 days per degree of temperature rise. The winter season will cease to exist when the temperature rises by more than 2.5°C; predicted to occur by mid-century. The fall season will initially lengthen as temperature rises due to shorter winters but, with continued warming, will shorten as summer lengthens.
- Changing season duration impacts the seasonal contribution to total pavement damage. The late spring and summer seasons currently contribute more than 90% of the total pavement damage at this site. Rutting damage becomes more prevalent during other times of the year, especially during the expanding fall season as the winter season

shortens. For temperature increases greater than 3.5°C, early spring also contributes to the total pavement damage. At 4.5°C temperature rise and above, the damage is spread much more evenly throughout the year.

- Downscaled climate model output for RCP 4.5, 6.0 and 8.5 was used to identify plausible temperature increases and the timing of the effects [*Taner et al.*, 2017]. Temperature rise ranging from 0.7 to 0.8°C is projected to occur during years 2000 through 2020, 1.3 to 1.6°C for 2020 to 2040, 2.0 to 2.8°C in 2040 to 2060 and 2.5 to 4.0°C in 2060 to 2080. For all periods except 2060 to 2080, the adaptation needs are relatively insensitive to these temperature ranges.
- A straightforward, preliminary adaptation analysis shows that if the existing base-layer remains structurally sound with 85% reliability, required HMA-thickness increases range from 7% for early century to 32% (costing $60,000/km) by late mid-century. If the base layer fails and needs to be replaced, additional base-layer thickness costing approximately $35,000/km (material costs) plus HMA replacement, agency, and user costs will be needed to maintain 85% reliability through late-mid-century. If actions are not taken to prevent premature pavement failure from temperature rise the costs of widespread base-layer reconstruction will be much higher than the costs of asphalt overlays.
- The hybrid bottom-up/top-down approach is an effective investigatory method for analyzing pavement response to climate-change-induced temperature rise. While computationally-intensive, the bottom-up portion of the analysis shows the effects of incremental temperature rise on season length, seasonal average temperatures, pavement material properties, and pavement life. It also reveals trends in pavement damage and projected pavement response to rehabilitation actions. A more complete understanding of the

pavement's climate-stress response supports more effective adaptation strategies. The top-down portion, in which the temperature change is defined, is used to determine the timing of impacts to support staged-adaptation planning and budgeting.

This research can be expanded both nationally and globally because the methodology is applicable to other regions (inland and coastal) where temperature rise and climate-change-induced seasonal changes will impact pavement performance. The adaptation approach, that is calculating the pavement layer thickness required to maintain a specified reliability level, provides practitioners with actionable guidance to address rising temperatures and changing seasons. We are currently building on this research to develop a staged-adaptation approach in which multiple adaptation pathways will be evaluated. Rehabilitation and reconstruction costs will be accumulated along these pathways and robust solutions will be sought to address uncertainties in climate-change projections *(26, 28)*. Other adaptation options should also be evaluated including, but not limited to, different base materials (crushed stone, reclaimed stabilized base, crushed gravel) and HMA binder grades.

Future research on coastal-road infrastructure will build on previous research showing pavement-life reduction with sea-level-rise-induced groundwater rise [*Knott et al.,* 2018b; *Knott et al.,* 2017]. The hybrid approach will be used to determine the combined effect of temperature and groundwater rise on coastal roads. Adaptation pathway analysis *(26, 28)* will be used to identify combinations of HMA and base-layer thicknesses that minimize damage costs caused by increased moisture content, temperature and traffic. Future research should utilize the latest pavement analysis and design tools to better capture pavement response mechanics and durability (moisture damage and aging) in pavement performance evaluation.

CHAPTER 6: DESIGNING A CLIMATE-READY COASTAL ROAD IN THE NORTHEAST

6.1 INTRODUCTION

Pavements are typically designed with the assumption that climate is stationary or not changing with time. This assumption is no longer valid leading to the question: How should pavements be designed when climate parameters affecting pavement performance are expected to change? This problem is further complicated by an uncertain climate future [*Hayhoe et al.,* 2015; *Meagher et al.,* 2012; *Melillo et al.,* 2014; *van Aalst et al.,* 2008]. Two approaches have been used in climate-change adaptation planning: the top-down or scenario-based approach and the bottom-up or asset-based approach.

The top-down approach begins with the choice of climate-change scenarios and is useful in identifying potential future pavement-life reductions and promoting climate resiliency through enhanced pavement design [*Chinowsky et al.,* 2013; *Ray and Brown,* 2015; *van Aalst et al.,* 2008]. The results are dependent on the chosen climate-change scenarios, however, and designs may cease to be effective if the climate-change predictions change in the future [*de Bruin et al.,* 2009; *Kwadijk et al.,* 2010; *Smith et al.,* 2009]. The top-down approach was used in the analyses presented in Chapters 3 and 4 investigating impacts and adaptation strategies of SLR-induced groundwater rise.

The bottom-up approach in pavement design begins with evaluating the effect of various combinations of environmental/climate parameters on pavement life. Climate-change scenarios are used only to identify the possible range in the climate/environmental parameters. Pavement design is dependent on local conditions including: traffic, geologic materials, hydrology, local

climate, and historical practices [*Muthadi and Kim,* 2008]. Road infrastructure is designed, constructed and maintained by state DOTs and municipalities. Knowledge of pavement sensitivity to select environmental parameters is useful in pavement design, maintenance and rehabilitation. Climate-change impacts to road infrastructure occur on a local scale and, consequently, adaptation plans involving local stakeholders are more likely to be adopted [*Butler et al.,* 2015]. While the bottom-up approach provides asset-specific performance information, it is not able to pinpoint the timing of critical environmental conditions. In Chapter 5, a hybrid bottom-up/top-down approach was introduced to investigate the impact of rising temperatures on pavement life. Pavement life at a case-study site was first evaluated for incremental temperature rise using the bottom-up approach. Downscaled GCM output was then used to determine the timing of the effects and to investigate simple adaptation options [*Knott et al.,* 2019].

The vulnerability and adaptation analyses presented in Chapters 3 and 4 focus exclusively on rising groundwater with pavement temperature assumed to be constant at 20°C. The temperature analysis in Chapter 5 considered only temperature rise and seasonal groundwater fluctuations but did not include long-term SLR-induced groundwater rise. In reality, both long-term temperature and groundwater rise will impact coastal-road infrastructure [*Meyer et al.,* 2014; *Wang et al.,* 2016]. A more complete vulnerability and adaptation analysis will consider the combined effect of both temperature and the unbound material moisture content controlled by groundwater level [*Wang et al.,* 2016].

In this chapter, a general hybrid bottom-up/top-down framework [*Kwadijk et al.,* 2010; *Kwakkel, Haasnoot et al.,* 2016; *Kwakkel, Walker et al.,* 2016; *Ray and Brown,* 2015; *Taner et al.,* 2017] is introduced for designing a climate-ready road focusing only on flexible pavements. The hybrid approach utilizes both bottom-up and top-down methodologies, beginning with a

bottom-up assessment of flexible pavement sensitivity to many possible combinations of environmental/climate forcings. This quantifies the pavement's sensitivity to environmental conditions. A top-down assessment using downscaled GCMs is then employed to identify the plausible variable combinations and to determine the timing of the effects. Adaptation pathways consisting of multiple adaptation actions will be demonstrated as a flexible, staged approach to adaptation planning [*Haasnoot et al.,* 2013; *Kwakkel, Haasnoot et al.,* 2016; *Kwakkel, Walker et al.,* 2016]. A general framework will be presented and then demonstrated at the coastal road case-study site evaluated in Chapter 5. The case study demonstrates the type of information that the method provides to stakeholders regarding pavement-design sensitivity to temperature and groundwater rise and the resultant staged-adaptation plan.

6.2 PAVEMENT BACKGROUND

Pavement design is based on traffic loading, the availability of base materials, subgrade soil properties, and environmental factors. Flexible pavements are typically designed for 20 years, but the base materials can be in place for 50 or more years. In practice, pavement service life can be extended out 60 years or longer through pavement management systems. These systems keep track of pavement inventory, overall pavement performance over the pavement's lifetime, maintenance/rehabilitation schedules, and costs [*Christopher et al.,* 2006; *Menendez and Gharaibeh,* 2017; *Tavakoli et al.,* 1992].

Many methods are used for repairing damaged flexible pavements including crack sealing, patch, drainage repair, surface coat, overlays (direct overlay and mill and overlay), and reconstruction [*Goodspeed et al.,* 1994]. Two of the most common maintenance/rehabilitation techniques are crack sealing and mill and overlay [*AASHTO,* 2008; *Chinowsky et al.,* 2013;

Christopher et al., 2006; *DeCarlo et al.,* 2017; *Tanquist,* 2012]. Agencies determine which rehabilitation method will be used and when to implement according to the road's functional classification and the severity and extent of pavement distresses [*Goodspeed et al.,* 1994; *Menendez and Gharaibeh,* 2017; *Tavakoli et al.,* 1992]. This is all part of the pavement management system, i.e. determining the right treatment at the right time to keep the overall system in good condition and to minimize overall costs. This sometimes means letting a road deteriorate until it gets to a point when rehabilitation is needed instead of spending money on maintenance that will only last a short time. In NH, pavement overlays for interstates and statewide connectors (state-maintained roads) are designed for 10 years and are based on average daily truck traffic and reduced material stiffness consistent with the level of pavement surface distress. Regional connectors and local roads receive a 20 mm overlay every 7 to 8 years to maintain the road's serviceability (NHDOT, personal communication). Local agencies will have their own schedule of when action is taken sometimes based on a pavement management system or sometimes on a strict schedule, i.e. every road is paved every 10 years.

In current practice, pavement rehabilitation/reconstruction is typically implemented when pavement distresses reach a certain threshold determined by a local DOT field distress survey [*Tavakoli et al.,* 1992]. This threshold can be defined in terms of rutting, fatigue cracking, the international roughness index (IRI) [*Christopher et al.,* 2006] or other parameters such as weathering, bleeding, transverse and longitudinal cracking, or potholes [*Tavakoli et al.,* 1992]. For example, moderately severe fatigue cracking (3.2 mm crack width) over more than 30% of the pavement surface area is a threshold for underlying layer reconstruction [*Goodspeed et al.,* 1994]. Exceedance of a distress threshold indicates that the HMA layer is no longer protecting the underlying layers [*Goodspeed et al.,* 1994; *Menendez and Gharaibeh,* 2017; *Tavakoli et al.,*

1992]. When the underlying layers no longer provide adequate support, maintenance paving becomes ineffective [*NHDOT,* 2015].

Current observations or historical practice cannot be used for long-term adaptation planning with environmental change. Weak pavement structures will require more frequent treatments or rehabilitation as the climate becomes less favorable and the costs to maintain the existing service life will increase. With changing environmental/climate conditions, the optimum pavement structure for the current design cycle may not be optimum for future pavement-design cycles. The point at which pavement base-layer rehabilitation or reconstruction is necessary can be thought of as an adaptation tipping point [*Kwadijk et al.,* 2010], defined here as the point when top-layer maintenance and rehabilitation is no longer effective within the new environmental/climate state. The tipping point could be defined in terms of standard maintenance practice or cost. For example, a tipping point occurs when the projected maintenance paving frequency exceeds the acceptable frequency as determined by the DOT. In terms of cost, a tipping point occurs when the maintenance-paving costs exceed pavement-reconstruction costs. Rebuilding the pavement structure with a more robust design may be the more cost-effective solution going forward.

Pavement performance metrics are useful for evaluating pavement-design alternatives. One performance metric is the ratio of the projected N_f with the new environmental/climate condition to the N_f for the current (designed) condition (N_f ratios). Adaptation strategies based on projected N_f ratios result in a stiffer pavement structure that is projected to achieve the same performance level despite adverse changes in environmental/climate conditions. This performance metric is used in Chapter 4. Another performance metric is the damage factor defined as the number of equivalent single axle loads (ESALs) predicted to travel the road over a defined

period (ESALs) divided by the calculated N_f for the pavement structure [*Tanquist,* 2001; *Tanquist,* 2012]. If the ESALs/N_f ratio is greater than one, the pavement is predicted to fail. A third metric is the HMA thickness required to achieve a pre-defined reliability level (Optimal HMA or O-HMA thickness); for example, roads with less than 1 million ESALs are typically built to achieve 85% reliability [*Tanquist,* 2012]. Finally, a cost metric that can be used individually or in combination with other metrics is adaptation costs, defined as the total cost of modifying the existing structure to maintain the designed service life (or reliability) in a changing climate [*Chinowsky et al.*, 2013; *Ray and Brown*, 2015]. The total adaptation costs include the capital costs to modify the pavement structure plus accumulated maintenance/rehabilitation costs over a defined period. Pavement designs with the smallest adaptation cost over the pavement management period are the most desirable.

Flexible pavement design typically uses an empirical approach in the United States based on field performance data measured at the AASHTO road test performed from 1958 to 1960 (*AASHTO*, 1993; *HRB*, 1961). A combined mechanistic and empirical approach has been used for pavement design primarily in research and in some states, such as Minnesota. In this approach, mechanistic-empirical models, calibrated to observed pavement performance, are used to calculate stresses and strains in the pavement structure in response to simulated traffic loading [*AASHTO*, 2008; *Tanquist,* 2012]. These models are useful in calculating pavement response to loading for future climate/environmental conditions which may be different from those experienced in the AASHTO road test. Mechanistic analysis, based on layered-elastic theory [*Burmister,* 1943], is used to determine the layer thicknesses necessary to prevent pavement failure over a specified design period, typically 20 years. The horizontal tensile strain at the bottom of the asphalt layer predicts fatigue cracking and the vertical compressive strain on the top of the

subgrade predicts rutting. Model inputs include traffic loading, expressed as ESALs over a design period; the pavement structure, including the number of layers and layer thicknesses; and material properties, such as resilient modulus and Poisson's ratio [*Christopher et al.*, 2006].

The resilient modulus is the most important material property for predicting the pavement response to traffic loading. The asphalt resilient modulus is sensitive to temperature and the unbound material resilient modulus is sensitive to both temperature and moisture content which is influenced by groundwater levels. Some models, such as MnPAVE [*Tanquist,* 2012] and Pavement ME [*AASHTO,* 2008], use climate inputs to calculate material resilient modulus from empirical relationships and can calculate seasonal changes in HMA properties through seasonal multipliers based on local weather information [*AASHTO,* 2008; *Tanquist,* 2001; *Tanquist,* 2012]. Others, such as KENLAYER [*Huang,* 2003], require user-defined material properties. Simulation of long-term changes, i.e. beyond the pavement design period, in material properties due to environmental/climate change currently requires a step-wise approach.

Pavement design alternatives vary by location and the functional classification of roadways. Local roads and regional connectors typically have simple pavement structures and, consequently, may be more vulnerable to climate change [*Knott et al.*, 2017]. State DOT engineers and local planners are valuable resources when determining what alternatives are feasible in the local area. Alternatives include variations in asphalt mix design, binder grade, unbound layer type, layer thicknesses, materials, geotextiles, the use of chemical additives for base-layer strengthening, and drainage design. In this research, local stakeholders and researchers chose the case-study site and agreed that pavement-layer thicknesses would be evaluated to demonstrate the methodology.

6.3 GENERAL ADAPTATION FRAMEWORK

A general framework is presented that can be used for various environmental/climate forcings such as temperature, groundwater, precipitation, flooding frequency, traffic, etc. It can be applied to flexible pavements along the coast or inland.

6.3.1 Bottom-Up/Top-Down Analysis

A combination of three approaches described in the literature is proposed to evaluate adaptation options for road infrastructure [*Kwakkel, Walker et al.,* 2016]. These approaches are decision scaling, robust decision making (RDM) [*Kasprzyk et al.,* 2013; *Lempert et al.,* 2006], and dynamic adaptive policy pathways (DAPP) [*Haasnoot et al.,* 2013; *Kwadijk et al.,* 2010; *Kwakkel, Haasnoot et al.,* 2016]. Three characteristics of pavement design make it uniquely well suited for these approaches. First, the pavement structure controls pavement performance. Various pavement structures are evaluated and compared using the decision scaling climate stress test [*Ray and Brown,* 2015; *Taner et al.,* 2017]. Second, some pavement structures are more resilient than others to environmental/climate change and these robust designs can be identified using RDM. Third, pavement adaptation can be flexible through relatively short-term (20 year) pavement design cycles and maintenance/rehabilitation practices. Adaptation tipping points, described in the DAPP approach, can be identified as the point when the more robust and capital-intensive adaptation strategies, i.e. underlying layer modification or reconstruction, are needed. The figures presented in this section are used to illustrate the methodology and are not based on a real analysis.

The *decision scaling* climate stress test is used to determine pavement performance sensitivity to environmental/climate change [*Ray and Brown,* 2015; *Taner et al.,* 2017]. Various

pavement structural designs are evaluated for all possible combinations of the chosen climate variables providing the stakeholders with a Pavement/Climate Sensitivity Catalog (PCSC). The performance metric can be N_f ratios, damage factors, O-HMA thickness, or adaptation costs, etc. The environmental/climate variables are chosen based on the study objectives, stakeholder priorities, and the study location. Temperature, groundwater levels, precipitation, flooding frequency, and freeze-thaw parameters are all important to pavement life [*Daniel et al.*, 2017; *Knott et al.*, 2017; *Ping et al.*, 2010; *Roshani*, 2014; *Salour and Erlingsson*, 2014] and can be analyzed using the climate stress test. This process is used to provide stakeholders with increased knowledge of the pavements' structural response to environmental/climate change.

An example PCSC using temperature and groundwater rise is presented in Figure 6-1 (modified from [*Taner et al.*, 2017]. Each box labeled (a) through (l) represents a different pavement structural design. The two environmental/climate variables used in this example are SLR-induced groundwater rise and temperature increase plotted on the x and y-axes, respectively. For each two-variable combination, the N_f ratio (pavement N_f for the specific variable combination/N_f for the existing structure and no climate change) is calculated. N_f ratios less than one, indicating projected pavement life less than the existing pavement's designed life, are highlighted in red. N_f ratios greater than one, indicating projected pavement life greater than the existing pavement's designed life, are highlighted in green.

Robust pavement structures are those whose pavement life equals or exceeds the design life for many combinations of environmental/climate variables. Robust pavement designs with thick asphalt and base layers address environmental/climate change uncertainty, but do not explicitly address adaptation costs. Robust structures are expensive to construct and may not be necessary until later in the century when changes in climate parameters are more pronounced

than in the short term. Using the example presented in Figure 6-1, structural designs (j), (k), and (l) are all robust, i.e. they out live the design life for most of the climate-variable combinations, but their relatively high cost may be a barrier to implementation early in the pavement management period because of budgetary constraints. Other factors such as unanticipated traffic changes, asphalt mix design advances, maintenance improvements, and budget allocation, etc. all affect pavement service life and necessitate flexibility in pavement design and maintenance/rehabilitation practices. Short-term planning cycles within the longer pavement management period [*NHDOT*, 2016] allow for some flexibility.

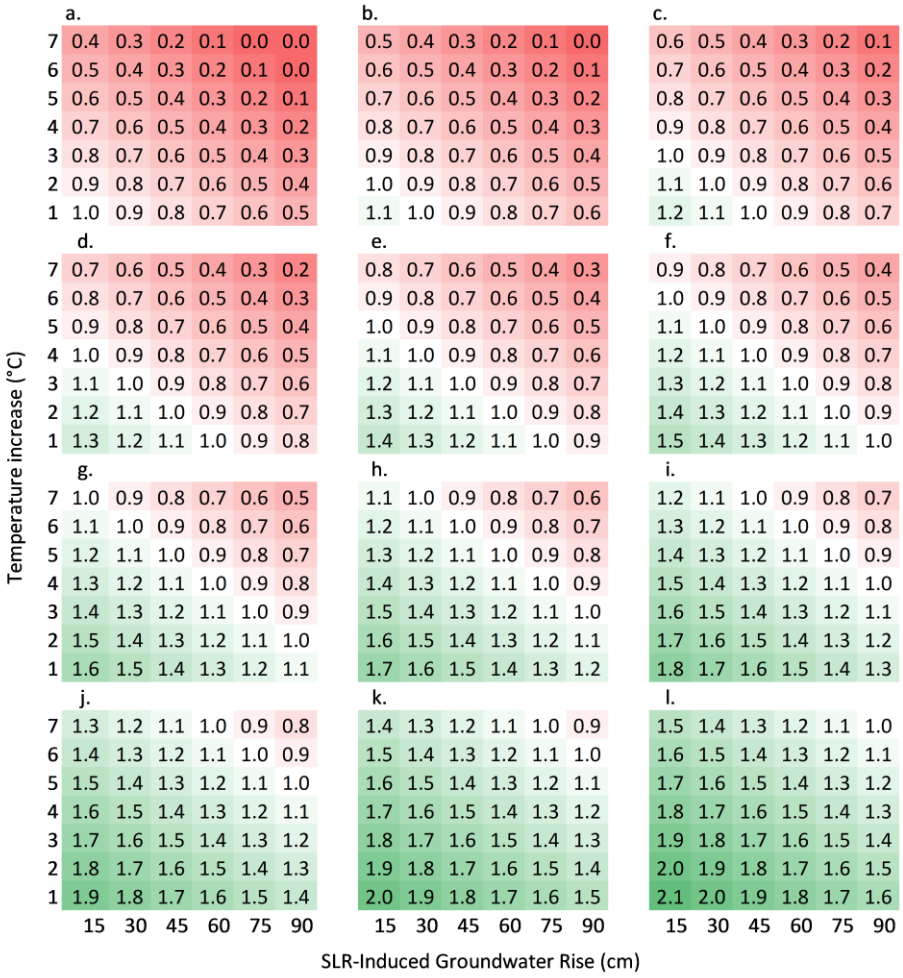

Figure 6- 1. Example of a Pavement/Climate Sensitivity Catalog (PCSC) presented to illustrate the methodology (modified from [*Taner et al.*, 2017]) - Pavement structural designs, ordered from weak to strong are shown in boxes (a) through (l). N_f ratios are shown for each climate-variable combination. Projected N_f less than the design N_f are highlighted in red, equal to the design life are white, and exceeding the design N_f are highlighted in green. Note: This figure is for illustration only and is not based on real data.

An alternative approach chooses the pavement structures that maintain the designed service life, i.e. have N_f ratios equal or close to one despite environmental/climate change. These structures, identified in the PCSC (Figure 6-1), are summarized in Figure 6-2.

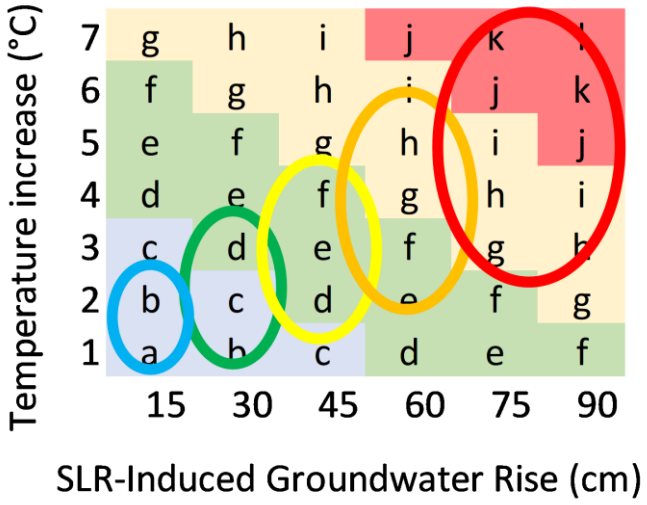

Figure 6- 2. Optimal PCSC– Pavement structures (a) through (l) with N_f ratios close to 1. The cell colors highlight the optimum pavement structures for various GW and temperature rise combinations. The ovals represent plausible areas of temperature/groundwater rise combinations based on downscaled GCMs with oval colors from blue to red representing climate projections from early to late mid-century. This figure is used to illustrate the methodology and is based on Figure 6-1 not real data.

This figure, hereafter referred to as the *Optimal PCSC*, presents only those pavement structural designs that meet this criterion. For example, options (a), (b), and (c), highlighted in light blue, are optimal for air temperature rise from 0 to 2°C and groundwater rise from 0 to 30 cm. Options (j), (k) and (l), highlighted in red, are optimal for air temperature rise from 5 to 7°C and groundwater rise from 60 to 90 cm.

The PCSC documents the environmental/climate sensitivity of the various pavement structures but does not address the timing of these changes. Taner et al. (2017) used downscaled GCMs to narrow the set of *possible* combinations of environmental/climate parameters to a smaller set of *plausible* combinations based on RCP 4.5 and 8.5 [*IPCC,* 2013]. Plausible climate combinations can also be identified within user-defined time periods. Important time intervals for pavement management include the 10-year planning cycle, 20-year design period, or 60-year pavement management period [*AASHTO,* 2008; *Christopher et al.,* 2006; *Tanquist,* 2012]. The U.S. DOT CMIP Climate Data Processing Tool can be used for processing the U.S. Bureau of Reclamation's Downscaled CMIP5 Climate and Hydrology Projections (DCHP) [*Reclamation,* 2016] at geographical scales appropriate for transportation assets. CMIP5 data is available from 1950 through 2099 to project temperatures and precipitation for future periods of interest [*ICF International,* 2016]. Future groundwater levels, if chosen for analysis, can be determined using a groundwater model [*Bjerklie et al.,* 2012; *Habel et al.,* 2017; *Knott et al.,* 2017; *Walter et al.,* 2016] forced by SLR projections [*Sallenger et al.,* 2012a; *Sweet et al.,* 2017].

Plausible areas of environmental/climate variable combinations from the downscaled climate models are superimposed on the Optimal PCSC as shown on Figure 6-2. These plausible areas can represent climate-projections from multiple climate models and two or more scenarios. The size of the plausible areas increases with increasing uncertainty for longer-range projections. Plausible areas of temperature rise were calculated in Chapter 5 and shown on Figure 5-7. If the climate projections change in the future, the PCSC and Optimal PCSC will still be relevant and the plausible areas can simply be changed accordingly, introducing flexibility into the analysis. This demonstrates the hybrid nature of the approach where a bottom-up methodology establishes

the asset's sensitivity to environmental/climate change and the top-down (scenario-based) approach identifies the plausible climate-variable combinations over time.

6.3.2 Staged Adaptation Planning

Pavement structural modifications can be relatively simple through surface-layer rehabilitation, or complex through base-layer rehabilitation/reconstruction. Short-term adaptation strategies can consist of relatively low-cost HMA overlays, the timing and frequency of which can be estimated using pavement simulations. When a pavement is projected to fail, simulated pavement life can be extended by simulating direct HMA overlay or mill and overlay [*AASHTO,* 2008; *Tanquist,* 2012]. Staged adaptation planning with changing environmental/climate conditions must answer three questions. (1) When should the existing pavement structure be replaced? (2) What should the new pavement structure look like? (3) What is the right balance between pavement performance and costs over stakeholders' time period of interest? In other words, what is the most cost-effective combination of HMA maintenance/overlays and base-layer rehabilitation/reconstruction with changing environmental/climate conditions?

The DAPP approach introduces the concepts of adaptation pathway mapping, tipping points, and an adaptation scorecard [*Haasnoot et al.,* 2013; *Kwakkel, Haasnoot et al.,* 2016; *Kwakkel, Walker et al.,* 2016]. Pathway mapping and tipping points can be used to address question (1). Adaptation pathway mapping provides a dynamic mechanism for systematically evaluating adaptation strategies, or pathways including multiple adaptation actions, throughout the pavement management period (60 years). Adaptation tipping points are points along the pathway where the current strategy is no longer effective and a new action is warranted [*Haasnoot et al.,* 2013; *Kwadijk et al.,* 2010; *Kwakkel, Haasnoot et al.,* 2016; *Kwakkel, Walker et al.,* 2016].

An adaptation tipping point in pavement management may occur when the groundwater moves into the base layers of the pavement structure resulting in pavement life reduction [*Knott et al.,* 2017]. Other tipping points include road-surface inundation with groundwater rise or surface-water flooding requiring radical adaptation actions such as raising the road, road abandonment, or active pumping. Temperature non-stationarity may introduce the need to repave with a different asphalt binder grade [*Chinowsky et al.,* 2013]. The combined effect of changes in two or more environmental/climate parameters may also affect the nature and timing of adaptation tipping points.

The PCSC and Optimal PCSC described above are powerful tools to help stakeholders answer question (2): "What should the new structure look like?" The Optimal PCSC (Figure 6-2) can be used to identify pavement structural designs that maintain the desired service life with projected environmental/climate change when the existing pavement structure ceases to perform according to historical norms. Some structural designs will be optimal early in the century, others later in the century, and some may be optimal for a wide range of climate-variable combinations.

An adaptation pathways map and scorecard [*Haasnoot et al.,* 2013; *Kwakkel, Walker et al.,* 2016; *Kwakkel, Haasnoot et al.,* 2016] can be used to answer question (3): "What is the right balance between pavement performance and costs over the time periods of interest for stakeholders?" A total of 10 hypothetical adaptation pathways are illustrated on a pathways map (Figure 6-3) and described in an adaptation score card (Table 6-1) [*Haasnoot et al.,* 2013]. The pavement designs used in the adaptation pathway map are chosen from the Optimal PCSC (Figure 6-2) and include the existing pavement structure and structural designs that perform well for the plausible environmental/climate combinations projected to occur during the pavement

management period. The options presented in Figure 6-3 and Table 6-1 are used to illustrate the methodology and are not based on a real analysis.

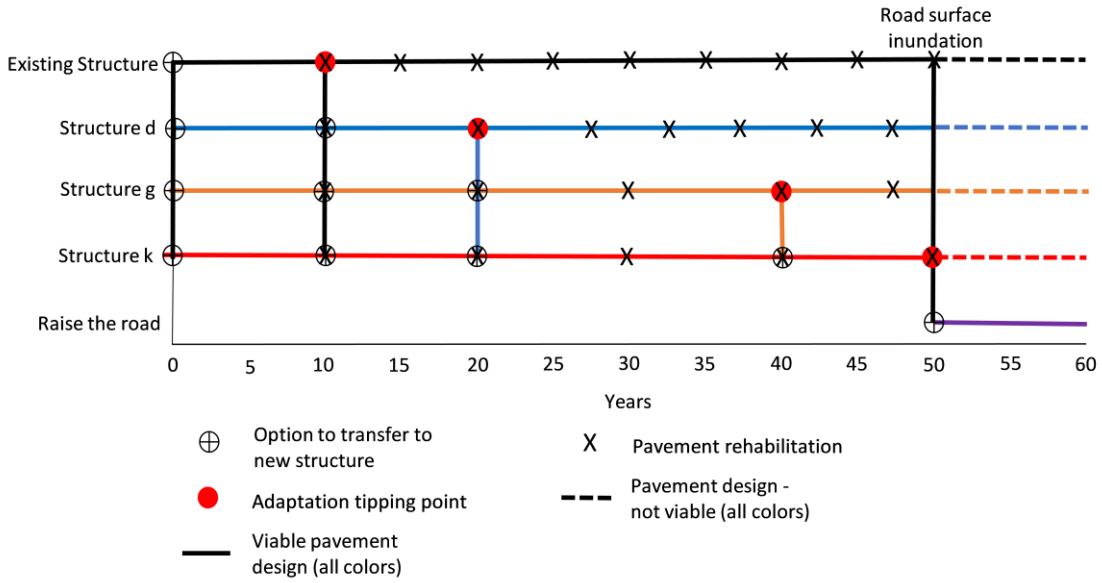

Figure 6- 3. Example of an adaptation pathways map, modified from [*Haasnoot et al.*, 2013], showing maintenance paving actions (X) and adaptation tipping points (red circles) where maintenance paving with the current base layer is no longer effective. Note: This figure is for illustration only and is not based on real data.

Pavement performance simulations are run for each optimal pavement design with climate-variable parameters changed in time steps based on the pavement-life sensitivity and/or stakeholder preference. The climate-variable parameters are determined using downscaled climate models for two or more RCP scenarios. The timing of adaptation actions is performance-based and not tied to a pre-determined rehabilitation cycle. For this example, adaptation strategy 1 begins with the existing structure (ES) as illustrated by the top horizontal line on the adaptation pathways map (Figure 6-3). The points at which maintenance paving (MP), or HMA overlay, is needed to avoid simulated pavement failure are illustrated with "X". The road is abandoned when inundated at year 50. Adaptation strategies 2 through 4 begin by modifying the ES

to achieve each new structural design. Adaptation strategies 5 through 7 begin with the existing structure and investigate changing structures when the existing structure is projected to fail.

Table 6- 1. Adaptation score card showing adaptation pathways, the costs per pavement cycle, and the 50-year total cost assuming the road is abandoned once inundated. ES= existing structure, Sd= structure d, CC(d) = capital cost to construct structure d, MP = maintenance paving cost (modified from [*Haasnoot et al.*, 2013]). Note: This table is to illustrate the methodology and is based on Figure 6- 3 not real data.

Adapt. Strategy No.	Path Actions	1st 20-Year Cycle Adapt. Capital Cost (CC)	1st 20-Year Cycle Maint. Paving Cost (MP)	2nd 20-Year Cycle Adapt. Capital Cost (CC)	2nd 20-Year Cycle Maint. Paving Cost (MP)	3rd 20-Year Cycle Adapt. Capital Cost (CC)	3rd 20-Year Cycle Maint. Paving Cost (MP)	Total Cost	Road Elevation in 2070	Side Effects
1	ES	0	2MP	0	4MP	0	3MP	9MP	-	-
2	Sd	CC(d)	MP	0	4MP	0	2MP	CC(d)+7MP	-	-
3	Sg	CC(g)	MP	0	2MP	0	2MP	CC(g)+5MP	-	-
4	Sk	CC(k)	MP	0	2MP	0	2MP	CC(k)+5MP	-	-
5	ES to Sd	CC(d)	0	0	4MP	0	2MP	CC(d)+6MP	-	-
6	ES to Sg	CC(g)	0	0	2MP	0	2MP	CC(g)+4MP	-	-
7	ES to Sk	CC(k)	0	0	2MP	0	2MP	CC(k)+4MP	-	-
8	ES to Sd to Sg	CC(d)	0	CC(g)	MP	0	2MP	CC(d)+CC(g) +3MP	-	-
9	ES to Sd to Sk	CC(d)	0	CC(k)	MP	0	2MP	CC(d)+CC(k) +3MP	-	-
10	ES to Sd to Sg to Sk	CC(d)	0	CC(g)	MP	CC(k)	MP	CC(d)+CC(g) +CC(k)+2MP	-	-

The present-value costs of base-layer reconstruction (CC) and maintenance paving (MP) are tallied in the adaptation scorecard (Table 6-1). For example, adaptation strategy 5, ES to structure d (Sd), represents constructing Sd from ES when the pavement model predicts ES failure at the first X on the ES pathway. The costs include the capital costs of constructing Sd (CC(d)) from the ES in the first pavement cycle, 4MP in the second cycle, and 2MP in the third cycle. The total cost for adaptation strategy 5 is CC(d) + 6MP. The remaining strategies investigate implementing more than one structural modification in addition to maintenance paving over the pavement management period.

6.4 CASE STUDY

The general methodology is demonstrated at a NH coastal road case-study site. In this location, changes in seasonal and long-term temperature and SLR-induced groundwater rise both have the potential to impact pavement life [*Knott et al.,* 2019; *Meyer et al.,* 2014; *Wang et al.,* 2016]. This case study considers the combined effect of groundwater-controlled moisture content and temperature rise on pavement life.

6.4.1 Methodology

The hybrid bottom-up/top-down methodology is presented and demonstrated at a pavement evaluation site on Route 286, a regional corridor and coastal evacuation route in southern NH. Route 286 has a simple pavement structure with 140 mm HMA and 406 mm bank-run gravel base overlying a sand subgrade [*NHDOT,* 2016]. The resilient modulus (M_R) of the HMA, the gravel base, and the sand subgrade, respectively, are 1493 MPa at 25°C [*Nemati et al.,* 2018]; 103 MPa from AASHTO correlation charts [*Christopher et al.,* 2006] and NHDOT layer coefficients [*Janoo,* 1994; *NHDOT,* 2014]; and 62 MPa from testing at the US Army Corps of Engineers Cold Regions Research and Engineering Laboratory (CRREL) [*Janoo et al.,* 1999]. The combined effect of climate-change-induced temperature rise and SLR-induced groundwater rise on these materials is evaluated using pavement performance modeling.

6.4.1.1 Pavement Performance Modeling

Pavement performance modeling was performed using MnDOT's software MnPAVE [*Tanquist,* 2012], a mechanistic-empirical model based on layered-elastic theory. MnPAVE was chosen because changes in season length, seasonal average temperatures, and seasonal resilient modulus

(M_R), needed to assess climate-change-induced impacts, can be simulated [*Tanquist,* 2001; *Tanquist,* 2012].

Adaptation Alternatives and Performance Metric

The adaptation design alternatives for the case study consist of four fixed gravel base-layer thicknesses, each with an HMA-layer thickness that can vary. The gravel base layer begins with the existing base-layer thickness of 406 mm and is increased in approximately 102 mm intervals to 508, 610, and 711 mm. The performance metric is the HMA thickness required to achieve 85% reliability (optimal-HMA thickness or O-HMA) using Monte Carlo simulation within MnPAVE [*Tanquist,* 2012]. This performance metric was chosen to provide actionable adaptation guidance as opposed to damage information. The cost metric is adaptation cost defined as the agency cost incurred for HMA overlays and/or pavement-structure rehabilitation and the user costs associated with work-zone delays. The costs are summed over the pavement management period from 2020 to 2080 and presented in present-value dollars [*FHWA,* 2017].

Pavement Analysis

There are four input categories in MnPAVE: environmental/climate variables, material properties, traffic, and pavement structure. The environmental/climate inputs include five seasonal average air temperatures (fall, winter, early spring, late spring, and summer), season duration, and frost depth. Spring is divided into early spring and late spring to account for changes in aggregate-base and subgrade-soil properties during the spring thaw period [*Tanquist,* 2001; *Tanquist,* 2012]. The seasonal average temperatures and the season durations were calculated from freezing and thawing indices and 3-day average temperatures [*Tanquist,* 2001; *Tanquist,* 2012] for current conditions and 0.5°C incremental temperature rise as described in Chapter 5 [*Knott et al.,* 2019]. A frost depth of 1020 mm, based on data from southern NH and

Massachusetts, was used as the early spring interface between the frozen and thawed soil in the pavement profile [*FHWA,* 2008; *Tanquist,* 2012]. Groundwater elevations measured in wells near the case-study site from 1970 through 2014 were evaluated and combined with LiDAR data [*NH Coastal Lidar,* 2011] to determine the annual average and seasonal groundwater depths beneath the pavement surface [*Barker,* 2016; *N.H. Department of Environmental Services,* 2016]. Groundwater depth is not entered directly into MnPAVE but is simulated indirectly through moisture content changes in material properties.

The material properties depend on the environmental/climate conditions. The HMA modulus was calculated as a function of temperature using the FHWA Long Term Pavement Performance Program (LTPP) temperature adjustment factor with the FHWA default slope parameter [*FHWA,* 1998a]. The asphalt temperature at one-third the pavement thickness was calculated from air temperature using the equation developed by Witczak [*Asphalt Institute,* 1982; *Shook et al.,* 1982; *Tanquist,* 2001]. The M_R of the unbound materials also changes with temperature. Relationships between M_R and temperature from laboratory tests [*Janoo et al.,* 1999] were established for gravelly-coarse sand and fine sand in Knott et al. (2019) [*Knott et al.,* 2019]. These relationships were used to calculate M_R at optimum moisture content ($M_{R,opt}$) for the gravel-base and sand subgrade with long-term annual-average temperature change and the corresponding seasonal-average temperature changes [*Knott et al.,* 2019].

The gravel base and subgrade M_R will also change with groundwater level fluctuations and frost depth [*Orr and Irwin,* 2006; *Ping and Ling,* 2008]. The unbound material M_R is adjusted for moisture content using the methodology described in Elshaer [*Elshaer,* 2017]. The pavement layers were divided into five sublayers (HMA, two base layers and two subgrade layers) to simulate saturation and consequential M_R changes within the pavement structure

[*Tanquist,* 2012]. For example, the groundwater table defines the top of the saturated lower subgrade layer. As the groundwater table rises, the thickness of the unsaturated subgrade layer is reduced. Eventually, with groundwater rise, both subgrade layers are saturated. As the groundwater rises in the base layer, the (initially thin) saturated base-layer thickness increases and the unsaturated base-layer thickness decreases. Seasonal groundwater variations are also simulated by varying layer thicknesses. The M_R for the unsaturated and saturated gravel-base and subgrade layers is calculated using the Witczak equation [*Elshaer,* 2017; *Witczak, Houston et al.,* 2000; *Witczak, Andrei et al.,* 2000]. The matric suction is estimated from the distance between each sublayer-midpoint and the groundwater table. The degree of saturation is determined from the soil water retention curve (SWRC) for each soil type and used in the Witczak equation to calculate the ratio of M_R at the current moisture condition to the $M_{R,opt}$ [*Elshaer,* 2017; *Witczak, Houston et al.,* 2000; *Witczak, Andrei et al.,* 2000]. This moisture-content adjustment factor ($M_R/M_{R,opt}$) is applied to the $M_{R,opt}$ calculated for the annual-average and seasonal-average temperature changes [*Knott et al.,* 2019] resulting in a MR adjusted for temperature and groundwater rise for each pavement layer.

Traffic loading is described in terms of ESALs where one ESAL is defined as one 80 kN dual tire axle with a 552 kPa tire pressure [*Tanquist,* 2012]. The average daily traffic is estimated to be 16,000 with 6% trucks, a truck factor of 0.24, and a lane distribution factor of 1 [*Seabrook Master Plan Steering Committee,* 2011].

6.4.1.2 Bottom-Up/Top-Down Analysis

Pavement Climate Sensitivity Catalog (PCSC)

A Pavement Climate Sensitivity Catalog (PCSC) was constructed based on the bottom-up framework [*Ray and Brown,* 2015; *Taner et al.,* 2017] to determine pavement-life sensitivity to

temperature and groundwater rise. A grid was created with temperature rise from 0 to 5°C in 0.5°C increments along the horizontal axis and groundwater rise from 0 to 700 mm in 100 mm increments along the vertical axis. The O-HMA thickness was calculated for the 70 temperature and groundwater rise combinations. The range of possible temperature increases for the time period from 2000 to 2080 was determined by analyzing projected daily average temperature rise from the U.S. Bureau of Reclamation's Downscaled Climate and Hydrology Projections (DCHP) [*Reclamation,* 2016] CMIP5 (Coupled Model Intercomparison Project Phase 5) with the high Representative Concentration Pathway RCP 8.5 [*IPCC,* 2013] as described in Chapter 5 [*Knott et al.,* 2019]. The maximum groundwater rise (700 mm) represents the water-table rise from the existing 700 mm average groundwater depth to the existing pavement surface. The calculations assume traffic at 0.938 ESALs and a 1.22% growth factor over a 20-year design life [*Rockingham Planning Commission,* 2017]. Traffic growth beyond the 20-year design life was not simulated. The pavement is assumed to have no pre-existing distresses.

Adaptation Pathways

Adaptation pathways are a collection of prescribed adaptation actions each taken in a specified order and at a specified time [*Haasnoot et al.,* 2013; *Kwakkel, Haasnoot et al.,* 2016; *Kwakkel, Walker et al.,* 2016]. Temperature, groundwater and traffic projections are needed to accomplish this and, consequently, the top-down portion of the hybrid approach is employed. In this study, the adaptation pathways are used to compare stepwise adaptation actions using various combinations of simple overlays and pavement rehabilitation needed to maintain a minimum of 85% reliability for traffic less than 1 million ESALS and 90% reliability for traffic greater than 1 million ESALs [*Tanquist,* 2012]. First, the O-HMA thickness must be determined for each base-layer thickness, and time-dependent traffic and environmental parameters. The O-

HMA was calculated with projected temperature rise, groundwater depth, and traffic adjusted in 10-year time steps as shown in Table 6-2.

Table 6- 2. Projected temperature rise, groundwater depth and traffic at Route 286 in coastal New Hampshire for three emissions scenarios: RCP 4.5, RCP 6.0, and RCP 8.5 and four SLR scenarios: Intermediate Low (IL), Intermediate (I), Intermediate High (IH), and High (H); F=Pavement Surface Flooded

	RCP 4.5 IL		RCP 6.0 I		RCP 8.5 IH		RCP 8.5 H		
Year	Temp Rise (°C)	GW Depth (mm)	Temp Rise (°C)	GW Depth (mm)	Temp Rise (°C)	GW Depth (mm)	Temp Rise (°C)	GW Depth (mm)	Traffic (Million ESALs)
2000	0.3	700	0.4	700	0.4	700	0.4	700	0.944
2010	0.7	672	0.7	663	0.8	644	0.8	630	0.944
2020	1.1	644	1.0	612	1.2	593	1.2	561	1.000
2030	1.5	612	1.3	565	1.7	514	1.7	482	1.061
2040	1.8	584	1.7	519	2.2	459	2.2	380	1.124
2050	2.1	552	2.0	463	2.7	371	2.7	273	1.191
2060	2.3	524	2.3	398	3.4	273	3.4	150	1.263
2070	2.5	512	2.7	343	4.0	187	4.0	16	1.337
2080	2.7	494	3.0	279	4.8	86	4.8	F	1.416

Projected annual temperature rise was determined from downscaled climate models for RCP 4.5, RCP 6.0, and RCP 8.5 [*IPCC*, 2013; *Reclamation*, 2016] as described in Chapter 5 [*Knott et al.*, 2019]. Projected groundwater rise at the case-study site is 46% of relative SLR determined using groundwater modeling of SLR-induced groundwater rise in coastal NH [*Knott et al.*, 2018a]. The relative SLR projections are from Sweet et al. (2017) [*Sweet et al.*, 2017]. Adaptation pathways were created for each RCP scenario to determine scenario sensitivity.

Next, adaptation pathway maps [*Haasnoot et al.*, 2013; *Kwakkel, Walker et al.*, 2016; *Kwakkel, Haasnoot et al.*, 2016] were constructed to investigate tipping points [*Kwadijk et al.*, 2010], i.e. the point at which pavement rehabilitation is done. In this study, pavement rehabilitation consists of removing the HMA layer, repairing and/or thickening the gravel base, and

replacing the HMA layer with the O-HMA thickness. Reclaimed stabilized base (305 mm) with additional gravel, if necessary, is used for increasing the base-layer thickness [*NHDOT,* 2018].

6.4.1.3 Adaptation Cost Analysis

The various adaptation pathways were simulated and the HMA overlay and pavement rehabilitation costs were tallied in present-value dollars over the 60-year pavement management period from 2020 to 2080. FHWA Real Cost software [*FHWA,* 2004; *FHWA,* 2017] was used to simulate life-cycle costs including agency and user costs. The agency costs included material, transportation, labor and equipment costs and were calculated using FHWA guidance [*FHWA, 2018* ; *FHWA,* 1998b] with NHDOT material costs [*NHDOT,* 2017; *NHDOT,* 2018]. The user costs consisted of work-zone delay costs only. Additional user costs, not considered in this study, include vehicle operating costs (gas, oil, maintenance, etc.) and crash costs that are related to pavement roughness and the overall condition of the roadway. Mean present-value and probabilistic costs were calculated using Monte Carlo simulation. HMA material-cost uncertainties associated with material M_R laboratory test variance [*Knott et al.,* 2019] as well as discount rate uncertainties based on 1979-2017 real treasury interest rate statistics (mean = 3.8%, std. dev. = 1.7%) [*Office of Management and Budget,* 2018] were included in the Monte Carlo simulations. The data used in the cost analysis are presented in Appendix B.

Comparisons were made between adaptation pathways including costs; low, medium, and high RCP scenarios; and road-surface inundation. The results are discussed in the context of a staged and flexible adaptation plan.

6.4.2 Results and Discussion

6.4.2.1 Pavement Climate Sensitivity Catalog (PCSC)

The PCSC is presented in Figure 6-4 with the O-HMA thickness given in each grid cell. Boxes (a) through (d) represent the four gravel-base thicknesses: 406, 508, 610, and 711 mm, respectively. The color shading shows O-HMA thickness less than the current thickness (140 mm) in green and O-HMA thickness greater than 140 mm in red. The PCSC illustrates that the O-HMA thickness decreases with increasing base-layer thickness. The reduction in O-HMA thickness needed for thicker gravel-base layers results in greater adaptation capacity through HMA overlays.

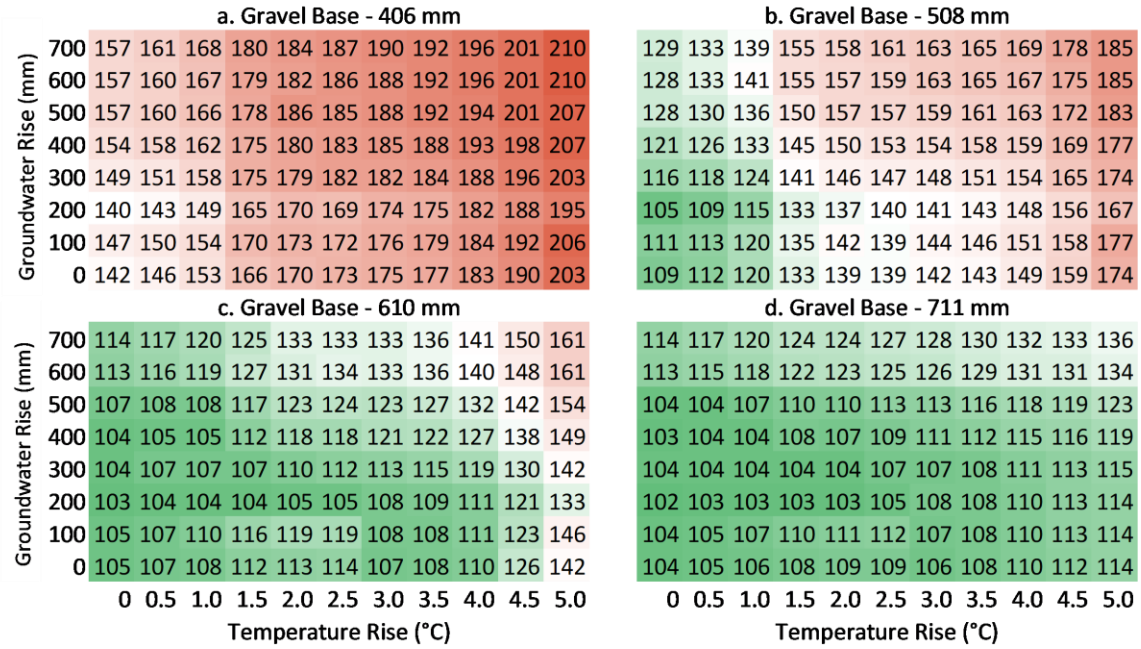

Figure 6- 4. Pavement Climate Sensitivity Catalog (PCSC) - shows the HMA thickness required to achieve 85% reliability (O-HMA) with incremental temperature rise and groundwater rise. The O-HMA color convention is: green < 140 mm < red. Four gravel-base thicknesses are shown: a. 406 mm, b. 508 mm, c. 610 mm, and d. 711 mm.

The O-HMA thickness is more sensitive to temperature increases than groundwater rise, but this is less pronounced with the thicker base layers. For example, the O-HMA thickness required for maximum groundwater rise is sufficient only for 1°C temperature rise with 406- and 508-mm

base-layer thicknesses. In comparison, the O-HMA thickness required for maximum groundwater rise is sufficient for 2.5°C and 5.0°C temperature rise with 610- and 711-mm gravel-base layer thicknesses, respectively.

The ratio of O-HMA at a given temperature and groundwater rise to O-HMA with no temperature and groundwater rise ($O\text{-}HMA_{T,\,GW}/O\text{-}HMA_{0,0}$) for each base-layer thickness provides a measure of each structure's resiliency (Figure 6-5).

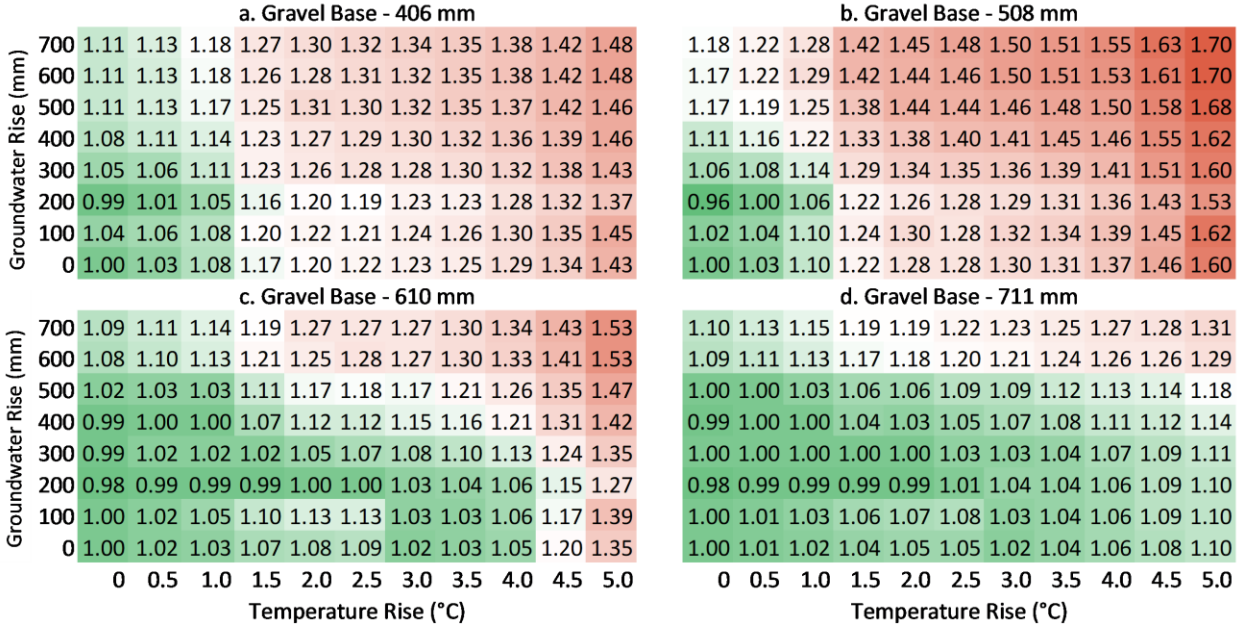

Figure 6- 5. Ratio of $O\text{-}HMA_{T,\,GW}$ / $O\text{-}HMA_{0,0}$ for incremental temperature and groundwater rise. The color convention is minimum (green) to maximum (red). Four gravel-base thicknesses are shown: (a) 406 mm, (b) 508 mm, (c) 610 mm, and (d) 711 mm.

Temperature rise from 0 to 3°C with no groundwater rise requires O-HMA thickness increases of 23%, 30%, 2%, and 2% with 406, 508, 610, and 711 mm base thicknesses, respectively. O-HMA thickness increases of 30%, 41%, 15%, and 7% are needed for temperature rise from 0 to 3°C and groundwater rise from 0 to 400 mm with 406, 508, 610, and 711 mm base thicknesses, respectively. Increasing the base-layer thickness from 406 to 508 mm does not improve temperature and groundwater rise resiliency. This base thickness provides a large reduction in the O-

HMA thickness under current temperatures and groundwater levels, but the benefit is severely reduced with temperature and groundwater rise. Gravel base thicknesses of 610 and 711 are the most resilient with temperature rise, but this resiliency is reduced with temperature rise greater than 4.0ºC for the 610-mm base layer and when groundwater moves within 300 mm of the pavement surface with both 610-mm and 711-mm base-layer thicknesses.

In summary, the O-HMA is thinner with thicker base layers for all temperature and groundwater rise combinations, but HMA increases are needed for all structures as temperatures and groundwater levels rise. The O-HMA thickness sensitivity to temperature rise is less for the 610- and 711-mm base layers, but these structures become more vulnerable when rising groundwater weakens the base layer.

6.4.2.2 Adaptation Pathways

The PCSC bottom-up approach illustrates pavement performance trends with incremental temperature and groundwater-rise. This analysis is independent of climate-change scenarios and traffic increases beyond the 20-year design life and the timing of adaptation actions are not considered. Conversely, the adaptation-pathway top-down analysis incorporates projected temperature, groundwater and traffic increases for the 60-year period from 2020 to 2080 leading to stepwise adaptation options for cost evaluation.

Pavement performance

Pavement performance by O-HMA thickness is shown in Figure 6-6. All four base-layer options require a minimum of 100 mm HMA thickness that increases as traffic, temperature and groundwater levels increase. As demonstrated with the PCSC, the O-HMA thickness decreases with increasing base-layer thickness. While the trends are the same, the O-HMA thicknesses

shown here differ from the O-HMA thicknesses in the PCSC due to the cumulative increase in traffic ESALs used in the pathway analysis.

Climate-change-scenario uncertainty increases with time for all base-layer thicknesses. Divergence between the maximum (RCP8.5H) and the minimum (RCP4.5IL) scenarios becomes prevalent by year 2040 when the RCP4.5IL O-HMA thickness levels off for base-layer thicknesses G406 through G610. For G711, the divergence is delayed until 2060 and then it increases sharply between 2060 and 2080.

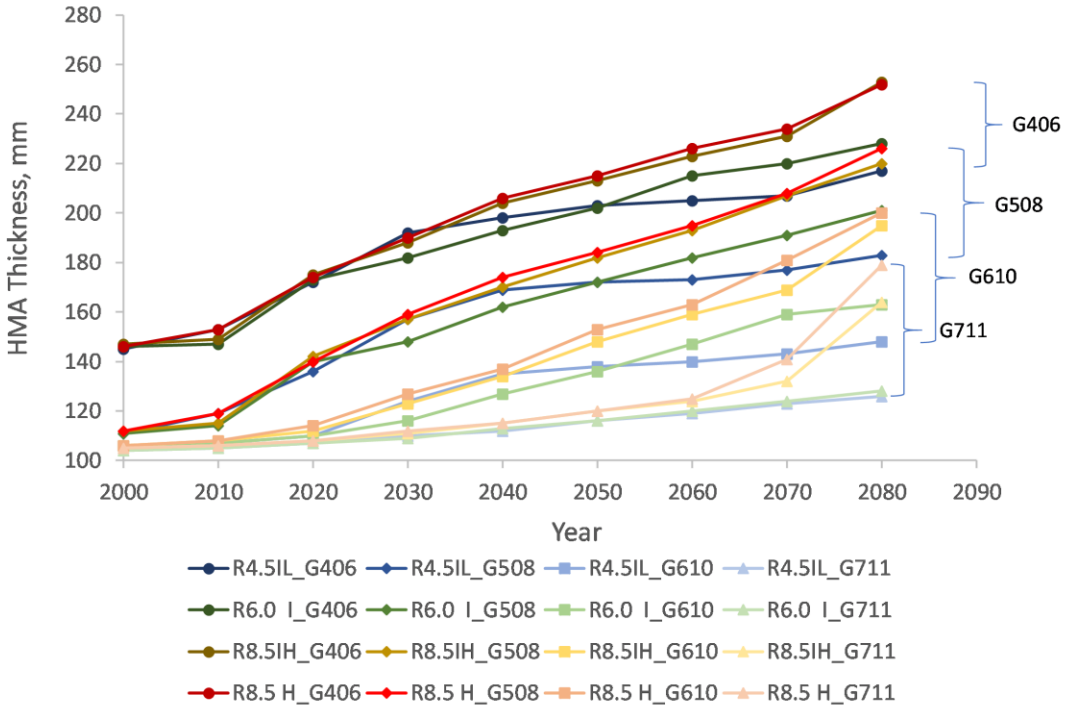

Figure 6- 6. O-HMA thickness versus time for four gravel base-layer thicknesses: G406, G508, G610, and G711 and for four climate-change scenarios: RCP4.5IL, RCP6.0I, RCP8.5IL, and RCP8.5H. Colors represent different climate-change scenarios. Markers represent changes in base-layer thickness.

The O-HMA thickness increase versus time is shown for all the climate change scenarios including no climate change (NCC) (i.e. traffic increases only) in Figure 6-7. All the

structures demonstrate a need for increased HMA thickness over time due to traffic increases and climate change. For the existing 406 mm base thickness, the mid-century O-HMA increase attributed to climate change (i.e. the difference between the O-HMA increase for the scenarios and the no-climate-change increase) ranges from 29 to 33 mm. The increase is less, 11 to 15 mm, for the 711 mm base thickness. By the end of the century, the O-HMA increases due to climate change are greater, 31 to 66 mm and 15 to 68 mm, respectively for the two structures. While the O-HMA thickness increase is less for structures with a thicker base, the relative O-HMA increase with climate change to the traffic-only increases is much higher. This result supports the PCSC finding that a thicker base improves pavement performance with traffic increases and modest climate change, but the resiliency is reduced when the groundwater moves higher in the base-layer triggering steep O-HMA thickness increases.

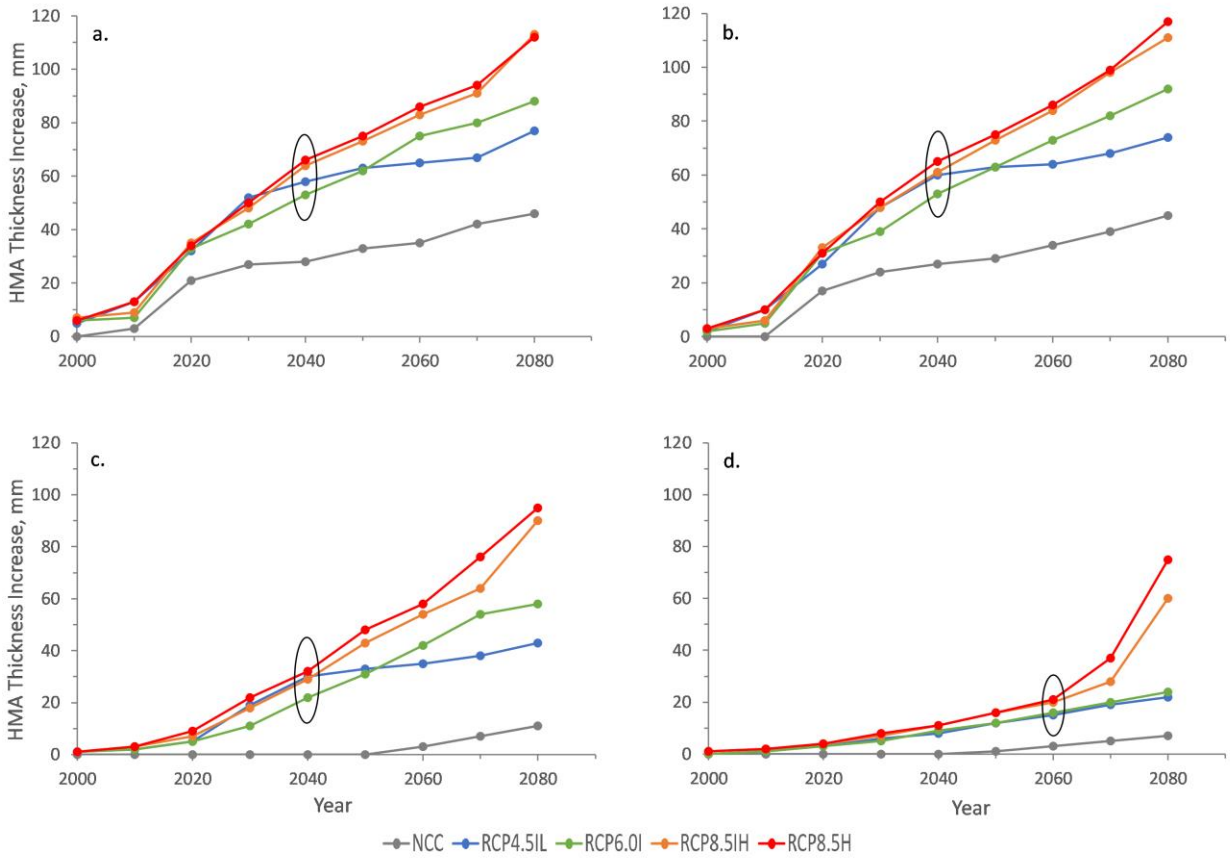

Figure 6- 7. HMA thickness increases needed to achieve O-HMA thickness for no climate change (NCC) and four climate-change scenarios: RCP4.5IL, RCP6.0I, RCP8.5IH, and RCP8.5H. Four gravel base-layer thicknesses are presented: (a) 406 mm, (b) 508 mm, (c) 610 mm and (d) 711 mm.

Points when the O-HMA thickness diverges based on the climate-change scenarios are identified with ovals on the charts. These are decision points at which adaptation pathways may change depending on which RCP scenario is most correct at that point in time. In practice, the decisions will be facilitated by increased knowledge about traffic loading, climate change, and pavement material properties.

Adaptation Pathway Maps

Thirteen adaptation pathways were chosen for cost evaluation based on the performance analysis. All 13 pathways were constructed for four scenarios: no climate change (NCC), RCP4.5IL, RCP8.5IH, and RCP8.5H. RCP6.0I is close to RCP4.5IL before mid-century and falls between RCP4.5IL and RCP8.5IH after mid-century; consequently, for simplicity, it was not included in the pathway analysis. While pathways were created for the NCC, RCP4.5, RCP8.5IH and RCP8.5H scenarios, only RCP8.5IH is shown here (Figure 6-8) with the adaptation pathways' first action occurring in 2020.

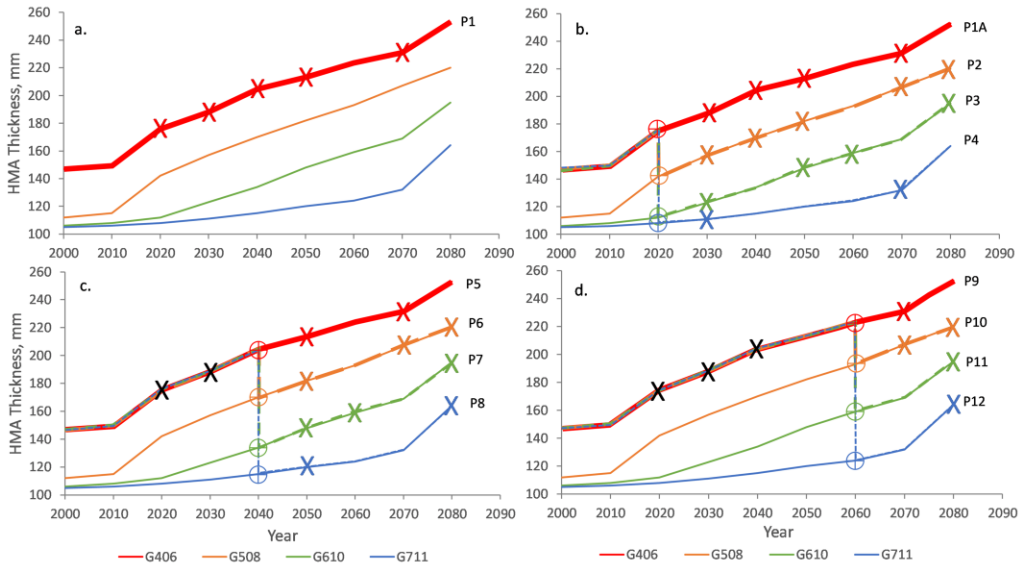

Figure 6- 8. Adaptation pathways (a) P1, (b) P1A to P4, (c) P5 to P8, and (d) P9 to P12 shown as the calculated O-HMA thickness versus time for RCP8.5IH. Colored X's represent the simple HMA overlays for individual pathways. Black X's represent overlays for all the pathways shown in each chart. Bullseyes represent tipping points for pavement rehabilitation.

All adaptation pathways begin with the existing structure. Pathway 1 (P1) consists of simple HMA overlays only with each overlay shown on Figure 6-8a with an X. In pathways P1A through P4, the existing HMA is removed and replaced with the O-HMA thickness as needed (Figure 6-8b). In P1A, the base layer is repaired without increasing the base-layer thickness. This action would be needed if the pavement had pre-existing rutting and/or fatigue cracking of a severity warranting base-layer rehabilitation. In pathways P2 through P4, the base-layer thickness is increased from 406 mm to 508, 610 and 711 mm, respectively, before laying the O-HMA. It is assumed that the old HMA will be recycled in place as reclaimed stabilized base. Any excess HMA will be removed for off-site recycling and new gravel base will be trucked to the site if needed to achieve the proposed thickness. In P1A through P4, base-layer rehabilitation occurs in 2020. In P5 through P8, the same structural assumptions are made, but base-layer rehabilitation is delayed until 2040. Prior to 2040 simple overlays are proposed to maintain the O-HMA thickness. In P9 through P12 base-layer rehabilitation is delayed until 2060.

6.4.2.3 Adaptation Costs

The average present-value agency and user costs for all the pathways and climate-change scenarios are shown in Figure 6-9. The climate-change scenario influences the pathway cost, but not the pathway ranking in most cases. Regardless of the climate-change scenario, P1 is the least expensive option and, consequently, may be the most desirable. There are situations where premature failure may occur, however, making base-layer rehabilitation necessary. These include pre-existing pavement distresses, failure to maintain the O-HMA thickness, road-surface inundation, unexpected increases in traffic loading or climate parameters, and a future beyond 2080. The two least-costly base-layer rehabilitation options for all climate-change scenarios are P11and P12 with base-thickness increases proposed for year 2060.

If circumstances other than cost drive the rehabilitation timing, the least costly structure is the 610 mm base achieved through pathways P3, P7, and P11. These pathways benefit from an optimal use of on-site-recycled stabilized base that minimizes trucking and user-delay costs. Of these, P11 is the least costly due to a combination of optimal on-site recycling and delayed rehabilitation. If reconstruction is necessary, the most-costly pathway is P1A: reconstruction without increasing the base-layer thickness.

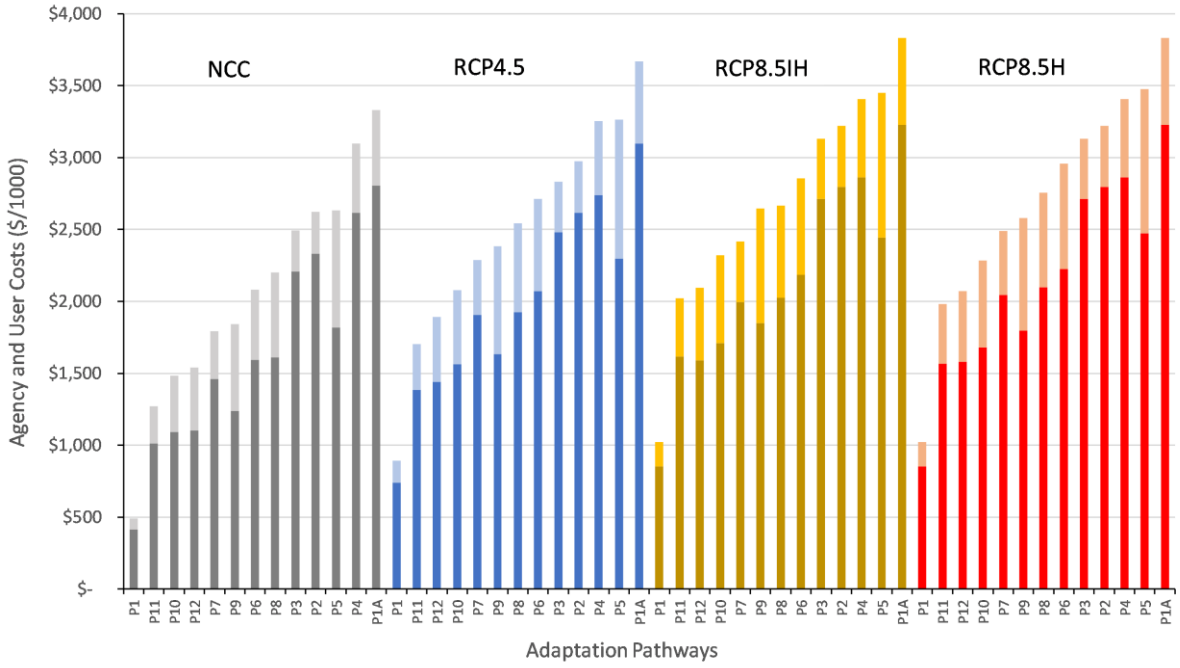

Figure 6- 9. Projected average agency and user costs for 13 adaptation pathways with NCC, RCP4.5, RCP8.5IH, and RCPH 3 scenarios. The dark shade represents the average agency cost and the lighter shade represents the user delay costs.

6.4.2.4 Adaptation Strategies

Cumulative probability distributions of total (agency and user) present-value costs from Monte Carlo simulations are shown for pathways P1, P1A, P3, P7 and P11 for RCP4.5, RCP8.5IH, and RCP8.5H in Figure 6-10.

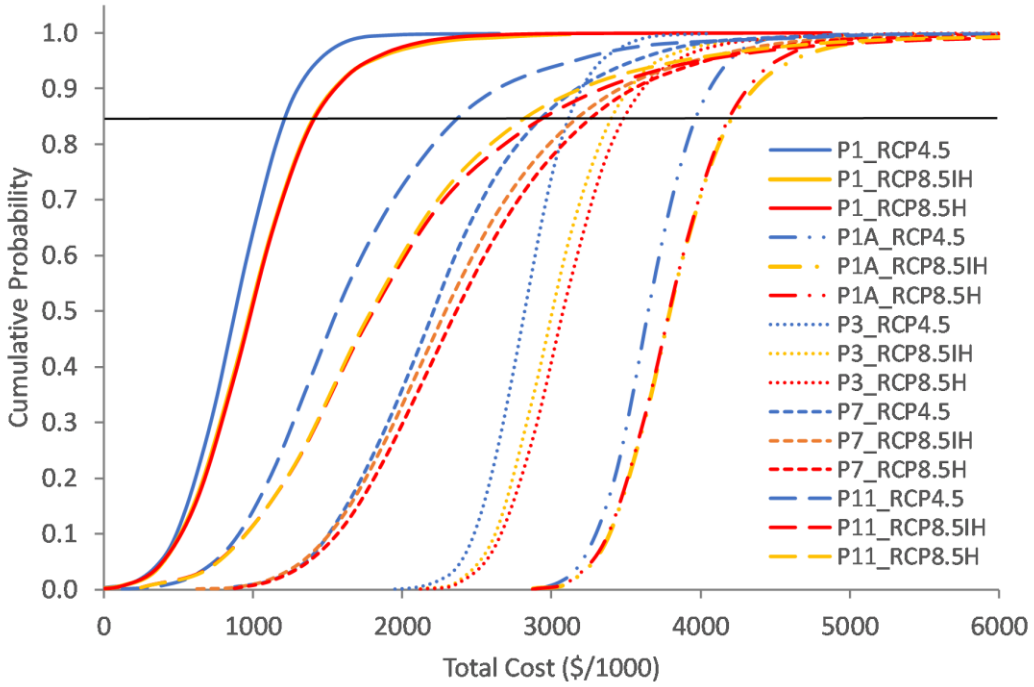

Figure 6- 10. Probability distributions for total costs associated with pathways P1, P1A, P3, P7, and P11 for RCP4.5IL, RCP8.5IH, and RCP8.5H.

All pathways demonstrate cost increases from the low to the high RCP scenarios. The low-cost pathways are consistent across scenarios, but the cost difference among the rehabilitation pathways are less pronounced for the high RCP scenarios as uncertainty increases. Delaying base-layer rehabilitation (P7 and P11) reduces the cost in present-value dollars but also increases cost uncertainty. The least cost base-layer rehabilitation pathway (P11) is approximately twice the overlay-only pathway (P1). Increasing the base-layer thickness from 406 mm to 610 mm (P3) saves 20% when compared to constant base-thickness rehabilitation (P1A) under RCP4.5 and 12% under RCP8.5H. Delaying rehabilitation from 2020 (P3) to 2060 (P11) saves an additional 24% for RCP4.5 and 10% for RCP8.5H. These results show that there is a large financial benefit to early adaptation with pavement overlays by avoiding the high cost of base-layer rehabilitation. Increased road-surface elevation associated with a thicker pavement structure also results in

ancillary costs to modify adjacent properties and connecting roads. This analysis focuses only on HMA and base-layer thickness increases, but if the subgrade is damaged because of a weak pavement structure, the costs of full pavement reconstruction including subgrade repair would be much higher.

Cost is not the only concern when designing a climate-ready coastal road. Some roads will be vulnerable to tidal water and/or groundwater road-surface inundation caused by SLR. At this case-study site, groundwater is projected to regularly inundate the road surface before tidal waters cause overland flooding. The projected groundwater elevation (relative to MSL) for RCP8.5IH and RCP8.5H is shown with the pavement-surface elevations for each adaptation pathway in Figure 6-11.

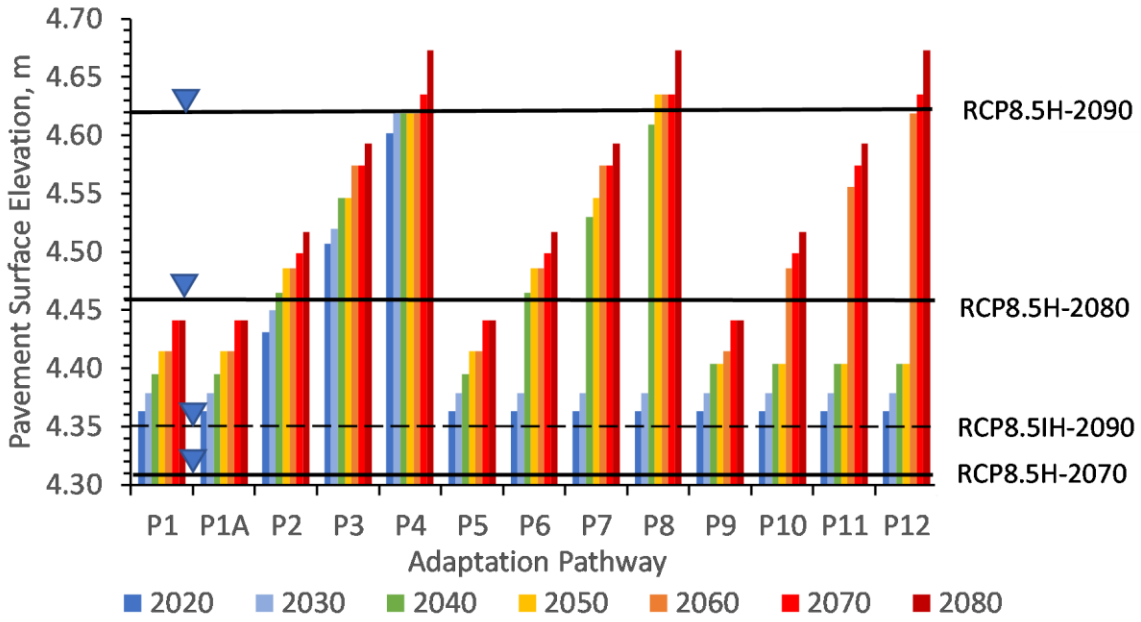

Figure 6- 11. Pavement surface elevation relative to MSL for the 13 adaptation pathways under RCP8.5IH and RCP8.5H. The projected groundwater elevation at the pavement evaluation site is shown for years 2070, 2080, and 2090.

For the RCP8.5IH scenario, groundwater is not projected to be above the existing road-surface elevation (4.33 mm) until 2090. Using the RCP8.5H scenario, projections suggest that in 2070, the groundwater will be only130 mm below the road surface for P1, P1A, P5, and P9, and in 2080, the groundwater will inundate the road surface. Properties at similar elevations served by this coastal road will also flood. Consequently, this case-study site is projected to have flooding problems after 2070 for RCP8.5H (but not the lower RCP scenarios) when following the least expensive (P1) adaptation pathway. Pathways P3, P7 and P11 will delay groundwater inundation at RCP8.5H with groundwater projected to be 260 mm and 130 mm below the road-surface elevation in 2070 and 2080, respectively. If the O-HMA is maintained and the costs of premature failure are avoided, P11 is the best choice because road-surface inundation costs and the additional costs of early base-layer rehabilitation will both be avoided. Adoption of P11 will also give practitioners the opportunity to re-evaluate adaptation strategies based on new information. Looking beyond 2080, the P3, P7 and P11 road surfaces will be flooded in 2090. This suggests, that if Route 286 is still needed to serve properties beyond 2080, P12, an even thicker base, or an elevated road (bridge) will be better than P11. This decision should be made prior to base-layer rehabilitation in 2060.

The overlay schedule and thicknesses required to maintain the O-HMA thickness for selected pathways under NCC, RCP4.5, RCP8.5IH, RCP8.5H are shown in Figure 6-12. The base-layer thickness is not shown but can be inferred from the pathway name.

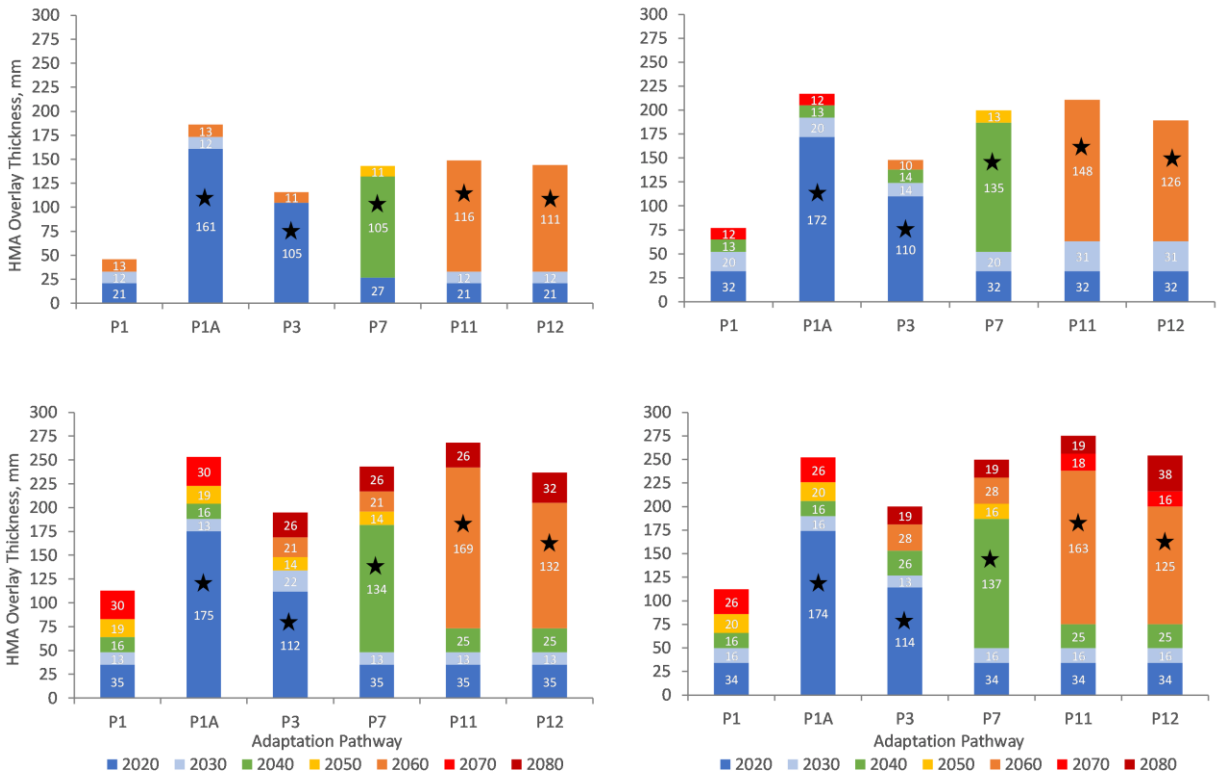

Figure 6- 12. Cumulative HMA overlays required to maintain O-HMA thicknesses for select pathways. Colors represent the timing of the overlay. Overlay thickness is indicated by white numbers. Black stars mark the HMA thickness to be placed after base-layer thickening. Each chart represents: (a) NCC, (b) RCP4.5, (c) RCP8.5IH, and (d) RCP8.5H.

An example of a flexible and step-wise approach to adaptation is as follows. (1) Choose adaptation pathway P11. When there are differences in the incremental overlay thickness between climate-change scenarios, it is recommended that the largest overlay thickness for that pathway and time period be used to avoid the high cost of premature pavement failure. (2) Just prior to 2040, the pavement condition, traffic predictions and climate-change scenarios should be re-assessed. Based on the results, practitioners can either decide to increase the base thickness in 2040, i.e. switching from P11 to P7 or continue with P11 overlays until 2060. (3) Just prior to 2060, a similar re-assessment should be conducted. At this point, groundwater inundation may be occurring in many-low lying areas along the coast and stakeholder options will include: (a) follow P11, (b)

switch to P12 or a thicker base, (c) elevate the roadway, or (d) abandon the roadway and relocate residents. P11 will enable continued travel over Route 286 through 2080, but road-surface flooding from groundwater inundation is projected before 2090. P12 will enable travel through 2090, but not much beyond that for RCP8.5H. Decision-making at or around 2080 will center around raising the road or road abandonment because further thickening of the base and HMA layers will not adequately address road inundation.

6.5 SUMMARY AND CONCLUSIONS

The combined effect of temperature and SLR-induced groundwater level increases on pavement life was investigated at a regional connector and coastal evacuation route in southern NH. A bottom-up/top-down approach was used, and seasonal and long-term changes were included in the study. Pavement season length and seasonal average temperature changes were determined using downscaled daily average temperatures [*ICF International,* 2016; *Reclamation,* 2016] and MnDOT season definitions [*Tanquist,* 2001] following the method described in Chapter 5 [*Knott et al.,* 2019]. Seasonal and long-term groundwater levels were determined from historical groundwater-monitoring records [*Barker,* 2016; *N.H. Department of Environmental Services,*] and numerical modeling of SLR-induced groundwater rise, respectively [*Knott et al.,* 2017]. Monte Carlo simulations within MnPAVE [*Tanquist,* 2001] were used to calculate the optimal HMA (O-HMA), i.e. the thickness required to achieve a minimum of 85% reliability.

The bottom-up approach [*Brown et al.,* 2012; *Ray and Brown,* 2015; *Taner et al.,* 2017] produced a PCSC in which the sensitivity of four pavement structures with increasing base-layer thicknesses was determined for 70 combinations of incremental temperature and groundwater rise. The following conclusions can be drawn from the PCSC. (1) The PCSC is a useful

screening step in adaptation planning because it illustrates the asset's sensitivity to incremental environmental change untethered to climate-change scenarios. (2) O-HMA layer thickness increases are needed for all four base-layer configurations as temperatures and groundwater rise. (3) Pavement performance is more sensitive to rising temperatures than to rising groundwater for the 406- and 508-mm base layers. Base-layer thicknesses of 610 and 711 mm show improved temperature resiliency. (4) Pavement resiliency is reduced when groundwater moves up in the gravel-base layer. (5) In coastal road infrastructure where both temperature and groundwater are expected to rise, HMA and base-layer thickness increases will be required to maintain pavement reliability.

After analyzing the pavement's sensitivity to temperature and groundwater rise, the top-down approach was used to determine adaptation pathways and costs. Thirteen adaptation pathways were analyzed for performance, cost, and road-surface inundation. O-HMA thickness increases are required across all adaptation pathways. Average total costs including present-value agency and user work-zone delay costs and cumulative present-value cost probabilities using Monte Carlo simulations for the 60-year pavement management period (2020 through 2080) were tallied and compared. The key findings are:

- Climate change is a cost multiplier, i.e. the costs of HMA overlays or pavement rehabilitation increase with rising temperatures and groundwater levels.
- The least-cost adaptation pathway consists of simple HMA overlays with prescribed HMA overlay thicknesses and implementation schedule. This pathway is projected to fail, however, between 2070 and 2080 under the high RCP and SLR scenario when groundwater is projected to inundate the road surface.

- If base-layer rehabilitation is needed because of pre-existing distresses, unexpected changes in loading and/or climate conditions, or projected road-surface inundation, the existing base-layer thickness should be increased from 406 to at least 610 mm at this location. Increasing the gravel-base layer to 711 mm is slightly more expensive when done after mid-century and may be a viable option if the road is to be used beyond 2080.
- The factors controlling the cost differential (in present-value dollars) between base-layer rehabilitation pathways are reclaimed stabilized base optimization and the timing of the rehabilitation actions. It is best to delay rehabilitation until necessary by implementing prescribed HMA overlays to maintain the O-HMA thickness.
- Base-layer rehabilitation with little or no base-layer thickness increase is the most expensive adaptation strategy and should be avoided.
- The hybrid adaptation approach has value in identifying optimal adaptation pathways as well as appropriate maintenance paving actions needed to prevent premature pavement failure.

A step-wise and flexible adaptation plan is presented where adaptation actions are taken every 10 years along adaptation pathways from 2020 through 2080. Re-evaluation is recommended every 10 to 20 years to determine (1) the pavement's condition, (2) changes in projected traffic, and (3) changes in climate projections. Based on these findings, the adaptation plan can remain on the same pathway or change to another. Early adaptation actions must maximize resiliency, minimize cost, and not preclude future actions. The benefits of implementing a prescribed HMA overlay plan include cost minimization and reduction in future uncertainties.

Recommended future work includes creating a PCSC with O-HMA thickness as a function of temperature, groundwater, and traffic increases that are possible through the period of

interest. In this PCSC study, traffic was assumed to increase at a steady rate over the 20-year design life; however, the more extreme temperature and groundwater changes will occur later in the century when traffic may also have changed. The usefulness of the PCSC to prescribe O-HMA thicknesses could be improved by including incremental traffic changes with incremental temperature and groundwater changes.

Investigating a wider range of adaptation options and considering the carbon footprint [*Thives and Ghisi,* 2017] of each adaptation pathway is also recommended. This analysis investigates the effect of changing layer thicknesses on resiliency. Other options include using a different HMA binder [*Mallick and El-Korchi,* 2013] and/or base-layer stabilization techniques such as different base-layer materials, additives, or geotextiles [*Christopher et al.,* 2006]. A desirable adaptation option would reduce the amount of HMA needed to achieve the desired performance, reduce carbon emissions and reduce costs.

This research suggests that the effectiveness of preventive maintenance without structural enhancements will decline when the pavement structure is weakened by temperature and moisture content increases. Future research should investigate the tradeoff between preventive maintenance and thicker pavement overlays with climate change. The effect of various pavement performance metrics on the choice of adaptation pathways should also be investigated.

CHAPTER 7: SUMMARY AND CONCLUSIONS

7.1 SUMMARY

SLR-induced groundwater rise and climate-change-induced temperature increases will have significant impacts on the service life of coastal-road infrastructure, but adaptation planning can decrease the cost of these impacts. The overall goal of this research was to investigate the effects of a changing climate on coastal-road pavement life and to develop adaptation planning methodologies for SLR-induced groundwater rise and temperature changes. First, the magnitude and areal extent of groundwater rise caused by SLR was determined in coastal NH. Maps were produced to identify the groundwater rise zone (GWRZ), i.e. the area where groundwater is projected to rise with SLR, and vulnerable coastal roadways. Second, the magnitude of pavement-life reduction from rising groundwater was investigated at five pavement evaluation sites on roads with different functional classifications. Two of these sites were then chosen to evaluate adaptation options to avoid premature pavement failure using the top-down approach for early-mid-century, mid-century, and end-of-century along the highest SLR scenario.

Next, a hybrid bottom-up/top-down approach was introduced and used to determine the seasonal and long-term effects of climate-change-induced temperature rise on pavement life. The sensitivity of the pavement to incremental temperature rise was determined and simple adaptation options with material-only costs were evaluated. Finally, a general framework for stepwise and flexible pavement adaptation was presented and demonstrated at a case-study site. In this study, the combined effect of both rising temperature and groundwater on pavement life was investigated. Adaptation pathways consisting of a series of adaptation actions were then

identified and compared in terms of performance and cost over a 60-year pavement management period.

7.2 CONCLUSIONS

One of the objectives of this research was to compare the top-down and hybrid bottom-up/top-down approaches to adaptation planning. The top-down adaptation results in terms of HMA thicknesses from Chapter 4 were compared with the hybrid results from Chapter 6. The three most cost-effective options for the top-down approach were compared with the closest adaptation pathways from the hybrid analysis. Direct comparisons are made with caution since there were differences in the analyses. The hybrid analysis included temperature rise, groundwater rise and traffic increases for the 60-year pavement management period, while the top-down approach considered only groundwater rise. Keeping these differences in mind, some observation can be made.

Both approaches dismissed the 508-mm base layer thickness as a viable option at the case-study site. The top-down approach yields robust designs based on the HMA thickness needed to prevent pavement failure in 2060 as opposed to a stepwise HMA overlay approach. This results in a recommended HMA thickness greater than what is needed in 2030. In addition, the top-down designs will need additional HMA overlays and/or base-layer thickness to prevent failure beyond 2060. In comparison, the hybrid analysis prescribes "just-in-time" stepwise HMA-thickness increases continuing out to 2080 and possibly beyond. The top-down adaptation plan is effective and does not preclude future adaptation actions, but it is more expensive than the comparable P3 and P4 hybrid pathways. In addition, the cost analysis presented in Chapter 6 shows that the P3 and P4 pathways are significantly more expensive than the most cost-effective

base-layer rehabilitation pathways of the hybrid adaptation approach. This demonstrates that the hybrid adaptation approach yields a more cost-effective climate-change adaptation plan than the top-down (scenario-based) adaptation approach at this pavement evaluation site.

The main findings of this dissertation are:

- Climate parameters affecting pavement life are changing with climate change and adaptation plans to strengthen the pavement surface layers are needed now to avoid the high cost of base-layer rehabilitation or reconstruction.
- Coastal groundwater will rise with sea-level rise three to four times farther inland than overland inundation, contributing to premature failure of coastal infrastructure and impacting natural ecosystems. This has implications for built and natural systems including coastal road and underground infrastructure, surface and groundwater quality, drinking water, historical properties, and human and ecosystem health.
- Coastal roads located within the groundwater rise zone (GWRZ) where the groundwater table depth is less than 10 feet below the pavement surface are at risk for reduced pavement life. The GWRZ and vulnerable roads (23% of the region's roads) have been identified in coastal NH.
- Adaptation actions, such as increasing the HMA and/or base-layer thicknesses, can reduce the impact of rising groundwater on pavement life; however, choosing when to implement these actions within the long-term pavement management period is challenging.
- Climate-change-induced temperature rise will change season durations and seasonal average temperatures, a phenomenon that should not be ignored in adaptation planning. The winter pavement season in northern regions is projected to end by mid-century, replaced by a lengthening fall season. Seasonal pavement damage, currently dominated by the late

spring and summer, is projected to be distributed more evenly throughout the year as temperatures rise.

- The top-down adaptation approach results in robust and protective adaptation actions but lacks the detail to define a cost-effective actionable adaptation plan.
- An adaptation framework employing the hybrid approach coupled with adaptation pathway mapping and cost accumulation over a 60-year pavement management period provides a stepwise and flexible approach to adaptation planning with opportunities to re-evaluate when new climate and traffic projections are available.
- Costs within each adaptation pathway increase with higher emissions scenarios and factors unrelated to climate, such as pavement rehabilitation efficiencies, recycling, and the timing of rehabilitation actions are important. Additional considerations when choosing adaptation pathways include pre-existing pavement condition, budgetary constraints, carbon emissions, and future road and property inundation.
- The hybrid adaptation framework provides value for systems that have considerable operation and maintenance costs. It is computationally intensive but results in stepwise and flexible adaptation pathways of cost-effective maintenance and rehabilitation actions to avoid premature failure associated with a changing climate.
- The optimal HMA thickness (O-HMA) is a useful metric for pavement performance with a changing climate by providing stakeholders with actionable guidance for maintenance overlays.

7.3 RECOMMENDATIONS AND FUTURE WORK

This dissertation introduces the hybrid adaptation framework for use in flexible pavement management in both coastal- and inland-road infrastructure when planning for climate change. This is a preliminary study that provides a new way of looking at infrastructure operations and management considering a changing climate. Future work is needed to make this approach operational.

When considering an entire pavement system, project-level management and reactive maintenance and rehabilitation are expensive. This research has focused on project-level climate adaptation, but the hybrid-adaptation approach is well suited for expansion and incorporation into Pavement Management Systems (PMS). Pavement management is a systematic method for selecting maintenance and rehabilitation actions, determining priorities and optimizing repair frequency by predicting future pavement condition and minimizing costs [*Shahin*, 2005]. A PMS involves pavement asset inventory definition, inspection and condition assessment, condition forecasting and analysis, and maintenance and rehabilitation budget prioritizing/optimization [*Shahin*, 2005]. Because most transportation agencies have PMS to assist in decision-making, incorporating climate-change adaptation planning into an existing framework is an appropriate approach for making pavements climate resilient [*Meyer et al.*, 2010].

The first step in PMS is defining the pavement asset inventory including the network, branches and sections for condition assessment. Next, a pavement performance model is chosen to estimate the type and timing of maintenance and rehabilitation actions as part of a multiyear improvement project for the network. The model is used to predict time to failure, optimize a combination of projects, evaluate long-term impacts, provide feedback loops, and estimate life-cycle costs [*Shahin*, 2005]. The modeling requires data for all the variables that affect pavement

performance. The next steps in the PMS system include grouping the maintenance and rehabilitation strategies and budget prioritization/optimization [*Shahin*, 2005].

This section discusses how climate-change adaptation planning can be incorporated into PMS using the hybrid approach and what additional information is needed. This engineering-based approach requires engineering judgment to identify climate-related pavement stressors in each region, network, branch, and pavement section; and choosing the appropriate pavement performance model, performance metrics, and adaptation options for evaluation.

The foundation of any successful PMS is data, accurate pavement modeling, and ease of implementation. The following additional research is necessary to help DOTs incorporate climate-change adaptation planning in PMS.

- Field and laboratory data are needed to define material M_R as a function of temperature and moisture content. These relationships need to be established for HMA, base, and subgrade materials in all regions of the country and for projected future ranges of temperatures, season lengths, and saturation frequency and duration.
- Pavement performance models used for design may need to be re-calibrated with future climate conditions.
- Pavement Climate Sensitivity Catalogs (PCSCs) need be created for pavement-sensitive climate stressors in all regions of the country and for typical pavement structures corresponding with each functional classification.
- Adaptation options to be evaluated in PCSCs include various layer thicknesses, binder grades, base materials and stabilization additives, improved drainage,

and/or geotextiles. The carbon footprint of the adaptation alternatives should also be considered when choosing adaptation options.

- Pavement performance models should be improved to simplify the input of climate-sensitive material properties that vary both seasonally and over the long term.
- The use of other pavement performance metrics should be investigated. Common PMS metrics include the Pavement Condition Index (PCI), International Roughness Index (IRI), Pavement Serviceability Index (PSI), etc. [*Wolters et al.*, 2011].
- The case-studies in this dissertation focused on pavement life reduction due to fatigue cracking and rutting induced by traffic loading with climate change. Rising temperatures can also increase age-hardening of asphalt binder and pavement inundation can result in asphalt moisture damage, both leading to asphalt durability decline [*FHWA*, 2015]. These processes must also be included in future climate-change adaptation research and planning.

The first step in incorporating climate-change adaptation into PMS is to identify the most important environmental stressors for each region of the country and networks within each region. Each region will face different threats from climate change [*Jay et al.*, 2018]. For example, the northern regions are expected to experience seasonal changes in freeze-thaw cycles, coastal regions will experience sea-level and groundwater rise impacts, and the southwest is expected to experience extreme heat [*Jacobs et al.*, 2018]. The pavement network is a logical grouping of pavements for maintenance and rehabilitation management and a branch within the network has a specific use or functional classification [*Shahin*, 2005]. This definition could be expanded to include specific climate vulnerabilities as well. The vulnerable pavement systems,

such as coastal roads vulnerable to tidal-water flooding or SLR-induced groundwater rise, roads close to rivers that are projected to flood more frequently, or areas with projected extreme heat, are identified and targeted for specific climate analysis including the creation of PCSCs.

Once the climate-stressors and the vulnerable branches in a PMS network have been identified, a pavement performance model and the performance metric are chosen. The ideal model for climate-change adaptation planning should be capable of processing changing temperatures, season duration, and moisture content as well as material properties on annual, seasonal, and possibly daily time scales. A model that relies on historical climate data will underestimate future pavement damage and costs. The performance metric used in this dissertation's case study is the optimal HMA thickness (O-HMA). The O-HMA criteria assumes that overlays are applied at a performance-based prescribed frequency and thickness to maintain the pavement's reliability at a predetermined level. This differs from the typical PMS approach where a pavement condition index (PCI) is calculated, falling between 0 and 100 [*Shahin*, 2005]. A low PCI suggests that the pavement condition is poor. When the PCI drops to the critical PCI (typical range is 55 to 70), the point at which the PCI loss increases with time, the cost of preventative maintenance increases dramatically, and major rehabilitation is considered [*Shahin*, 2005].

Once the pavement performance model and performance metric is selected, a PCSCs can be created for the vulnerable branches and sections within the PMS network. The creation of PCSCs is not currently part of PMS but could be produced by pavement research groups and would be an important PMS resource. The PCSC is created for the identified important environmental stressors and traffic. The pavement's response to loading is influenced by environmental parameters such as temperature (maximum, minimum, average, seasonal average, etc.), moisture content, saturation duration, flooding, freeze-thaw cycles, etc. The response is also a function of

traffic; consequently, PCSCs should be created for different levels of expected traffic in addition to various combinations of climate stressors. The PCSC provides practitioners with information about how the typical pavement section will respond to many possible climate futures. If climate projections change due to a reduction in greenhouse gas emissions or accelerated climate change, practitioners will still have actionable guidance for the new conditions.

Using the asset-specific information from the PCSC on the asset's climate sensitivity, adaptation pathways can be established using downscaled climate-model output and evaluated using the maintenance and rehabilitation prioritization methodologies in PMS. If many adaptation pathways are to be evaluated, project-level budget optimization [*Santos and Ferreira*, 2012] in addition to network-level optimization [*Shahin*, 2005] can be used to identify the most cost-effective adaptation strategies. In PMS, cost is not the only factor to consider when prioritizing maintenance and rehabilitation strategies. Safety is also a factor. This is also true with climate-change adaptation pathways, especially in areas expected to experience more frequent coastal storms, sea-level rise, wildfires, and river flooding. Adaptation plan flexibility, stakeholder involvement, engineering judgment, and regular re-evaluation through PMS feedback loops are all essential in the adaptation planning process.

Once the hybrid adaptation framework and lessons learned from this research are incorporated in PMS, practitioners will be able to: (1) identify roads that are vulnerable to changes in climate and more frequent extreme weather events, (2) enhance pavement-life forecasting by including climate change in predictive models, (3) gain increased knowledge of a pavement's response to loading with changing environmental conditions using a PCSC, (4) identify stepwise adaptation pathways, (5) use life-cycle cost analysis with probabilistic present-value cost

distributions to compare adaptation pathways, (6) choose a cost-effective adaptation plan that is stepwise and flexible, and (7) re-evaluate and modify the plan if necessary.

7.4 CONTRIBUTIONS TO KNOWLEDGE

This research has applied recent advances in climate-change adaptation planning with uncertainty to pavement management. To date, it has resulted in three published papers and one accepted for publication in peer-reviewed journals. Two additional papers will be submitted for publication. The work has been presented in regional, national and international conferences and has spurned additional research. It has raised awareness of SLR-induced groundwater rise in coastal areas and its' potential impacts on natural ecosystems and infrastructure in low-lying areas. The pavement adaptation framework presented in Chapter 6 provides stakeholders with an important first step in incorporating performance-based climate-adaptation in PMS.

LIST OF REFERENCES

AASHTO (1996), Guide for design of pavement structures.

AASHTO (2008), Mechanistic-Empirical Pavement Design Guide (MEPDG). A Manual of Practice, Interim Edition.

AASHTO (2017), AASHTO M 320 - Standard Specification for Performance-Graded Asphalt Binder, 8.

Aerial Photos (2011), 2010-2011 1-ft Color Aerial Photos.

Asphalt Institute (1982), Research and Development of the Asphalt Institute's Thickness Design Manual (MS-1) Ninth Edition, 204 p.

ASTM (2011), Standard Practice for Classification of Soils for Engineering Purposes (Unified Soil Classification System), *American Society for Testing and Materials, D 2487-11*.

Ayotte, J. D. and K. W. Toppin (1995), Geohydrology and water quality of stratified-drift aquifers in the middle Merrimack River Basin, south-central New Hampshire, *U.S. Geological Survey Water-Resources Investigations Report 92-4192*, 52 p.

Barker, G. (2016), GEOLOGS, *New Hampshire Geological Survey, New Hampshire Department of Environmental Services*.

Batouli, M. and A. Mostafavi (2016), Assessment of Sea-Level Rise Adaptations in Coastal Infrastructure Systems: Robust Decision Making under Uncertainty, Construction Research Congress 2016: Old and New Construction Technologies Converge in Historic San Juan, CRC 2016, May 31, 2016 - June 2, 2016.

Bear, J. (1979), *Hydraulics of Groundwater*, McGraw-Hill Inc., New York.

Bhave, A. G., A. Mishra, and N. S. Raghuwanshi (2014), A combined bottom-up and top-down approach for assessment of climate change adaptation options, *Journal of Hydrology, 518*, 150-161, doi: http://dx.doi.org.libproxy.unh.edu/10.1016/j.jhydrol.2013.08.039.

Bizjak, K. F., A. Dawson, I. Hoff, L. Makkonen, J. S. Ylhaisi, and A. Carrera (2014), The impact of climate change on the european road network, *Proceedings of the Institution of Civil Engineers: Transport, 167*(5), 281-295, doi: 10.1680/tran.11.00072.

Bjerklie, D. M., J. R. Mullaney, J. R. Stone, B. J. Skinner, and M. A. Ramlow (2012), Preliminary investigation of the effects of sea-level rise on groundwater levels in New Haven, Connecticut, *U.S. Geological Survey Open-File Report, 2012-1025*, 46.

Brown, C., Y. Ghile, M. Laverty, and K. Li (2012), Decision scaling: Linking bottom-up vulnerability analysis with climate projections in the water sector, *Water Resour. Res., 48*(9), doi: 10.1029/2011WR011212.

Burmister, D. M. (1943), The Theory of Stresses and Displacements in Layered Systems and Applications to the Design of Airport Runways, *Highway Research Board, 23*, 126-144.

Butler, J. R. A., R.M. Wise, T.D. Skewes, E.L. Bohensky, N. Peterson, W. Suadnya, Y. Yanuartati, T. Handayani, P. Habibi, K. Puspadi, N. Bou, D. Vaghelo, W. Rochester (2015), Integrating Top-Down and Bottom-Up Adaptation Planning to Build Adaptive Capacity: A Structured Learning Approach, *Coast. Manage., 43*, 346-364.

Cedergren, H. (1988), Why all Important Pavement Should be Well Drained, *Transportation Research Record: Journal of the Transportation Research Board*, 56-62.

Chinowsky, P. S., J. C. Price, and J. E. Neumann (2013), Assessment of climate change adaptation costs for the U.S. road network, *Global Environmental Change, 23*(4), 764-773, https://doi.org/10.1016/j.gloenvcha.2013.03.004.

Christopher, B. R., C. Schwartz, and R. Boudreau (2006), Geotechnical Aspects of Pavements, *FHWA NHI-05-037*.

Church, J. A., P. L. Woodworth, T. Aarup, and W. S. Wilson (2010), *Understanding Sea-Level Rise and Variability*, Blackwell Publishing, Ltd.

Coastal NH (2013), 1-ft Resolution Imagery for Coastal New Hampshire.

Cooper, H., C. Zhang, and D. Selch (2015), Incorporating Uncertainty of Groundwater Modeling in Sea-Level Rise Assessment: a Case Study in South Florida, *Clim. Change, 129*(1-2), 281-294, http://dx.doi.org/10.1007/s10584-015-1334-1.

Cooper, H. M., Q. Chen, C. H. Fletcher, and M. M. Barbee (2013), Assessing vulnerability due to sea-level rise in Maui, Hawaiâ€˜i using LiDAR remote sensing and GIS, *Clim. Change, 116*(3), 547-563, doi: 10.1007/s10584-012-0510-9.

Cornell University (2016), Typical Values of Youngs Elastic Modulus and Poissons Ratio for Pavement Materials, *2016*.

Daniel, J. S., J. M. Jacobs, H. Miller, A. Stoner, J. Crowley, M. Khalkhalia, and A. Thomas (2017), Climate change: potential impacts on frost–thaw conditions and seasonal load restriction timing for low-volume roadways, *Road Materials and Pavement Design*.

Daoulas, J., M. Elfino, H. Nair, and S. Nelson (2011), Forensic investigation and remediation of pavement performance affected by groundwater seepage, *Transp. Res. Rec.*(2212), 65-73, doi: 10.3141/2212-07.

de Bruin, K., R.B. Dellink, A. Ruijs, L. Bolwidt, A. van Buuren, J. Graveland, R.S. de Groot, P.J. Kuikman, S. Reinhard, R.P. Roetter, V.C. Tassone, A. Verhagen, and E.C. van Ierland (2009), Adapting to climate change in The Netherlands: an inventory of climate adaptation options and ranking of alternatives, *Clim. Change, 95*, 23-45.

DeCarlo, C., W. Mo, E. Dave, and J. Locore (2017), Sustainable Pavement Rehabilitation Strategy using Consequential Life Cycle Assessment: An Example of Interstate 95, Proceedings of the 10th International Conference on the Bearing Capacity of Road, Railways, and Airfields (BCRRA 2017), Athens, Greece.

DeConto, R. M. and D. Pollard (2016), Contribution of Antarctica to past and future sea-level rise, *Nature, 531*, 591–597.

Deser, C., A. Phillips, V. Bourdette, and H. Teng (2012), Uncertainty in climate change projections: The role of internal variability, *Climate Dynamics, 38*, 527-546.

Dripps, W. R. and K. R. Bradbury (2007), A simple daily soil-water balance model for estimating the spatial and temporal distribution of groundwater recharge in temperate humid areas, *Hydrogeol. J., 15*, 433-44.

Elshaer, M. (2017), *Moisture Dependent Performance of Flexible Pavements*, Doctoral Dissertation, University of New Hampshire, Durham, NH.

Elshaer, M., J. Daniel, M. Ghayoomi, and E. Dave (2015), Sensitivity Analysis for Pavement Structure Evaluation During Flooding, Transportation Research Board 95th Annual Meeting, Washington, D.C.

Elshaer, M., M. Ghayoomi, and J. S. Daniel (2017a), Impact of Subsurface Water on the Structural Performance of Inundated Flexible Pavements, *International Journal of Pavement Engineering, 1-11*.

Elshaer, M., M. Ghayoomi, J. Daniel, and E. Dave (2015), Impact of Subgrade Moisture Content on the Performance of Pavement Structure, Presented at the 95th Annual Meeting of the Transportation Research Board.

Elshaer, M., M. Ghayoomi, and J. S. Daniel (2017b), Methodology to evaluate performance of pavement structure using soil moisture profile, *Road Materials and Pavement Design*, 1-20.

Ezer, T. and L. P. Atkinson (2014), Accelerated flooding along the U.S. East Coast: On the impact of sea-level rise, tides, storms, the Gulf Stream, and the North Atlantic Oscillations, *Earth's Future, 2*, 362-382.

FHWA (1998a), LTPP Guide to Asphalt Temperature Prediction and Correction, *FHWA-RD-98-085*.

FHWA (1998b), Life-Cycle Cost Analysis in Pavement Design — Interim Technical Bulletin, *FHWA-SA-98-079*.

FHWA (2004), Real Cost Life-Cycle Cost Analysis-User Manual, *2.1*.

FHWA (2008), Long-Term Pavement Performance Computed Parameter: Frost Penetration, Frost penetration analysis results, *FHWA-HRT-08-057, Chapter 7*.

FHWA (2015), Climate Change Adaptation for Pavements, *FHWA-HIF-15-015*.

FHWA (2017), Real Cost Life-Cycle Cost Analysis, *2.5*.

FHWA (2018), Cost-Based Unit Price: HMA and Aggregate Base.

Fleming, E., J. Payne, W. Sweet, M. Craghan, J. Haines, J. F. Hart, H. Stiller, and A. Sutton-Grier (2018), Coastal Effects. In Impacts, Risks, and Adaptation in the United States: Fourth National Climate Assessment, Volume II, 322–352.

Forbes, P. W. (2015), Pease Tradeport groundwater monitoring data. United States Airforce Civil Engineer Center, *2015*.

Goddard, P. B., J. Yin, S. M. Griffies, and S. Zhang (2015), An extreme event of sea-level rise along the Northeast coast of North America in 2009–2010., *Nat. Commun., 6:6346*.

Goodspeed, C.H., E.R. Schmeckpeper, and R.L. Lemieux (1994), Road Surface Management System, 3rd International Conference on Managing Pavements, 12/08.

Groves, D. G. and R. J. Lempert (2007), A new analytic method for finding policy-relevant scenarios, *Global Environmental Change, 17*(1), 73-85, https://doi.org/10.1016/j.gloenvcha.2006.11.006.

Gudipudi, P. P., B. S. Underwood, and A. Zalghout (2017), Impact of climate change on pavement structural performance in the United States, *Transportation Research Part D: Transport and Environment, 57*, 172-184, https://doi-org.libproxy.unh.edu/10.1016/j.trd.2017.09.022.

Haasnoot, M., J. H. Kwakkel, W. E. Walker, and J. ter Maat (2013), Dynamic adaptive policy pathways: A method for crafting robust decisions for a deeply uncertain world, *Global Environmental Change, 23*(2), 485-498, https://doi.org/10.1016/j.gloenvcha.2012.12.006.

Habel, S., C. H. Fletcher, K. Rotzoll, and A. I. El-Kadi (2017), Development of a model to simulate groundwater inundation induced by sea-level rise and high tides in Honolulu, Hawaii, *Water Research, 114*, 122-134.

Hall, J. A., S. Gill, J. Obeysekera, W. Sweet, K. Knuuti, and J. Marburger (2016), Regional Sea Level Scenarios for Coastal Risk Management: Managing the Uncertainty of Future Sea Level Change and Extreme Water Levels for Department of Defense Coastal Sites Worldwide, 224.

Harbaugh, A. (2005), MODFLOW-2005, The U.S. Geological Survey modular ground-water model—the Ground-Water Flow Process, *U.S. Geological Survey Techniques and Methods, 6-A16*.

Harbaugh, A., E. Banta, M. Hill, and M. McDonald (2000), MODFLOW-2000, The U.S. Geological Survey Modular Ground-Water Model—User Guide to Modularization Concepts and the Ground-Water Flow Process, *U.S. Geological Survey Open-File Report - 00-92*, 121.

Harvey, J. W. and W. E. Odum (1990), The influence of tidal marshes on upland groundwater discharge to estuaries, *Biogeochemistry, 10*, 217-236.

Hawkins, E. and R. Sutton (2011), The potential to narrow uncertainty in projections of regional precipitation change, *Climate Dynamics, 37*, 407-418.

Hawkins, E. and R. Sutton (2009), The Potential to Narrow Uncertainty in Regional Climate Predictions, *Bull. Amer. Meteor. Soc., 90*, 1095-1107.

Hayhoe, K., C. Wake, T. Huntington, L. Luo, M. Schwartz, J. Sheffield, E. Wood, B. Anderson, J. Bradbury, A. DeGaetano, T. Troy, and D. Wolfe (2006), Past and Future Changes in Climate and Hydrological Indicators in the U.S. Northeast, *Climate Dynamics, 28*, 381-407.

Hayhoe, K., A. Stoner, S. Abeysundara, J. S. Daniel, J. M. Jacobs, P. Kirshen, and R. Benestad (2015), Climate projections for transportation infrastructure planning, operations and maintenance, and design, *Transp. Res. Rec., 2510*, 90-97, doi: 10.3141/2510-11.

Heath, R. C. (1983), Ground-Water Hydrology, *U.S. Geological Survey Water-Supply Paper 2220, Water-Supply Paper 2220*, 84.

Hemond, H. F. and J. L. Fifield (1982), Subsurface flow in salt-marsh peat—A model and field-study, *Limnology and Oceanography, 27*, 126-136.

Herman, J. D., P. M. Reed, H. B. Zeff, and G. W. Characklis (2015), How Should Robustness Be Defined for Water Systems Planning under Change?, *Journal of Water Resources Planning and Management*, 1-14.

Holmes, R. R., Jr., P. J. Terrio, M. A. Harris, and P. C. Mills (2001), Introduction to Field Methods for Hydrologic and Environmental Studies, *U.S. Geological Survey Open-File Report 01-50*, 245.

Hoover, D. J., K. O. Odigie, P. W. Swarzenski, and P. Barnard (2017), Sea-level rise and coastal groundwater inundation and shoaling at select sites in California, USA, *Journal of Hydrology: Regional Studies, 11*(Supplement C), 234-249, doi: https://doi.org/10.1016/j.ejrh.2015.12.055.

Horton, B. P., S. Rahmstorf, S. E. Engelhart, and A. C. Kemp (2014), Expert Assessment of Sea-Level Rise by AD 2100 and AD2300. *Quaternary Science Reviews,* 84, 2014, pp. 1-6., *Quaternary Science Reviews, 84*, pp. 1-6.

Huang, Y. (2003), KENPAVE - A Computer Package for Pavement Analysis and Design.

ICF International (2016), U.S. DOT CMIP Climate Data Processing Tool, User Guide.

IPCC (2007), *Contribution of Working Group I to the Fourth Assessment Report of the Intergovernmental Panel on Climate Change 2007*, Cambridge University Press, Cambridge, UK and New Yor, NY.

IPCC (2013), Climate Change 2013: The Physical Science Basis. Contribution of Working Group I to the Fifth Assessment Report of the Intergovernmental Panel on Climate Change, 1535.

IPCC (2014), Climate Change 2014: Synthesis Report, Contribution of Working Groups I, II and III to the Fifth Assessment Report of the Intergovernmental Panel on Climate Change [Core Writing Team, R.K. Pachauri and L.A. Meyer (eds.)]. , 151.

Jacobs, J. M., L. R. Cattaneo, W. Sweet, and T. Mansfield (2018), Recent and Future Outlooks for Nuisance Flooding Impacts on Roadways on the U.S. East Coast, *Transp. Res. Rec., 2672*, 1-10.

Jacobs, J. M., M. Culp, L. Cattaneo, P. Chinowsky, A. Choate, S. DesRoches, S. Douglass, and R. Miller (2018), Transportation. In *Impacts, Risks, and Adaptation in the United States: Fourth National Climate Assessment, Volume II*, 479-511.

Janoo, V. (1994), Layer Coefficients for NHDOT Pavement Materials, *Special Report 94-30*, 53.

Janoo, V., J. J. Bayer, G. D. Durell, and C. E. Smith (1999), Resilient Modulus for New Hampshire Subgrade Soils for Use in Mechanistic AASHTO Design, *Special Report 99-14*, 1-43.

Jay, A., D.R. Reidmiller, C.W. Avery, D. Barrie, B.J. DeAngelo, A. Dave, M. Dzaugis, M. Kolian, K.L.M. Lewis, K. Reeves, and D. Winner (2018), Overview, In: *Impacts, Risks, and Adaptation in the United States: Fourth National Climate Assessment, Volume II* [Reidmiller, D.R., C.W. Avery, D.R. Easterling, K.E. Kunkel, K.L.M. Lewis, T.K. Maycock, and B.C. Stewart (eds.)]. U.S. Global Change Research Program, Washington, DC, USA, pp. 33–71. doi: 10.7930/NCA4.2018.CH1.

Johnston, A., P. Slovinsky, and K. L. Yates (2014), Assessing the vulnerability of coastal infrastructure to sea level rise using multi-criteria analysis in Scarborough, Maine (USA), *Ocean Coast. Manage., 95*, 176-188.

Karmalkar, A. V. and R. S. Bradley (2017), Consequences of Global Warming of 1.5°C and 2°C for Regional Temperature and Precipitation Changes in the Contiguous United States, *PLoS ONE, 12*.

Kasprzyk, J. R., S. Nataraj, P. M. Reed, and R. J. Lempert (2013), Many objective robust decision making for complex environmental systems undergoing change, *Environmental Modelling & Software, 42*(Supplement C), 55-71, https://doi.org/10.1016/j.envsoft.2012.12.007.

Kemp, A. C., B. P. Horton, J. P. Donnelly, M. E. Mann, M. Vermeer, and S. Rahmstorf (2011), Climate related sea-level variations over the past two millennia, *Proc. Natl. Acad. Sci. U. S. A., 108*, 11017-11022.

Kirshen, P., L. Caputo, R. M. Vogel, P. Mathisen, A. Rosner, and T. Renaud (2014), Adapting Urban Infrastructure to Climate Change: A Drainage Case Study, *Journal of Water Resources Planning Management*.

Kirshen, P., C. Wake, M. Huber, K. Knutti, and M. Stampone (2014), Sea-Level Rise, Storm Surges, and Extreme Precipitation in Coastal New Hampshire: Analysis of Past and Projected Future Trends.

Knott, J. F., J. S. Daniel, J. M. Jacobs, P. Kirshen, and M. Elshaer (2017), Assessing the Effects of Rising Groundwater from Sea-Level Rise on the Service Life of Pavements in Coastal Road Infrastructure, *TRB Research Record: Journal of Transportation Research Board, 2639*.

Knott, J. F., J. Jacobs, J. S. Daniel, and P. Kirshen (2018a), Modeling the Effects of Sea-Level Rise on Groundwater Levels in Coastal New Hampshire, *Journal of Coastal Research, 35*, 143-157.

Knott, J. F., J. E. Sias, E. V. Dave, and J. M. Jacobs (2019), Seasonal and Long-Term Changes to Pavement Life Caused by Rising Temperatures from Climate Change, *Transportation Research Record: Journal of the Transportation Research Board, In Press.*

Knott, J. F., J. S. Daniel, J. M. Jacobs, and P. Kirshen (2018b), Adaptation Planning to Mitigate Coastal-Road Pavement Damage from Groundwater Rise Caused by Sea-Level Rise, *Transp. Res. Rec.*, 0361198118757441.

Kopp, R. E., R. M. DeConto, D. A. Bader, R. M. Horton, C. C. Hay, S. Kulp, M. Oppenheimer, D. Pollard, and B. H. Strauss (2017), Implications of Antarctic ice-cliff collapse and ice-shelf hydrofracturing mechanisms for sea-level projections., *Earth's Future*.

Kopp, R. E., R. M. Horton, C. M. Little, J. X. Mitrovica, M. Oppenheimer, D. J. Rasmussen, B. H. Strauss, and C. Tebaldi (2014), Probabilistic 21st and 22nd century sea-level projections at a global network of tide-gauge sites, *Earth's Future, 2*, 383-406.

Kossin, J. P., T. Hall, T. Knutson, K. E. Kunkel, R. J. Trapp, D. E. Waliser, and M. F. Wehner (2017), Extreme Storms. Climate Science Special Report: Fourth National Climate Assessment, Volume I, 257–276.

Kumlai, S., P. Jitsangiam, and P. Pichayapan (2017), The implications of increasing temperature due to climate change for asphalt concrete performance and pavement design, *KSCE Journal of Civil Engineering, 21*, 1222-34.

Kwadijk, J. C. J., M. Haasnoot, J.P.M. Mulder, M.M.C. Hoogvliet, A.B.M. Jeuken, R.A.A. van der Krogt, N.G.C. van Oostrom, H.A. Schelfhout, E.H. van Velzen, H. van Waveren, and M.J.M de Wit (2010), Using adaptation tipping points to prepare for climate change and sea level rise: a case study in the Netherlands, *Wiley Interdisciplinary Reviews: Climate Change, 1*, 729-740.

Kwakkel, J. H., M. Haasnoot, and W. E. Walker (2016), Comparing Robust Decision-Making and Dynamic Adaptive Policy Pathways for model-based decision support under deep uncertainty, *Environmental Modelling & Software, 86*, 168-183.

Kwakkel, J. H., W. E. Walker, and M. Haasnoot (2016), Coping with the Wickedness of Public Policy Problems: Approaches for Decision Making under Deep Uncertainty, *J. Water Resour. Plann. Manage., 142*, 01816001.

Lempert, R. J., N. Kalra, S. Peyraud, Z. Mao, S. B. Tan, D. Cira, and A. Lotsch (2013), Ensuring Robust Flood Risk Management in Ho Chi Minh City, *Working Paper No. 6465*.

Lempert, R. J. and M. T. Collins (2007), Managing the Risk of Uncertain Threshold Responses: Comparison of Robust, Optimum, and Precautionary Approaches, *Risk Analysis, 27*, 1009-1026.

Lempert, R. J., D. G. Groves, S. W. Popper, and S. C. Bankes (2006), A General, Analytic Method for Generating Robust Strategies and Narrative Scenarios, *Management Science, 52*, 514-528.

Levenberg, K. (1944), A method for the solution of certain nonlinear problems in least squares, *Quarterly Journal of Applied Mathematics, 2*, p. 164-168.

Lorah, M. M. and L. D. Olsen (1999), Natural attenuation of chlorinated volatile organic compounds in a freshwater tidal wetland: Field evidence of anaerobic biodegradation, *Water Resour. Res., 35*, 3811-3827.

Lyons, J. B., W. A. Bothner, R. H. Moench, and J. B. Thompson Jr. (1998), A New Bedrock Geologic Map of New Hampshire, revised.

Mack, T. J. (2009), Assessment of ground-water resources in the Seacoast region of New Hampshire, *U.S. Geological Survey Scientific Investigations Report, 2008-5222*, 188.

Mack, T. J. (2004), Assessing the potential for saltwater intrusion in a coastal fractured-bedrock aquifer using numerical modeling, Fractured-Rock Conference, Denver, Colorado, National Ground Water Association, p. 220-221, Portland, Maine, September 13-15, 2004.

Mallick, R. B. and T. El-Korchi (2013), *Pavement Engineering Principals and Practice, Second Edition*, CRC Press, Taylor and Francis Group, LLC, Boca Raton, FL.

Mallick, R. B., J. M. Jacobs, B. J. Miller, J. S. Daniel, and P. Kirshen (2016), Understanding the impact of climate change on pavements with CMIP5, system dynamics and simulation, 1-9, doi: 10.1080/10298436.2016.1199880.

Mallick, R. B., M. J. Radzicki, J. S. Daniel, and J. M. Jacobs (2014), Use of system dynamics to understand long-term impact of climate change on pavement performance and maintenance cost, *Transp. Res. Rec., 2455,* 1-9, doi: 10.3141/2455-01.

Manda, A. K., M. S. Sisco, D. J. Mallinson, and M. T. Griffin (2015), Relative role and extent of marine and groundwater inundation on a dune-dominated barrier island under sea-level rise scenarios, *Hydrol. Process., 29,* 1894-1904.

Marquardt, D. W. (1963), An algorithm for least-squares estimation of nonlinear parameters, *Journal of the Society of Industrial and Applied Mathematics, 11*, p. 431-441.

Masterson, J. P. (2004), Simulated Interaction Between Freshwater and Saltwater and Effects of Ground-Water Pumping and Sea-Level Change, Lower Cape Cod Aquifer System, Massachusetts, *U.S. Geological Survey Scientific Investigations Report, 2004-5014*, 72.

Masterson, J. P., M. N. Fienen, E. R. Thieler, D. B. Gesch, B. T. Gutierrez, and N. G. Plant (2014), Effects of sea-level rise on barrier island groundwater system dynamics - ecohydrological implications, *Ecohydrology, 7*, 1064-1071.

Masterson, J. P. and S. P. Garabedian (2007), Effects of Sea-Level Rise on Ground Water Flow in a Coastal Aquifer System, *Ground Water, 45*(2), 209-217, doi: 10.1111/j.1745-6584.2006.00279.x.

McCobb, T. D. and P. K. Weiskel (2003), Long-term hydrologic monitoring protocol for coastal ecosystems, *02-497*, 94.

Meagher, W., J. S. Daniel, J. Jacobs, and E. Linder (2012), A Methodology to Evaluate the Implications of Climate Change on the Design and Performance of Flexible Pavements, *Transportation Research Record, 2305*, 111-120.

Medalie, L. and R. B. Moore (1995), Ground-water resources in New Hampshire—Stratified-drift aquifers:, *U.S. Geological Survey Water Resources Investigtions Report 95–4100*, 31 p.

Meehl, G. A., T.F. Stocker, W. Collins, P. Friedlingstein, A.T. Gaye, J.M. Gregory, A. Kitoh, R. Knutti, J.M., A. Noda, S.C.B. Raper, I.G. Watterson, A.J. Weaver, and Z.C. Zhao (2007), Global climate projections. Climate Change 2007: the physical science basis. Cambridge University Press, Cambridge, *Climate Change 2007: the physical science basis*.

Melillo, J., T. Richmond, and G. Yohe (2014), Climate Change Impacts in the United States: The Third National Climate Assessment. Chapter 1: Overview and Report Findings, 841.

Menendez, J. R. and N. G. Gharaibeh (2017), Incorporating Risk and Uncertainty into Ifrastructure Asset Managment Plans for Pavement Networks, *Journal of Infrastructure Systems, 23*.

Meyer, M. D., A. Amekudzi., and J. P. O'Har (2010). Transportation Asset Management Systems and Climate Change: Adaptive Systems Management Approach. *Transportation Research Record, 2160*(1), 12–20. https://doi.org/10.3141/2160-02

Meyer, M., M. Flood, J. Keller, J. Lennon, G. McVoy, C. Dorney, K. Leonard, R. Hyman, and J. Smith (2014), Strategic Issues Facing Transportation, Volume 2: Climate Change, Extreme Weather Events, and the Highway System. Transportation Research Board of the National Academies, Washington, D.C, *750*.

Mills, B. N., S. L. Tighe, J. Andrey, J. T. Smith, and K. Huen (2009), Climate Change Implications for Flexible Pavement Design and Performance in Southern Canada, *Journal of Transportation Engineering-ASCE, 135*, 773-782.

Minnesota Department of Transportation (2014a), Process for seasonal load limit starting and ending dates, *Technical Memorandum No. 14-10-MAT-02*.

Minnesota Department of Transportation (2014b), Process for seasonal load limit starting and ending dates, *Technical Memorandum No. 14-10-MAT-02*.

Moffett, K. B., S. M. Gorelick, R. G. McLaren, and E. A. Sudicky (2012), Salt marsh ecohydrological zonation due to heterogeneous vegetation–groundwater–surface water interactions, *Water Resour. Res., 48*, n/a-n/a.

Moftakhari, H. R., A. AghaKouchak, B. F. Sanders, D. L. Feldman, W. Sweet, R. A. Matthew, and A. Luke (2015), Increased nuisance flooding along the coasts of the United States due to sea level rise: Past and future, *Geophysical Research Letters, 42, 9846-9852., 42*, 9846-9852.

Moore, R. B. (1990), Geohydrology and water quality of stratified-drift aquifers in the Exeter, Lamprey, and Oyster River Basins, southeastern New Hampshire, *Water-Resources Investigations Report*.

Moser, S., M. Davidson, P. Kirshen, P. Mulvaney, J. Murley, J. Neuman, L. Petes, and D. Reed (2014), Coastal Zone Development and Ecosystems, *Chapter 25 of the US National Climate Assessment 2014 Report*.

Moss, R., M. Babiker, S. Brinkman, E. Calvo, T. Carter, J. Edmonds, I.Elgizouli, S. Emori, L. Erda, K. Hibbard, R. Jones, M. Kainuma, J. Kelleher, J.F. Lamarque, M. Manning, B. Matthews, J. Meehl, L. Meyer, J. Mitchell, N. Nakicenovic, B. O'Neill, R. Pichs, K. Riahi, S. Rose, P. Runci, R. Stouffer, D. van Vuuren, J. Weyant, T. Wilbanks, J.P. van Ypersele, and M. Zurek (2008), Towards New Scenarios for Analysis of Emissions, Climate Change, Impacts, and Response Strategies. Geneva: Intergovernmental Panel on Climate Change. p. 132, 132.

Muench, S. and T. Van Dam (2015), Climate Change Adaptation for Pavements, *DTFH61-10-D-00042*.

Muthadi, N. and Y. Kim (2008), Local calibration of mechanistic-empirical pavement design guide for flexible pavement design, *Transportation Research Record: Journal of the Transportation Research Board*, 131-141.

N.H. Department of Environmental Services (2016), One Stop Data and Information, *2016*.

National Geodetic Survey (2016), Orthometric Height Conversion.

National Research Council (Ed.) (2011), *Climate Stabilization Targets: Emissions, Concentrations, and Impacts Over Decades to Millennia, the National Academies Press, Washington DC*, The National Academies press, Washington, DC.

Natural Resources Conservation Service (NRCS) (2016), Guide Sheet 1- General relationship of systems used for classifying soil samples. USDA. Official Soil Series Descriptions, *2016*.

Nemati, R., E. V. Dave, and J. S. Daniel (2018), Comparative Evaluation of New Hampshire Mixtures on Basis of 1 Laboratory Performance Tests Comparative Evaluation of New Hampshire Mixtures on Basis of Laboratory Performance Tests, International Society of Asphalt Pavement (ISAP) Conference Proceedings.

NH Coastal Lidar (2011), Coastal New Hampshire Lidar - 2011.

NH Hydrography (2006), New Hampshire Hydrography Data Set.

NH State Geologist (2004), Surficial Geology.

NHDOT (2014), Highway Design Manual, *Appendix 7-1 Flexible Pavement Analysis*, 1-7.

NHDOT (2015), NHDOT Pavement Strategy - Summary.

NHDOT (2016), New Hampshire Department of Transportation. Project Viewer, *2016*.

NHDOT (2017), Weighted Average Unit Prices for projects between 4/1/2016 and 3/31/20.

NHDOT (2018), New Hampshire Department of Transportation - Weighted Average Unit Prices for projects between 7/1/2017 and 6/30/2018.

NOAA (2016), https://tidesandcurrents.noaa.gov/datums.html?id=8423898, *2016.*

Office of Management and Budget (2018), OMB Circular Number A-94 - Appendix C. Real Treasury Interest Rates from 1979 through 2017., *2018*.

Orr, D. P. and L. H. Irwin (2006), Seasonal Variations of In Situ Materials Properties in New York State - Final Report, *CLRP Report No. 06-6*.

Oude Essink, G. H. P., E. S. van Baaren, and P. G. B. de Louw (2010), Effects of climate change on coastal groundwater systems: A modeling study in the Netherlands, *Water Resour. Res., 46*.

P. Oude Essink, G., E. van Baaren, and P. B de Louw (2010), Effects of climate change on coastal groundwater systems: A modeling study in the Netherlands, *Water Resour. Res.*, *46*(00), http://dx.doi.org.libproxy.unh.edu/10.1029/2009WR008719.

Parris, A., P. Bromirski, V. Burkett, D. Cayan, M. Culver, J. Hall, R. Horton, K. Knutti, R. Moss, J. Obeysekera, A. Sallenger, and J. Weiss (2012), Global Sea Level Rise Scenarios for the US National Climate Assesment, *NOAA Technical Memo OAR CPO-1*, 252.08-37.

Pierce, D. W., D. R. Cayan, and B. L. Thrasher (2014), Statistical downscaling using Localized Constructed Analogs (LOCA), *Journal of Hydrometeorology*, *15*, 2558-2585.

Ping, W. V. and C. Ling (2008), Design Highwater Clearances For Highway Pavements, *FL/DOT/RMC/BD-543-13*, 473.

Ping, W. V., B. Sheng, C. Ling, B. Dietrich, and D. Horhota (2010), Influence of base clearance on subgrade resilient modulus of Florida roadway pavements, *Transportation Research Record: Journal of the Transportation Research Board*(2154), 176-186, doi: 10.3141/2154-18.

Pitz, C. (2016), Predicted Impacts of Climate Change on Groundwater Resources of Washington State.

Ray, P. A. and C. M. Brown (2015), Confronting Climate Uncertainty in Water Resources Planning and Project Design: The Decision Tree Framework.

Reclamation (2016), Downscaled CMIP3 and CMIP5 Climate and Hydrology Projections.

Rockingham Planning Commission (2015), Tides to Storms: Preparing for New Hampshire's Future Coast, *2016*.

Rockingham Planning Commission (2017), 2040 Long Range Transportation Plan.

Roshani, A. (2014), Road Infrastructure Vulnerability to Groundwater Table Variation Due to Sea Level Rise, Master of Applied Science Thesis, Queensland University of Technology, Australia.

Rotzoll, K. and C. H. Fletcher (2013), Assessment of groundwater inundation as a consequence of sea-level rise, *Nature Climate Change*, *3*(5), 477-481, doi: http://dx.doi.org/10.1038/nclimate1725.

Rumbaugh, J. and D. Rumbaugh (2011), Guide to Using Groundwater Vistas.

Sallenger, A. H., K. S. Doran, and P. A. Howd (2012a), Hotspot of accelerated sea-level rise on the Atlantic coast of North America, *Nature Climate Change, 2*, 884-888.

Sallenger, A. H., K. S. Doran, and P. A. Howd (2012b), Hotspot of accelerated sea-level rise on the Atlantic coast of North America. Nature Climate Change, *Nature Climate Change, 2*, 884-888.

Salour, F. and S. Erlingsson (2014), Impact of groundwater level on the mechanical response of a flexible pavement structure – A case study at the Torpsbruk test section along county road 126 using a Falling Weight Deflectometer., *VTI rapport, 808A*.

Salour, F., S. Erlingsson, and C. Zapada (2015), Model for Seasonal Variation of Resilient Modulus in Silty Sand Subgrade Soil, Evaluation with Falling Weight Deflectometer, *Transportation Research Record: Journal of the Transportation Research Board*, 65-73.

Salour, F., S. Erlingsson, and C. E. Zapata (2014), Modelling resilient modulus seasonal variation of silty sand subgrade soils with matric suction control, *Canadian Geotechnical Journal, 51*, 1413-1422.

Santos, J. and A. Ferreira (2012), Pavement Design Optimization Considering Costs and Preventive Interventions, Journal of Trnasportation Engineering, 137(7), pp. 911-923.

Seabrook Master Plan Steering Committee (2011), 2011-20 Town of Seabrook Master Plan, Chapter 5: Transportation and Circulation.

Shahin, M.Y. (2005), *Pavement Management for Airports, Roads and Parking Lots*, 2nd ed., Springer, USA.

Shapiro, S. S. and M. B. Wilk (1965), An Analysis of Variance Test for Normality (Complete Samples), *Biometrika, 52*, 591-611.

Shook, J. F., F. N. Finn, M. W. Witczak, and C. L. Monismith (1982), Thickness Design of Asphalt Pavements—The Asphalt Institute Method, 5th International Conference on the Structural Design of Asphalt Pavements.

Silva, B. A., L. I. Burden, and L. M. G. Motta (2014), Study of the Influence of Groundwater Table in Mechanical Behavior of a Full-Scale Pavement Structure Modeled in a Test-Pit, *Journal of Traffic and Transportation Engineering, 2*, 65-71.

Smith, J. B., J. M. Vogel, and J. E. Cromwell (2009), An architecture for government action on adaptation to climate change. An editorial comment, *Clim. Change, 95*, 53-61.

Stekl, P. J. and S. M. Flanagan (1992), Geohydrology and water quality of stratified-drift aquifers in the Lower Merrimack and coastal river basins, southeastern New Hampshire, *U.S. Geological Survey Water-Resources Investigations Report 91-4025*, 75 p., 7 pls.

Stoner, A. M. K., J. S. Daniel, J. M. Jacobs, K. Hayhoe, and I. Scott-Fleming (2019), Quantifying the Impact of Climate Change on Flexible Pavement Performance and Lifetime in the United States, *Transp. Res. Rec.*, 0361198118821877.

Stott, P. A., N. P. Gillett, G. C. Hegerl, D. J. Karoly, D. A. Stone, X. Zhang, and F. Zwiers (2010), Detection and attribution of climate change: a regional perspective, *Wiley Interdisciplinary Reviews: Climate Change, 1*, 192-211.

Sweet, W., R. Kopp, C. Weaver, J. Obeysekera, R. Horton, E. Robert Thieler, and C. Zervas (2017), *Global and Regional Sea Level Rise Scenarios for the United States.*

Swett, L. J. (2007), Seasonal Variations of Pavement Layer Moduli Determined
Using In Situ Measurements of Pavement Stress and Strain, Master of Science in Civil Engineering thesis, University of Maine, Orno, Maine.

Taner, M. Ü, P. Ray, and C. Brown (2017), Robustness-based evaluation of hydropower infrastructure design under climate change, *Climate Risk Management, 18*(Supplement C), 34-50, doi: https://doi.org/10.1016/j.crm.2017.08.002.

Tanquist, B. A. (2001), Reliability, Damage, and Seasonal Considerations in the MnPAVE Mechanicanistic-Empirical Asphalt Pavement Design Computer Program.

Tanquist, B. A. (2012), MnPAVE, MNDOT Flexible Pavement Design, Mechanical-Empirical Method, Version 6.2, User's Guide.

Tavakoli, A., M. S. Lapin, and J. L. Figueroa (1992), PMSC: Pavement Management System for Small Communities, *Journal of Transportation Engineering, 118*, 270-280.

Taylor, K. E., R. J. Stouffer, and G. A. Meehl (2012), An Overview of CMIP5 and the Experiment Design, *Bulletin of the American Meteorological Society, 93*, 485-498.

Thives, L. P. and E. Ghisi (2017), Asphalt mixtures emission and energy consumption: A review, *Renewable and Sustainable Energy Reviews, 72*, 473-484, https://doi.org/10.1016/j.rser.2017.01.087.

Timm, D., D. Newcomb, and B. Birgisson (1999), Mechanistic-Empirical Flexible Pavement Thickness Design: The Minnesota Method, *MN/RC-P99-10*.

Transport & ICT (2015), Moving Toward Climate-Resilient Transport: The World Bank's Experience from Building Adaptation into Programs.

TRB (2009), A Transportation Research Program for Mitigating and Adapting to Climate Change and Conserving Energy.

Trombulak, S. C. and R. Wolfson (2004), Twentieth-century climate change in New England and New York, USA, *Geophys. Res. Lett., 31*.

U.S. Census Bureau (2016), *2016*.

U.S. Fish and Wildlife Service (2001), National Wetlands Inventory.

USGCRP (2017), Climate Science Special Report: Fourth National Climate Assessment, Volume I, 470.

Valle, O., Y. Qiao, E. Dave, and W. Mo (2017), Life cycle assessment of pavements under a changing climate, Pavement LCA Conference, Illinois.

van Aalst, M. K., T. Cannon, and I. Burton (2008), Community level adaptation to climate change: The potential role of participatory community risk assessment, *Global Environmental Change, 18*(1), 165-179, doi: https://doi.org/10.1016/j.gloenvcha.2007.06.002.

van Vuuren, D. P., J. Edmonds, M. Kainuma, K. Riahi, A. Thompson, K. Hibbard, G.C. Hurtt, T. Kram, V. Krey, J. Lamarque, T. Masui, M. Meinshausen, N. Nakicenovic, S.J. Smith, and S.K. Rose (2011), The representative concentration pathways: an overview, *Climatic Change, 109*, 5-31.

Vermeer, M. and S. Rahmstorf (2009), Global Sea Level Linked to Global Temperature, *Proceedings of the National Academy of Sciences*.

Vose, R. S., S. Applequist, M. Squires, I. Durre, M. J. Menne, C. N. Williams, C. Fenimore, K. Geason, and D. Arndt (2017), Improved historical temperature and precipitation time series for Alaska climate divisions, *Journal of Service Climatology*.

Vose, R. S., S. Applequist, M. Squires, I. Durre, M. J. Menne, J. Williams C.N., C. Fenimore, K. Gleason, and D. Arndt (2014), Improved historical temperature and precipitation time series for U.S. climate divisions, *Journal of Applied Meteorology and Climatology, 53*, 1232-1251.

Walter, D. A., T. D. McCobb, J. P. Masterson, and M. N. and Fienen (2016), Potential effects of sea-level rise on the depth to saturated sediments of the Sagamore and Monomoy flow lenses on Cape Cod, Massachusetts:, *U.S. Geological Survey Scientific Investigations Report 2016–5058*, 55 p.

Wang, W., S. Qiu, S. Wang, P. Wang, and J. Zhang (2016), Investigation of seasonal variations of Beijing pavement condition data using unevenly spaced dynamic panel data model, *International Journal of Pavement Engineering*.

Wilby, R. L. and I. Harris (2006), A framework for assessing uncertainties in climate change impacts: Low-flow scenarios for the River Thames, UK, *Water Resourches Research, 42*.

Wilson, K., J. Kelley, A. Reeve, and D. Belknap (2012), Morphological Controls on Maine's Salt Marshes: Dynamic Salt Marsh Pools, Groundwater, and Sea-Level Rise, 2012 Annual Meeting of the Geological Society of America, Charlotte Convention Center, Charlotte, North Carolina, Nov 4, 2012.

Witczak, M. W., D. Andrei, and W. N. Houston (2000), Resilient Modulus as Function of Soil Moisture – Summary of Predictive Models. Development of the 2002 Guide for the Development of New and Rehabilitated Pavement Structures, *NCHRP 1-37 A, Inter Team Technical Report (Seasonal 1)*.

Witczak, M. W., W. N. Houston, and D. Andrei (2000), Resilient Modulus as Function of Soil Moisture – A Study of the Expected Changes in Resilient Modulus of the Unbound Layers with Changes in Moisture for 10 LTPP Sites. Development of the 2002 Guide DD-3.35 for the Development of New and Rehabilitated Pavement Structures., *NCHRP 1-37 A, Inter Team Technical Report (Seasonal 2)*.

Wolfe, D. W., A. T. DeGaetano, G. M. Peck, M. Carey, L. H. Ziska, J. Lea-Cox, A. R. Kemanian, M. P. Hoffmann, and D. Y. Hollinger (2018), Unique challenges and opportunities for northeastern US crop production in a changing climate, *Clim. Change, 146*, 231-245.

Wolters, A., K. Zimmerman, K. Schattler, A. Rietgraf (2011), Implementing Pavement Management Systems for Local Agencies, Illinois Center for Transportation: ICT-R27-87,1-40.

Wu, S., R. Najjar, and J. Siewert (2009), Potential impacts of sea-level rise on the Mid- and Upper-Atlantic Region of the United States, *Clim. Change, 95*, 121-138.

APPENDICES

APPENDIX A

Table A- 1. Global Climate Models (GCMs) used in the temperature analyses presented in Chapters 5 and 6

RCP4.5		RCP6.0		RCP8.5	
Models:		Models:		Models:	
Model 1	access1-0.1.rcp45	Model 1	bcc-csm1-1.1.rcp60	Model 1	access1-0.1.rcp85
Model 2	bcc-csm1-1.1.rcp45	Model 2	ccsm4.1.rcp60	Model 2	bcc-csm1-1.1.rcp85
Model 3	canesm2.1.rcp45	Model 3	gfdl-cm3.1.rcp60	Model 3	canesm2.1.rcp85
Model 4	ccsm4.1.rcp45	Model 4	gfdl-esm2g.1.rcp60	Model 4	ccsm4.1.rcp85
Model 5	cesm1-bgc.1.rcp45	Model 5	gfdl-esm2m.1.rcp60	Model 5	cesm1-bgc.1.rcp85
Model 6	cnrm-cm5.1.rcp45	Model 6	ipsl-cm5a-lr.1.rcp60	Model 6	cnrm-cm5.1.rcp85
Model 7	csiro-mk3-6-0.1.rcp45	Model 7	ipsl-cm5a-mr.1.rcp60	Model 7	csiro-mk3-6-0.1.rcp85
Model 8	gfdl-esm2g.1.rcp45	Model 8	miroc-esm.1.rcp60	Model 8	gfdl-cm3.1.rcp85
Model 9	gfdl-esm2m.1.rcp45	Model 9	miroc-esm-chem.1.rcp60	Model 9	gfdl-esm2g.1.rcp85
Model 10	inmcm4.1.rcp45	Model 10	miroc5.1.rcp60	Model 10	gfdl-esm2m.1.rcp85
Model 11	ipsl-cm5a-lr.1.rcp45	Model 11	mri-cgcm3.1.rcp60	Model 11	inmcm4.1.rcp85
Model 12	ipsl-cm5a-mr.1.rcp45	Model 12	noresm1-m.1.rcp60	Model 12	ipsl-cm5a-lr.1.rcp85
Model 13	miroc-esm.1.rcp45			Model 13	ipsl-cm5a-mr.1.rcp85
Model 14	miroc-esm-chem.1.rcp45			Model 14	miroc-esm.1.rcp85
Model 15	miroc5.1.rcp45			Model 15	miroc-esm-chem.1.rcp85
Model 16	mpi-esm-lr.1.rcp45			Model 16	miroc5.1.rcp85
Model 17	mpi-esm-mr.1.rcp45			Model 17	mpi-esm-lr.1.rcp85
Model 18	mri-cgcm3.1.rcp45			Model 18	mpi-esm-mr.1.rcp85
Model 19	noresm1-m.1.rcp45			Model 19	mri-cgcm3.1.rcp85
				Model 20	noresm1-m.1.rcp85

Source: Data from the Downscaled CMIP5 Climate and Hydrology Projections archive at http://gdo-dcp.ucllnl.org/downscaled_cmip_projections.

Table A- 2. Grid coordinates for the four spatial grids of downscaled daily temperature observations and projections for southeastern New Hampshire used in the temperature-rise analysis presented in Chapters 5 and 6

Grid 1	Grid 2
Latitude bounds: (42.75, 42.875)	Latitude bounds: (42.875, 43.0)
Longitude bounds: (289.0, 289.125)	Longitude bounds: (289.0, 289.125)
Grid 3	Grid 4
Latitude bounds: (42.875, 43.0)	Latitude bounds: (43.0, 43.125)
Longitude bounds: (289.125, 289.25)	Longitude bounds: (289.125, 289.25)

Table A- 3. Simulated daily average temperature rise (ΔT) calculated as the difference between Early-Century (ec), Early-Mid-Century (emc), Mid-Century (mc), Late-Mid-Century (lmc) projections for RCP 4.5, 6.0 and 8.5 scenarios and the baseline daily average temperatures (calculated for years 1979-1999)

	ec_4.5	ec_6.0	ec_8.5	emc_4.5	emc_6.0	emc_8.5	mc_4.5	mc_6.0	mc_8.5	lmc_4.5	lmc_6.0	lmc_8.5
Ave ΔT (°C)	0.71	0.71	0.80	1.42	1.31	1.63	2.10	1.99	2.79	2.53	2.68	4.03
Max ΔT (°C)	1.67	1.75	1.66	2.27	2.17	2.50	3.09	2.88	3.78	3.63	3.53	4.99
Min ΔT (°C)	-0.09	-0.11	-0.21	0.30	0.27	0.72	1.13	1.17	1.73	1.63	1.66	2.82
SD (°C)	0.29	0.32	0.28	0.30	0.34	0.31	0.32	0.32	0.35	0.34	0.36	0.47
N	365	365	365	365	365	365	365	365	365	365	365	365
95% LL_ΔT	0.68	0.68	0.77	1.39	1.28	1.59	2.07	1.96	2.75	2.50	2.64	3.98
95% UL_ΔT	0.74	0.74	0.83	1.45	1.35	1.66	2.14	2.02	2.82	2.57	2.71	4.08

APPENDIX B

Table B- 1. Input parameters for Real Cost analysis [*FHWA*, 2004; *FHWA*, 2017]

Project Details	
State Route	Route 286
Region	NH Seacoast
County	Rockingham
Length of Project (km)	3.792
Analysis Options	
User costs	Yes
Traffic Direction	Both
Analysis Period (Years)	60
Beginning of Analysis Period	2020
Discount Rate (%)	3.8
Economic Variables	
Value of time - passenger cars ($/hour)	13.60
Value of time - single unit tucks ($/hour)	27.20
Value of time - conbination trucks ($/hour)	27.20
Traffic Data	
AADT (total for both directions)	16,000
Cars as percentage of AADT (%)	94
Combination trucks as percentage of AADT (%)	6
Annual growth rate of traffic (%)	1.3
Speed limit (kph)	80
Number of lanes in each direction	1
Free flow capacity (vphpl)	2200
Traffic distribution	Rural
Queue dissipation capacity (vphpl)	1748
Maximum AADT (total for both directions)	83,495
Maximum queue length (km)	3.8

Table B- 2. Calculation of Hot Mix Asphalt (HMA) costs including assumptions, equipment and labor, materials, and haul and placement costs. This example is for 3,503 tons of HMA. [*FHWA*, 2018; *FHWA*, 1998b; *NHDOT*, 2018]

Cost-Based Unit Price:
Hot Asphalt Concrete Pavement

Project Name and Number: Route 286, Coastal NH Regional Connector

Pay Item Number: 40101-0600
Description: SUPERPAVE PAVEMENT, 1/2-INCH NOMINAL MAXIMUM SIZE AGGREGATE, 0.3 TO <3 MILLION ESAL
Quantity: 3,503
Unit: TON

ASSUMPTIONS

Description	Assumed Value	Remarks
Type of truck	Belly Dump	
Truck haul capacity (tons)	20	See RS Means for truck haul capacity
Number of trucks	15	
Load time (minutes)	5	Default = 5
Dump time (minutes)	10	Default = 10; includes turnaround time
Haul speed (MPH)	25	Slower speed when fully loaded
Return speed (MPH)	35	Speed limit along haul route
Haul distance (miles)	19	Distance from pit to project
Shift length (hours)	10	
Efficiency Factor	90%	Default = 90%; inefficiencies include breakdowns, weather, coffee breaks, etc

EQUIPMENT (COST PER HOUR)

Description [1]	Quantity	Cost / Hour	Total Cost / Hour
Haul truck (owner / operators) [2]	15	$ 90.00	$ 1,350.00
Cat CS-433E Roller	2	$ 23.95	$ 47.90
Cat PS-360C Pneumatic Roller	1	$ 18.75	$ 18.75
Asphalt Paver, 130 H.P.	1	$ 78.05	$ 78.05
Bobcat Skidster	1	$ 23.95	$ 23.95
TOTAL			**$ 1,518.65**

(1) These are typical types of equipment used in this operation. Adjust for any project-specific requirements.
(2) Assume that the cost of the truck drivers are included in the cost of the truck for owner / operators.

LABOR (COST PER HOUR)

Description [1]	Quantity	Cost / Unit [2]	Subtotal	Payroll Burden [3]	Subtotal	Overhead [4]	Subtotal	Profit [5]	Total Cost / Unit
Foreman w/truck	1	$ 51.50	$ 51.50	35%	$ 69.53	10%	$ 76.48	10%	$ 84.13
Laborers	5	$ 19.29	$ 96.45	35%	$130.21	10%	$143.23	10%	$ 157.55
Equipment Operators	5	$ 31.52	$ 157.60	35%	$212.76	10%	$234.04	10%	$ 257.44
									$ -
TOTAL									**$ 499.12**

(1) These are typical types of labor used in this operation. Adjust for any project-specific requirements.
(2) Use Davis-Bacon labor rates (http://www.gpo.gov/davisbacon/allstates.html). Include fringes. Not all labor classifications have rates in Davis-Bacon, use judgement where rates aren't available.
(3) Default payroll burden = 35%
(4) Default overhead = 10%
(5) Default profit = 10%

Table B-2. Calculation of Hot Mix Asphalt (HMA) costs including assumptions, equipment and labor, materials, and haul and placement costs (continued)

CYCLE TIME

	Hours	Remarks
Load Time =	0.08	
Haul Time =	0.76	
Dump Time =	0.17	
Return Time =	0.54	
HOURS PER CYCLE	**1.72**	Adjusted by efficiency factor

Number of Cycles =	12			
Total Number of Hours =	20.6		Calculated Number of Haul Days* =	2
Total Cost to Haul and Place Hot Asphalt Concrete Pavement =	$ 41,646.69			
Haul and Place Unit Price =	**$ 11.89**		*Add time for weekends and expected rain delays	
H AND P UNIT PRICE =	**$ 11.89**	**per ton**		

MATERIALS

Description	Cost / Unit	Unit	Prime Mark-up	Total Cost / Unit
Material Price at Pit	$ 74.72	ton	10%	$ 82.19
MATERIALS UNIT PRICE =	**$ 82.19**	**per ton**		
TOTAL UNIT PRICE (HAUL + MATERIAL) =	**$ 94.08**	**per ton**		

Table B- 3. Assumptions used in the cost analysis [*NHDOT*, 2018]

HMA density (tons/m^3)	2.649
HMA material cost ($/ton)	74.72
Gravel density (tons/m^3)	2.618
Gravel material cost ($/ton)	13.86
12" RSB cost ($/$m^2$)	5.98
HMA milling cost ($/$m^2$-mm)	0.035
Route 286 width (m)	13.410
Route 286 length (km)	3.792

Table B- 4. Calculation of the thirty-year discount rate used in the present-value cost analysis [*Office of Management and Budget*, 2018]

Real Treasury Interest Rates (from OMB)			
Year	10-Year	20-Year	30-Year
1979	4.6		5.4
1980	3.3		3.7
1981	4.4		4.8
1982	7.8		7.9
1983	5.3		5.6
1984	6.1		6.4
1985	7.1		7.4
1986	5.9		6.7
1987	3.8		4.4
1988	5.1		5.6
1989	5.8		6.1
1990	4.2		4.6
1991	3.9		4.2
1992	3.6		3.8
1993	4.3		4.5
1994	2.7		2.8
1995	4.8		4.9
1996	2.8		3.0
1997	3.5		3.6
1998	3.6		3.8
1999	2.7		2.9
2000	4.0		4.2
2001	3.2		3.2
2002	3.1		3.9
2003	2.5		3.2
2004	2.8	3.4	3.5
2005	2.5	3.0	3.1
2006	2.8	3.0	3.0
2007	2.8	3.0	3.0
2008	2.6	2.8	2.8
2009	2.4	2.9	2.7
2010	2.2	2.7	2.7
2011	1.3	2.1	2.3
2012	1.1	1.7	2.0
2013	0.1	0.8	1.1
2014	1.0	1.6	1.9
2015	0.9	1.2	1.4
2016	1.0	1.2	1.5
2017	0.1	0.5	0.7
Mean			**3.80**
SD			**1.67**